Energy Storage Materials 81 (2025) 104461

Contents lists available at ScienceDirect

Energy Storage Materials

journal homepage: www.elsevier.com/locate/ensm

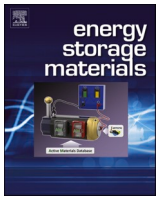

Effects of external pressure on all-solid-state batteries: comprehensive review and analysis

John Adjah [a,b,e,**], Benjamin Agyei-Tuffour [a,**], Ridwan A. Ahmed [b], Desmond Edem Primus Klenam [b,c,e], David Dodoo-Arhin [a], Emmanuel Nyankson [a], Kwadwo Mensah-Darkwa [d], Winston Wole Soboyejo [e,*]

[a] Department of Materials Science and Engineering, School of Engineering Sciences, University of Ghana, Legon-Accra, Ghana
[b] Department of Mechanical Engineering, Materials Science and Engineering, Worcester Polytechnic Institute, Worcester, MA, 01609, USA
[c] Next Frontiers in Advanced Manufacturing Laboratory, School of Chemical and Metallurgical Engineering, University of the Witwatersrand, 1 Jan Smut Avenue, Johannesburg, WITS 2001, South Africa
[d] Department of Materials Engineering, Kwame Nkrumah University of Science and Technology, Kumasi, Ghana
[e] SUNY Polytechnic Institute, College of Engineering, 100 Seymour Rd, Utica, NY 13502, USA

ARTICLE INFO

Keywords:
All-solid-state batteries
Solid electrolytes
Pressure-induced solid-state batteries
Deformation mechanisms
Interfacial impedance
Stack pressure

ABSTRACT

All-solid-state batteries (ASSBs) offer next-generation energy storage solutions with high energy density and enhanced safety. A central challenge remains the solid-solid interfacial contact between electrodes and solid electrolytes. While external pressure improves contact and ionic conductivity, excessive pressure induces cracking and mechanical degradation. This review discusses the interplay of mechanical factors in sulfide, oxide, and polymer electrolytes, as well as lithium metal and alloy anodes and layered oxide cathodes. We assess the material-specific pressure requirements and their impact on structural integrity and electrochemical performance. Strategies for optimizing fabrication and operational pressure are discussed to enable robust, scalable ASSB designs.

1. Introduction

The global challenges associated with energy shortages and environmental pollution are enormous, driven primarily by a heavy reliance on fossil fuels, which account for >40 % of the global energy mix [1–5]. This urgent situation necessitates a shift towards a more environmentally friendly and low-carbon energy landscape [6]. One critical area of focus is to develop strategies to advance the electric vehicle industry while reducing energy consumption and emissions [6,7]. Despite a significant increase in global battery sales, scientific and technological advancements have slowed, affecting all types of battery technologies, including nickel-cadmium, nickel-metal hydride, and lithium-ion batteries [8–10].

Lithium-ion batteries, due to their enhanced power density, superior energy efficiency, and extended cycle life, have become prevalent in modern society. They power a diverse range of devices, from smartphones and laptops to electric vehicles and renewable energy storage systems. To mitigate the risk of battery-related fires and explosions, non-flammable solid-state electrolytes have emerged as substitutes for flammable liquid electrolytes in conventional lithium-ion batteries. The demand for improved safety, increased energy density, longer cycle life, broader operating temperature ranges, and greater sustainability is driving the shift from conventional Li-ion batteries to solid-state batteries. Solid electrolytes (SEs) with high ionic conductivity hold the potential to eliminate bottlenecks and provide a safer solution for durable lithium batteries [11,12].

By employing high-capacity lithium (Li) metal anodes instead of traditional graphite anodes, all-solid-state batteries (ASSBs) can substantially improve the gravimetric and volumetric energy densities of lithium-ion batteries. ASSBs typically comprise a solid electrolyte, a negative electrode (anode), and a positive electrode (cathode) [13]. These batteries require external pressure to function at their maximum potential because, unlike liquid electrolytes, they facilitate ion conduction only in restricted regions of solid-solid contacts [14,15]. For

* Corresponding author at: Department of Engineering, SUNY Polytechnic Institute, 100 Seymour Road, NY, 13502, USA.
** Corresponding authors at: Department of Materials Science and Engineering, Off Anne Jiaggi Road, School of Engineering Sciences, University of Ghana, Legon, Accra, Ghana.
E-mail addresses: jadjah003@st.ug.edu.gh (J. Adjah), bagyei-tuffour@ug.edu.gh (B. Agyei-Tuffour), soboyew@sunypoly.edu (W.W. Soboyejo).

https://doi.org/10.1016/j.ensm.2025.104461
Received 1 May 2025; Received in revised form 30 June 2025; Accepted 15 July 2025
Available online 16 July 2025

instance, Zhang et al. [16] discussed "solid-solid" contact models and explored the impact of external and internal stresses on the interfacial behavior of ASSBs. There are two primary categories of external pressure: fabrication pressure and stacking pressure (Fig. 1). Fabrication pressure refers to the externally applied force during the manufacturing process of the electrode and solid-state electrolyte (SSE), such as compressing, pelletizing, densifying, and calendaring (Fig. 1a), while stacking pressure denotes the continuous external force exerted throughout the operational lifespan of the battery (Fig. 1b). The interaction between these pressures and the microstructure of battery components is pivotal for overall performance. Moderate pressures can enhance electrochemical performance by improving contact between active materials and solid electrolytes, whereas excessively high pressures can have detrimental effects, such as material extrusion and compromised electrode integrity. The fabrication or preparation pressure typically ranges from dozens to several MPa/GPa and affects the electrolyte and composite electrode's porosity, charge transport, and mechanical properties. The operation pressure (or stack pressure) is normally below 10 MPa for soft electrolytes, which affects the contact between the electrode and the solid electrolyte (SE).

External pressure plays a crucial role in ASSBs, enabling elastic solid electrolytes (SEs) to adapt to volume changes in electrode materials during charge and discharge cycles, which helps mitigate problems like charge-transfer resistance stemming from voids and cracks. A discrete element model incorporating plastic deformation and cold stamping has been developed, providing important insights into ionic conductivity relationships informed by percolation theory by analyzing the weak connectivity of SE aggregates. Simulation studies were conducted using various solid electrolyte layers and electrodes, as well as different mold pressures and active material ratios, which allowed for a thorough understanding of the cold pressing process. It has been observed that increased applied pressure improves the contact and relative density between solid sulfide electrolytes and active materials. Moreover, localized stresses may concentrate the forces between the active material particles by causing the solid sulfide electrolyte particles to deform more easily. The correlation between applied pressure, relative density, and ionic conductivity has also been studied experimentally. Prior research demonstrated that the absence of external pressure resulted in localized plating, which has detrimental effects on battery performance [17].

Regulating stack pressure during alkali metal stripping and plating is essential for reducing interfacial resistance and promoting uniform current distribution [28,29]. This enhances ASSB efficiency. Optimal stack pressure also prevents the formation of voids at the Li metal electrode interface by inducing permanent deformation in the malleable alkali metal [30]. However, excessive pressure can damage ASSB performance, potentially causing electrode material fracture and short-circuiting [31,32]. Non-uniform external pressure strongly affects the stability of solid-solid interfaces in ASSBs, with internal and external stressors at the electrode/electrolyte interface playing a critical role [33,34]. These investigations reveal the complex interplay of chemical and thermal stresses at these interfaces. The powder compaction process in electrolytes or electrodes typically involves aggregate breaking, nanoparticle rearrangement, and particle consolidation due to plastic deformation. Applied pressure significantly influences the interfacial contacts between electrode and SE particles during composite electrode formation experimentally [35]. A study using a customized cellular system with X-ray CT, pressure monitoring, and electrochemical analysis examined a 3D configuration of composite electrodes in ASSBs [36], revealing insufficient contact perpendicular to the pressure axis between the active material and SEs. Additionally, an electrochemical-mechanical model explored the effects of compressive pressures up to 10 MPa, focusing on variables like concentration gradients, local electrode potentials, and current density distribution, all indicating a tendency for lithium plating. Experimental validation using locally compressed pouch cells cycled at 1 C confirmed the model's predictions, with lithium being deposited under varying pressure conditions [36], (Fig. 2).

The selection of appropriate preparation processes and stack pressure is contingent upon the physical properties of solid electrolytes (SEs) and electrodes, playing a pivotal role in determining the optimal electrochemical performance of all-solid-state batteries (ASSBs). It has been observed that the distinct stiffness, flexibility, and creep properties of SEs and electrodes significantly influence the integrity and operational efficiency of the battery system [18–20]. The correlation between capacity fading in ASSBs and critical physical parameters, such as Young's modulus, shear modulus, and bulk modulus, in commonly used SEs have been investigated [21]. This was studied in positive and negative electrodes.

Achieving a uniform and optimal applied external pressure across

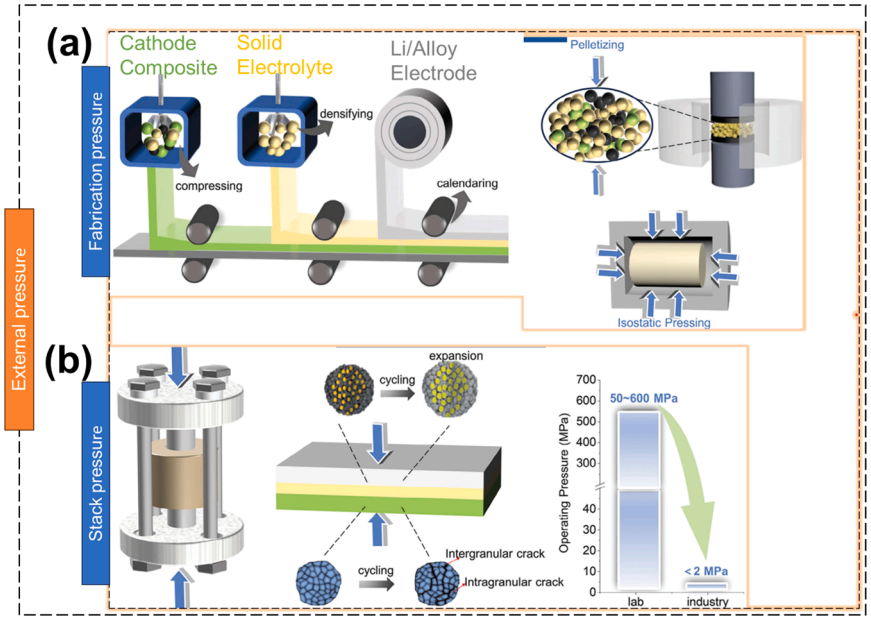

Fig. 1. Schematic of the two main forms and pressure-related problems in all-solid-state batteries: (a) Fabrication pressure is the pressure used in compressing, densifying, calendaring, and pelletizing. (b) Stack pressure is the external pressure applied during the battery cycling (Adapted from Zhang et al.) [22].

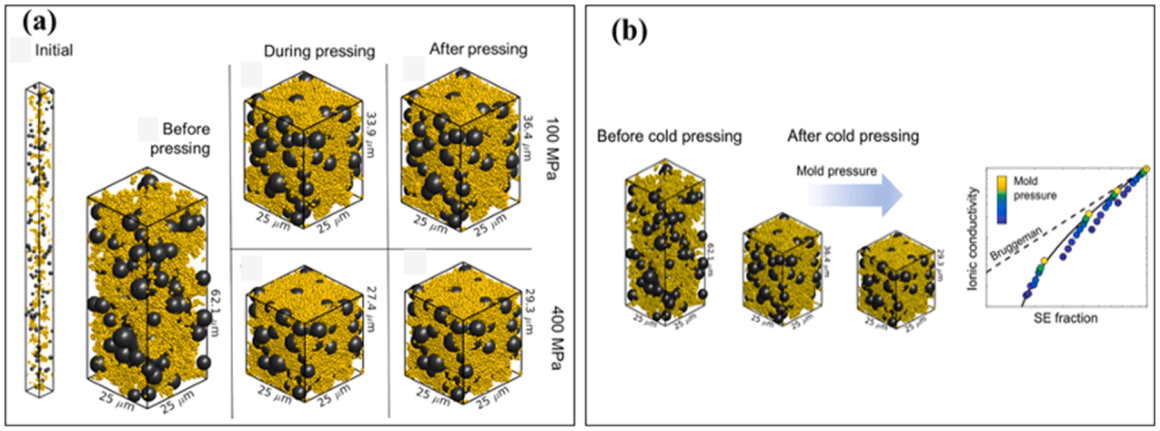

Fig. 2. (a) A 3D particle distribution chart showing that an anode electrode comprises 50 % AM particles. The anode layer experiences increased compression as pressure rises, and the electrode shows slight expansion upon release. (b) The relative conduction coefficient and its relationship with the volume fraction of the SE (Adapted from So et al.) [23].

all-solid-state batteries is challenging due to the close connection between the ideal external pressure and the physical characteristics of the electrode/electrolyte materials. Nonetheless, a comprehensive understanding of the interdependencies between the applied external pressure, electrode/electrolyte properties, and the electrochemical performance of solid-state batteries (SSBs) is imperative.

This review systematically examines the impact of external pressure on the electrochemical properties of electrolytes and electrode materials, the interfacial contact between electrodes and electrolytes, and the overall electrochemical performance of ASSBs. The analysis provides essential insights for determining the optimal external pressure levels required during the fabrication and operation of ASSBs. The review also outlines potential methods for reducing both fabrication and operation pressures by understanding the underlying electro-chemo-mechanical failure mechanisms, aiming to guide the development of low-operation-pressure ASSBs.

2. External pressure and structural integrity of ASSBs

The external pressure and structural integrity are critical for the design of ASSBs. Generally, the benefits of applying external pressure depend on various materials and design parameters. The main advantages associated with external pressure include enhancement of the energy density, improvement in the conductivity of the electrolyte, enhanced mechanical stability, and improved safety of the ASSBs. The enhancement in the energy density induced by the external pressure promoted high packing densities in the cell. This is due to the reduction in defects that are in the form of interparticle gaps, contributing to the increased contact between the electrodes and the solid electrolyte. For optimized battery storage capacity and performance, a more compact structure and design are desired.

Controlling the external pressure enables the effective transportation of the ions required to induce conductivity in the battery. This improves the electrolyte conductivity, leading to faster charging and discharging rates. The effects of applying moderate pressure can enhance the mechanical stability of the battery. This reduces internal defects such as porosity, cracks, and voids that might be present in the solid electrolyte. Thus, it enhances structural integrity and contributes to longevity.

In laboratory settings, high fabrication pressures for all-solid-state batteries (ASSBs) are produced using uniaxial or isostatic pressure devices, limiting production efficiency and cost improvements. While hydraulic presses are employed to create operational pressure in labs, they introduce difficulties when scaling up for industrial use, particularly with larger pouch cells. As the area of these cells expands, the force required to maintain uniform pressure can surpass the strength of the materials used in peripheral components, making it challenging to ensure consistent pressure distribution. This inconsistency can result in problems such as uneven lithium-ion flux and increased degradation. Therefore, it is crucial to lower the operational pressure to facilitate commercialization, with the acceptable threshold for original equipment manufacturers generally set at a maximum of 2 MPa, although this can vary significantly among different original equipment manufacturers. A lower operating pressure is generally preferred.

2.1. Residual stress-induced by pressure

Fabrication pressure plays a crucial role in inducing stress changes within the electrode and solid-state electrolyte (SSE) materials, which subsequently impact the electrochemical performance of all-solid-state batteries (ASSBs) (Table 1). Various surface treatment methods apply different pressures, leading to distinct stress distributions. For instance, Bo et al. [24] found that untreated LLZTO samples exhibited significant compressive stress, measured at 26 MPa, with one-quarter of the surface displaying this stress state. However, after polishing the samples, the average stress increased to 143 MPa, causing many areas to shift from compressive to tensile stress and creating a more uniform stress distribution, which could enhance lithium deposition consistency. Additionally, molecular dynamics simulations suggested that SSE surfaces under residual stress could effectively resist lithium dendrite penetration by reducing the likelihood of surface cracks due to high compressive stress. Despite these insights into the interplay between stress and electrochemical behavior in ASSBs, a notable lack of solid experimental evidence remains regarding how internal stress affects lithium-ion diffusion dynamics and dendrite growth processes.

2.2. Impact of operation pressure in ASSLMBs

Reducing the operational (stack) pressure in all-solid-state lithium metal batteries (ASSLMBs) is essential for their commercial viability. While high pressures are often employed in laboratory settings to ensure strong interfacial contact and to suppress dendrite growth, there is a significant gap between research conditions and industrial requirements. Many laboratory studies utilize stack pressures exceeding 50 MPa, whereas the industry seeks operational pressures below 10 MPa, ideally under 1 MPa [25]. This reduction is imperative because excessive pressure can lead to severe mechanical degradation and cell performance limitations. For instance, high pressures can damage the porous structure of the electrode materials, reduce porosity, and hinder crucial lithium-ion transport, which may lead to a complete breakdown of the electrode structure [25]. Furthermore, lithium metal, with a relatively low yield stress of ~ 0.8 MPa, is highly susceptible to plastic deformation and creep under excess external pressure [26]. This

Table 1
Summary of fabrication, stack pressures, and associated physicochemical properties of selected SSEs.

Electrolyte type	Material	Fabrication Pressure (MPa)	Stack Pressure (MPa)	ρ_{bulk}/ (ρ_{Rel}) g/cm (%)	E/GPa	G/ GPa	ν	σ/mS/cm	Refs.
Sulfide	Li_2S-P_2S_3	50 - 300	1 - 10	–	18 - 25	6.8	0.29	$\sim10^{-3}$	[29]
	$Li_{10}GeP_2S_{12}$	100 - 400	5 - 10	–	37.2	14.4	0.28	$\sim1.9\times10^{-3}$	[29]
	Li_6PS_5Cl	100 - 300	5 - 10	–	25	9.8	0.28	$\sim6.8\times10^{-3}$	[29]
	$25Li_2S_{0.75}P_2S_5$ glass	270	–	2.00(99)	13	5.0	0.30	–	[30]
	$50Li_2S_{0.50}P_2S_5$ glass	360	–	1.89(96)	18	6.9	0.27	–	[31]
	$70Li_2S_{0.30}P_2S_5$ glass	360	–	1.91(99)	22	8.3	0.31	–	[31]
	$70Li_2S_{0.30}P_2S_5$	360	–	1.67	14	5.5	0.29	–	[31]
	$75Li_2S_{0.25}P_2S_5$ (Li_3PS_4) glass	360	–	1.88(100)	23	8.7	0.32		[31]
	$75Li_2S_{0.25}P_2S_5$	180	–	1.45	8.8	3.4	0.28	–	[31]
	$75Li_2S_{0.25}P_2S_5$	360	–	1.68	15	5.9	0.30	–	[31]
	$75Li_2S_{0.25}P_2S_5$	360	–	1.86	20	7.4	0.32	–	[31]
	$75Li_2S_{0.25}P_2S_5$	360	–	1.89	21	8.0	0.32	–	[31]
	$75Li_2S_{0.25}P_2S_5$	360	–	1.88	23	8.7	0.32	–	[31]
	$80Li_2S_{0.20}P_2S_5$ glass	360	–	1.85(100)	25	9.5	0.31	–	[31]
	$50Na_2S_{0.50}P_2S_5$ glass	270	–	2.05(99)	15	5.5	0.33	–	[31]
	$67Na_2S_{0.33}P_2S_5$ glass	360	–	2.01(99)	19	7.0	0.35	–	[31]
	$75Na_2S_{0.25}P_2S_5$ glass	360	–	1.98(99)	19	7.1	0.34	–	[31]
	$75Na_2S_{0.25}P_2S_5$ glass	170	–	2.00	18	6.6	0.34	–	[31]
	$80Li_2S_{0.20}P_2S_5$ glass	190	–	1.85	25	9.5	0.31	–	[31]
	Li_6PS_5Cl	250	–	97.8	–	–	–	–	[32]
	$(Li_2S)_{70}(P_2S_5)_{30}$	200	–	98	–	–	–	–	
	$Li_{10}SnP_2S_{12}$	125	–	91.3	–	–	–	1.90/RT	[32]
	$(Li_2S)_{60}(SiS)_{28}(P_2S_3)_{12}$	–	0.1		–	–	–	1.80/RT	[33]
Halide	Li_3InCl_6	~370–500	~10–20	–	~20–30	~8 - 12	~0.2–0.30	$\sim1.0\times10^{-3}$	[34]
	Li_3YCl_6	~400	~5–10	–	~25	~10	~0.28	$\sim1.2\times10^{-3}$	[34]
	Li_3ScCl_6	~350–450	~5–15	–	~22	~9	~0.26	$\sim1.5\times10^{-3}$	[34]
	Li_3YBr_6	~300–400	~10	–	~18	~7	~0.29	$\sim2.0\times10^{-3}$	[34]
	Li_6PS_5Cl	–	2.0		–	–	–	–	[35]
	$Li_6PS_5Cl_{0.5}Br_{0.5}$	–	0.1		–	–	–	–	[36]
	$Li_{7-X}PS_{6-x}Cl_x$	–	3.0		–	–	–	–	[37]
	Li_6PS_6Cl	–	0.1		–	–	–	–	[36]
	Li_6PS_5Cl	50 - 370	5 - 70	–	–	–	0.22 – 3.02		[38]
Oxide	LLZO	300 - 500	10 - 30		150	57.7	0.26	–	[39]
	LATP	200 - 400	10 - 20		115	45	0.26	–	[39]
	LLTO	300 - 500	10 - 30		200	79	0.25	–	[39]
	Al-doped $Li_7La_3Zr_2O_{12}$	63	–	5.08(>98)	146	60	0.22	–	[40]
	$90Li_3BO_{3.10}Li_2SO_4$	360	–	1.92(92)	53	19	0.37	–	[29]
	$33Li_3BO_{3.33}Li_2SO_{4.33}Li_2CO_3$	360	–	0(97)	51	19	0.31	–	[41]
	$Li_7La_3Zr_2O_{12}$	200	–	94	–	–	–	0.635/RT	[42]
	$Li_7La_3Zr_2O_{12}$	132	–	99	–	–	–	0.12/RT	[42]
	$Li_{7.44}La_3Zr_2O_{12}$	300	–	95	–	–	–	0.167/RT	[42]
	$Li_{1.3}Al_{0.3}Ti_{1.7}(PO_4)_3$	504	–	90	–	–	–	0.052/RT	[42]
	Al-doped LLZO	150	–	95	–	–	–	0.071/RT	[42]
	$Li_{1.3}Al_{0.3}Ti_{1.7}(PO_4)_3$	504	–	94.2	–	–	–	0.30/RT	[42]
	$Li_{6.2}Ga_{0.3}La_{2.95}Rb_{0.05}Zr_2O_{12}$	250	–	95	–	–	–	1.62/RT	[42]
	$Li_{1.4}Al_{0.4}Ti_{1.6}(PO_4)_3$	200	–	93 - 94	–	–	–	0.183/RT	[42]
	$Li_7La_3Zr_2O_{12}Li_3BO_3$	300	–	86.4	–	–	–	0.0194/RT	[42]
	$Li_{6.4}La_3Zr_{1.4}Ta_{0.6}O_{12}$	200	–	95	–	–	–	0.35/RT	[42]
	$Na_{3.4}Mg_{0.1}Zr_{1.9}Si_{2.2}P_{0.8}O_{12}$	200	–	98.17	–	–	–	3.60/RT	[42]
	$Na_2Zn_2TeO_6$	300	–	83 - 85	–	–	–	0.40/RT	[42]
	NASICON	200	–	97 - 98	–	–	–	1.10/RT	[42]
	$Li_{3/8}Sr_{7/16-3x/2}LaxZr_{1/4}Ta_{3/4}O_3$	200	–	95	–	–	–	0.39/RT	[42]
	h-BN-LLZTO	–	0.1	93	–	–	–	0.13/RT	[43]
	LLZTO	–	2.4		–	–	–	–	[44]
	LLZTO-Au	–	3.3		–	–	–	–	[45]
	LBO-LLZO	–	0.4	–	–	–	–	–	[46]
	LLZO/LAGP/LATP	–	0.1	–	–	–	–	–	[47]
	LLZTO@ZnO	–	0.1	–	–	–	–	–	[48]
	LLZO	–	1.0	–	–	–	–	–	[49]
	PVDF-BaTiO-LLTO	–	4.9	–	–	–	–	–	[50]
	Al-LLZO	150	0.26	97.26	~9.0	–	0.26	~2.0	[51]
Polymer	PEO	5 - 20	0.1 - 1	0.07	0.026	0.35	10^{-4} – 10^{-2}	$\sim10^{-7}$ – $\sim10^{-5}$	[36]
	PMMA	10 - 30	1	4	1.48	0.35	10^{-4}	$\sim10^{-7}$	[35]
	LEO-LiTFSI	10 - 30	1	0.07	0.026	0.35	1.5×10^{-2}	$\sim1.5\times10^{-5}$	

phenomenon can result in the penetration of lithium through the grain boundaries of the ceramic electrolyte. This can potentially pose a significant risk of internal short circuits and catastrophic cell failure [25,26]. For example, silicon-based Li-ion batteries exhibit optimal cycling performance at 0.2 MPa, with capacity retention dropping from ~70 % (at 0.2 MPa) to around 47 % (at 0.4 MPa) after 50 cycles [25]. Similarly, a Li-In/Li_3InCl_6/NCM-83 cell experienced rapid capacity degradation, retaining only 65 % after 50 cycles when operated under 2 MPa [25].

Consequently, the need to reduce stack pressure drives the development of halide solid electrolytes and battery designs capable of functioning reliably under low-pressure conditions. Recent advancements in halide-based all-solid-state lithium-metal batteries (ASSLMBs) indicate that high performance can be attained at pressures significantly lower than typical laboratory standards. For instance, the halide-based $Li_3YBr_2Cl_4$ solid electrolyte has demonstrated successful operation at pressures as low as 0.1 MPa when paired with a Li-In anode, showing minimal capacity loss even when the pressure was decreased from 5 MPa to 0.1 MPa [27]. Another study by Gao et al. [28] confirmed reliable operation down to 0.1 MPa against a Li-In alloy and 0.2 MPa against a Li metal anode. This shows that pressure below 5 MPa did not impede rate capabilities, with 70 % of the C/20 capacity retained even at 1C discharge rate [28]. These results highlight that the mechanical characteristics, especially the hardness of the halide solid electrolyte, may play a more significant role than ionic conductivity in influencing galvanostatic cycling performance under low-pressure conditions [27]. Future R&D efforts should prioritize the development of advanced materials and interfaces designed to facilitate stable and efficient performance at low stack pressures that are relevant to industrial applications. This shift is essential to reduce dependency on mechanical compaction techniques and enhance operational reliability.

2.3. Effects of external pressure on electrolyte properties

The structural integrity of bulk solid-state electrolytes (SSEs) is fundamentally influenced by manufacturing parameters, which play a crucial role in determining their ion transport efficiency. High ionic conductivities are attained through the processing of inorganic SSEs, such as $Li_7La_3Zr_2O_{12}$ (LLZO) and amorphous sulfides (Li_2S-P_2S_5), at elevated temperatures and pressures. These conditions effectively reduce internal defects and minimize porosity [29,38,52].

LLZO demonstrates optimal performance when subjected to several hundred MPa during sintering and cold isostatic pressing, as this approach facilitates densification and lowers porosity [53,54]. Similarly, amorphous sulfides such as Li_2S-P_2S_5 benefit from pressures exceeding 350 MPa [29], which not only enhances their density but also increases their Young's moduli, thereby improving ionic conductivity—from 0.99 to 2.06 mS/cm, for example.

The pressure applied during the fabrication of solid-state electrolytes (SSEs) is a critical factor that affects their electrochemical and physicochemical properties, including compact density and ionic conductivity at room temperature. Variations in ionic conductivity for similar types of SSEs can often be attributed to differences in the fabrication or operational pressures used [55,56]. For instance, sulfide SSEs can be classified into amorphous, glass-ceramic, or microcrystalline types, each responding differently to fabrication pressure. Amorphous and glass-ceramic SSEs experience enhanced ionic conductivity with increasing fabrication pressure, which improves particle contact and facilitates ion transport. As the fabrication pressure rises from 100 MPa to 500 MPa, their compact density increases from 1.45 g cm^{-3} to 1.8 g cm^{-3}. In contrast, microcrystalline SSEs maintain a consistent ionic conductivity beyond 300 MPa and are more affected by operational pressure to close gaps between grains effectively [55]. Pellet annealing is essential to achieve high ionic conductivity in microcrystalline SSEs. Furthermore, applying high fabrication pressures can result in plastic deformation, influencing the amorphous phase ratio in glass-ceramic structures. Studies have shown that a fabrication pressure of approximately 0.5 GPa is ideal for reducing interfacial resistance and maximizing ionic conductivity in glass-ceramic thiophosphates. The porosity of SSEs is also closely tied to fabrication pressure; when lower pressures (~ 50 MPa) are used, increased porosity can lead to higher grain boundary impedance, adversely affecting battery performance [38]. In contrast, applying higher pressures, such as 370 MPa, has been shown to significantly enhance both capacity retention and rate performance in assembled all-solid-state batteries (ASSBs).

2.3.1. Garnet-type solid electrolytes

Oxide solid electrolytes (SEs) are gaining attention because of their high ionic conductivities, wide voltage ranges, and wide electrochemical stability windows [57–60]. Compared to sulfide solid electrolytes (SSEs), oxide solid electrolytes (SEs) exhibit high grain boundary resistance, resulting in decreased ionic conductivity [61]. Garnet-type, $Li_7La_3Zr_2O_{12}$ (LLZO) is an oxide solid electrolyte with a substantial Young's modulus of 150 GPa, signifying restricted elastic deformation under applied pressures. LLZO is a ceramic oxide material with high brittleness [62]. The conventional method for fabricating LLZO typically involves an initial pre-pressing step to ensure sufficient contact, followed by sintering under conditions of several hundred MPa and temperatures around 1000 °C [63,64].

LLZO exists as two crystal polymorphs: tetragonal and cubic. The cubic phase exhibits higher ionic conductivity compared to the tetragonal phase. This variation in ionic conductivity is attributed to differences in lattice structure, which influence the mobility of lithium ions within the material [58,65,66]. Achieving optimal ionic conductivity involves maintaining an appropriate bulk density, as lower densities lead to increased grain boundary resistance. Although high external pressure can enhance LLZO bulk density, research has shown that the relative density only reaches 73 % even when the cold-pressed pressure is raised to 800 GPa [67,68].

According to Zhao et al. [69], tetragonal LLZO (t-LLZO) with up to 93 % density can be achieved through the auto-consolidation of molten Li_2O without applying pressure during calcination at 1150 °C, and applying external pressure during sintering is advantageous for obtaining high-density cubic LLZO (c-LLZO) and minimizing Li source loss. However, higher temperatures and pressure accelerate lithium loss during LLZO preparation. High-density and high-purity c-LLZO bulk materials are difficult to synthesize. In the study of the pressure behavior of LLZO, Hirose et al. [70] observed phase transitions and the formation of denser phases under high-pressure conditions using X-ray diffraction and Raman spectroscopy. Monismith et al.'s [66,71] revealed that the application of uniaxial loading results in a cubic-to-tetragonal phase transition in the crystal structure, attributable to mechanical distortion (Fig. 3a and b).

A field-assisted sintering approach was used by Zhang et al. [72] to alter the surface-to-volume ratio and sintering pressure to analyze the phase composition and microstructural changes in LLZO. Their findings identified the optimal conditions for achieving a high-purity cubic phase and demonstrated the influence of pressure on the phase formation (Fig. 3c and d). In contrast to conventionally hot-pressed sintered samples, solid electrolytes (SEs) sintered using oscillating pressure sintering exhibit increased density and a more refined grain structure, leading to enhanced mechanical characteristics and elevated ionic conductivity. The density of the cubic LLZO phase material approached the theoretical value after it was sintered for 1 hour at 114 °C and 30 MPa of constant pressure, with pressure fluctuations of ±5 applied at 1 Hz.

Fig. 3 illustrates how the alternating pressure phenomenon leads to rapid compaction and regulated grain growth, which enhances the mechanical and electrical conductivity of the LLZO electrolyte manufactured using the oscillation pressure sintering (uses pressure that varies regularly when sintering, which helps to increase the densification of ceramic materials) [73]. The density and ionic conductivity of the oxide solid electrolyte (SE) are influenced by preparation pressure, which is a crucial factor in the sintering of SE pellets. Although stack

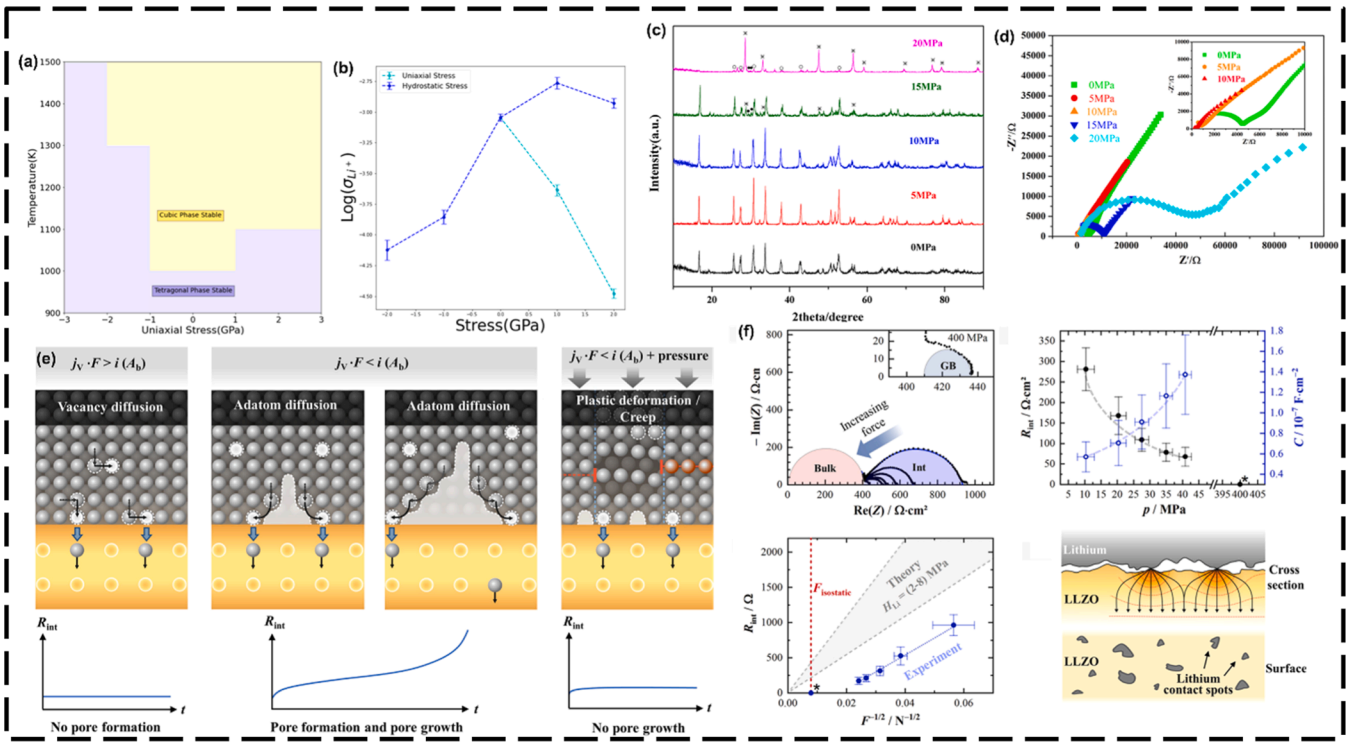

Fig. 3. (a) A potential phase diagram illustrating the behavior of LLZO under uniaxial stress and temperature, (b) The projected room temperature c-LLZO conductivity under hydrostatic (blue line) and uniaxial (green line) stresses. It was impossible to determine the conductivity under uniaxial compression for c-LLZO due to its phase-change behavior (Adapted from Monismith et al.) [71] (c) shows X-ray diffraction patterns of LLZO at different sintering pressures from 0 to 20 MPa (* denotes La_2ZrO_7, ● denotes La_2O_3, and° denotes cubic LLZO). (d) Nyquist plots show frequency ranges from 10 Hz to 1 MHz for samples sintered at 1150 °C with various pressures at 30 °C (Adapted from Zhang et al.) [78]. (e) The measured interfacial resistances (R_{int}) and the interface capacity values are dependent on the external pressure. (f) Estimating the interface resistances by considering a Vickers hardness for lithium varying from 2 to 8 (Adapted from Krauskopf et al.) MPa [79].

pressure helps lower the electrolyte's interfacial impedance, the intrinsic brittleness of oxide SEs limits its impact on bulk resistance. Preparation pressure plays a critical role in the sintering of oxide solid electrolyte (SE) pellets because it affects the electrolyte's density and ionic conductivity [74–77].

2.3.2. *Solid polymer electrolytes (SPEs)*

Solid polymer electrolytes (SPEs) have garnered attention owing to their favorable attributes. These include moderate toughness, ease of processing, and cost-effectiveness, making them well-suited for all-solid-state batteries (ASSBs) [80–82]. However, their mechanical and electrochemical qualities are insufficient, which limits their potential. The mechanical characteristics, such as tensile strength, modulus, elongation at fracture, fracture toughness, and elasticity, of the solid polymer were obtained from the stress-strain curve. Furthermore, owing to the cross-linking network formation of the polymer chain, the mechanical stability was improved [83–86].

PEO has garnered attention due to its broad electrochemical range and significant ion mobility, leading it to be one of the most researched solid polymer electrolytes (SPEs) [87–89]. The polyethylene oxide (PEO) exhibits a significant shear modulus of up to 200 MPa. However, the presence of rigid polymer chains within PEO inhibits ion transportation when complexed with lithium salts, thereby resulting in reduced ionic conductivity. In contrast to inorganic solid electrolytes, PEO exhibits an exceptionally lower Young's modulus and displays contrasting behavior under pressure [88–90].

The application of external pressure has been observed to enhance surface contact and bulk ionic conductivity in inorganic solid electrolytes. However, its impact on polymer solid electrolytes appears to be counterintuitive. Chen et al. [91] employed molecular dynamics to explore the correlation between ionic conductivity and pressure using a PEO/LiTFSI SPE as a model. The research offers new perspectives on how Li+ is transported within PEO/LiTFSI SPEs. In the simulation, the PEO/LiTFSI system was kept at a constant temperature of 393 K and was subjected to different pressures (0 MPa, 50 MPa, 100 MPa, and 150 MPa). The results indicated a steady decrease in the radius of gyration of the PEO polymer chain as pressure increased from 0 to 150 MPa, as shown in Fig. 4a–c [87–89]. Microscopic analysis revealed that the increased pressure twists and folds the PEO chains, which hinders the mobility of Li+ ions. Additionally, to evaluate the Li+ ions in solid PEO/LiTFSI polymer electrolytes, a total mean square displacement measurement was conducted as part of the study (Fig. 4d). Additionally, heightened concentrations of the lithium salt LiTFSI intensify the adverse effects of increased pressure on Li+ transport in PEO/LiTFSI solid polymer electrolytes (SPEs) due to the augmented binding energy between Li+ and TFSI− ions.

Nonetheless, the established correlation between pressure, lithium salt concentration, and ionic conductivity furnishes a theoretical foundation for the practical implementation of SPEs in high-pressure settings. Improving the mechanical properties and ionic conductivity of PEO requires addressing its low Young's modulus and increased elastic deformation through the combination of different materials [87–89,92]. Wang et al. [93] improved the mechanical properties of PEO by adding the solid plasticizer succinonitrile (SN) and creating blended solid electrolytes (SEs) with PEO, PVDF, $LiClO_4$, and SN, using a microporous PVDF membrane as a buffer. A sample with 15 % $LiClO_4$ and 15 % PEO showed significantly better tensile strength, achieving a peak stress of 3.37 MPa, which is ten times higher than that of the solid polymer electrolyte without the PVDF film.

2.3.3. *Sulfide solid electrolyte (SSE)*

The Young's modulus of sulfide solid electrolytes (SSEs) is relatively low (18–25 GPa), making them highly compressible at room temperature and desirable for their straightforward synthesis and efficient

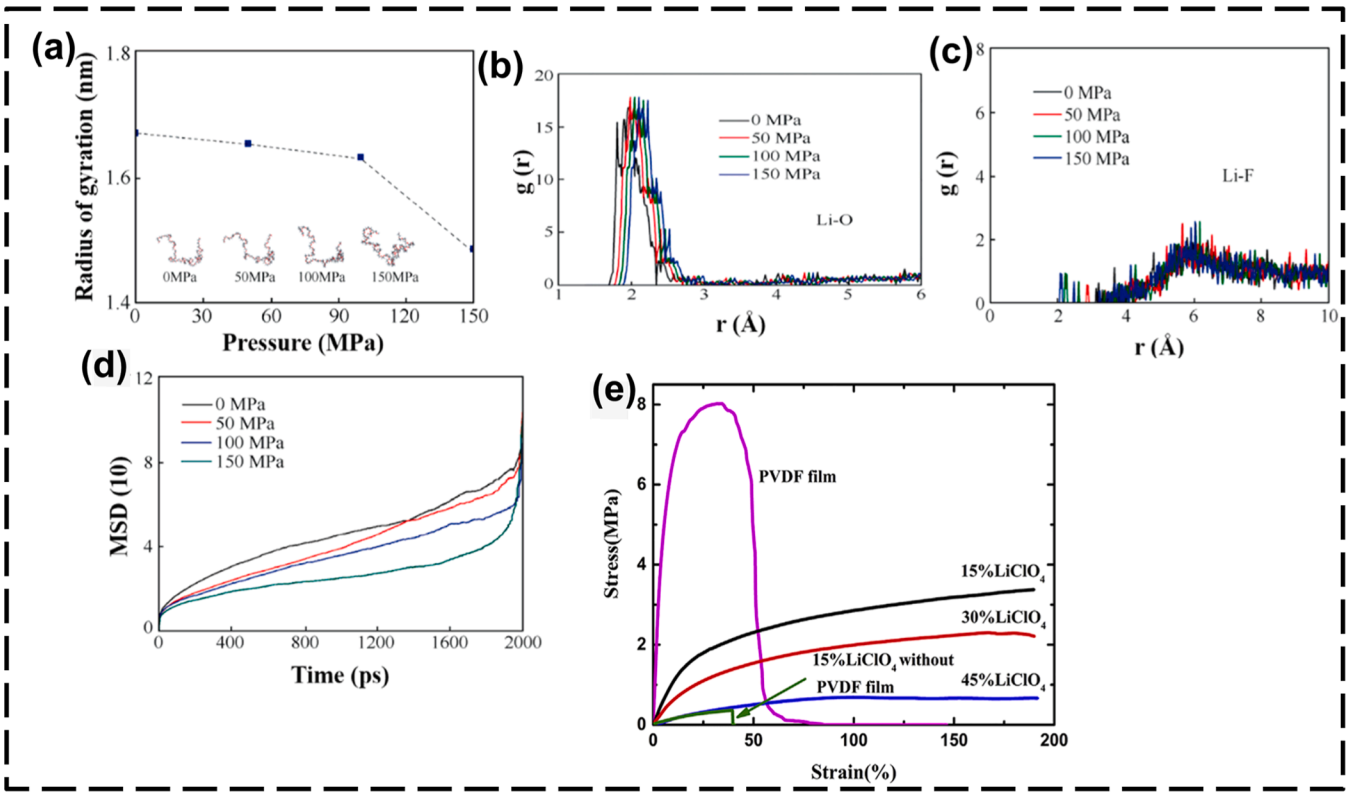

Fig. 4. (a) shows the correlation between the radius of gyration of PEO at 393 K and external pressure. The relation between the radial distribution of PEO polymer chains and the ions in LiTFSI is illustrated as follows: (b) displays the Li–O radial distribution under pressure, and (c) shows the Li–F radial distribution under pressure. The (d) illustrates the connection between the total mean square displacement of Li-ion in the system and the external pressure (Adapted from Chen et al.) [94] and (e) presents the ASPE stress-strain curve for different concentrations of $LiClO_4$ (Adapted from Wang et al.) [95].

lithium-ion conductivity (Fig. 5) [96–99]. SSEs like Li_3PS_4, $Li_{10}GeP_2S_{12}$, $Li_6PS_5Cl_5$, and Li_2S-$P_2S_{52}S_5$ can be produced using a simple cold pressing method without the need for annealing [100,101]. These sulfides are sensitive to atmospheric air and require processing in dry environments.

The response of highly microcrystalline solid electrolyte (μC-SSE) to preparation and stack pressure [105] exhibits significant variation, as presented in Fig. 6. At lower stack pressures, the ionic conductivity of μC-SSE decreases due to inadequate contact between the SSE and the electrode. However, as the stack pressure increases and stabilizes around 50 MPa, both nanocrystal-containing glass-ceramic solid sulfide electrolytes and amorphous sulfide solid electrolytes exhibit enhanced ionic conductivity. This illustrates how the solid electrolyte preparation pressure influences the results.

The implication is that higher preparation pressure causes the sample to become denser, which in turn decreases the number of voids in solid electrolytes and the ion transport barriers at grain boundaries. The correlation between ionic conductivity and pressure has a less apparent association at very high preparation pressures (400–500 MPa), suggesting a limit to bulk densification. In contrast to glass-ceramic sulfide solid electrolytes and amorphous sulfide solid electrolytes, microcrystalline solid electrolytes only reach a plateau in ionic conductivity at a high stack pressure of 250 MPa (Fig. 6a) [103,106]. This is because the particles' surface energy is decreased in these electrolytes due to pressure-induced sintering. The constancy of ionic conductivity is projected to persist amidst escalating stack pressures, provided that the stack pressure remains below the external pressure, due to the irreversibility of pressure-induced sintering (Fig. 6b).

Zeier et al. [104] reported that applying pressure to Li6PS5Br induces significant microstructural changes, primarily the formation of internal strain and dislocations within the material's lattice. These dislocations act as additional pathways that facilitate lithium ion movement, thereby enhancing ionic conductivity (Fig. 6d). The pressure causes broadening of diffraction reflections and a decrease in coherence length, indicating increased strain and defect density without causing phase transitions or amorphization (Fig. 6e-f).

Importantly, even after releasing the pressure (ex-situ), the induced strain and dislocation structures remain, leading to a sustained increase in ionic transport properties. This is evidenced by impedance spectroscopy, which shows higher ionic conductivity and the unchanged activation energy for Li+ hopping in strained samples. In essence, pressure introduces microstructural defects that promote faster ion migration, thereby improving the overall ionic transport in the electrolyte and battery electrodes [104].

Nevertheless, achieving irreversible sintering with preparation pressure alone for highly crystalline microcrystalline solid electrolytes with larger particle sizes is difficult, which leads to a different response to external pressure. Kodama et al. [108] used high-pressure X-ray computed tomography to observe the fragmentation of solid electrolyte particles and pressure-induced sintering at room temperature. The increased pressure led to improved ionic conductivity and facilitated sintering by fragmenting solid electrolyte particles and filling gaps between them (Fig. 7) [96,107]. This was validated by the experimentally obtained impedance measurements, which closely corresponded to numerical simulations based on computed tomography images.

Enhancing the density and reducing porosity of sulfide solid electrolytes optimizes their ionic conductivity, thereby increasing the efficiency of all-solid-state batteries (ASSBs). While a high preparation pressure is effective in boosting SSE ionic conductivity without altering their fundamental properties, it necessitates larger mold requirements, leading to increased ASSB costs. Employing cost-effective methods to manufacture SSEs and enhance their characteristics is a practical strategy, exemplified by Wang et al. [109] who utilized hot pressing to create SSE pellets. By preheating to 150 °C before pressing, degradation of Li10GeP2S12 (LGPS) is prevented, enhancing block density and

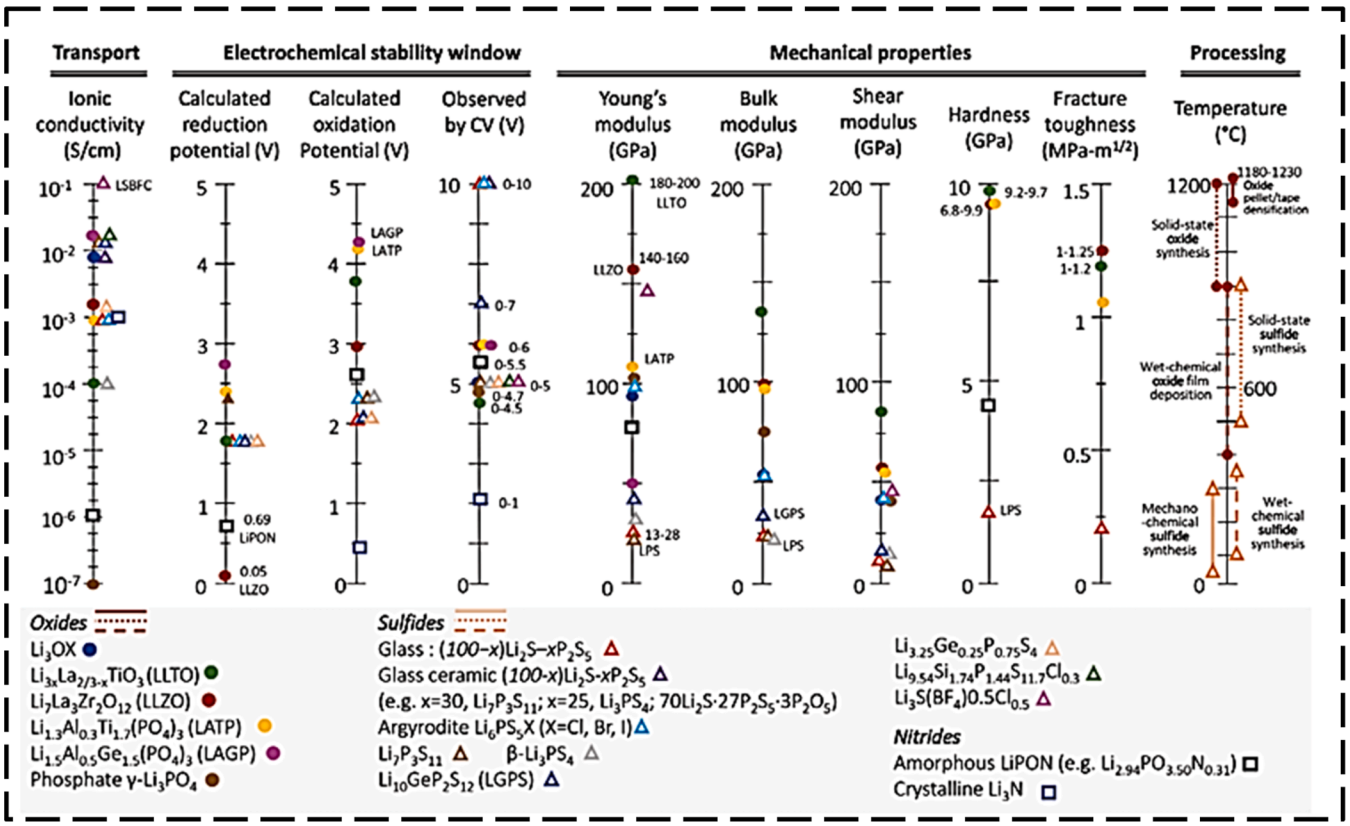

Fig. 5. Provides a summary of the specific characteristics of oxide, sulfide, and nitride solid electrolytes in terms of transport properties, electrochemical characteristics, mechanical stability, and processing temperature (Adapted from Kim et al.) [102].

mechanical strength, thereby further improving ionic conductivity.

Fitzhugh et al. [110] investigated how external pressure impacts both the ionic conductivity and electrochemical stability of solid-state electrolytes. Their study focused on the impact of mechanical constraints on solid-state electrolytes, which create energy barriers to prevent bulk and interfacial disintegration. This research aims to enhance the operational capacity of sulfide-based all-solid-state batteries. However, even at low stack pressures, large stresses may still form at the interface, which may impact the electrochemical deposition of Li metal and heighten its electro-chemo-mechanical degradation over cycling [111]. As such, increased stack pressure does not necessarily translate into improved battery performance.

The external pressure applied during the preparation of sulfide solid electrolytes (SSEs) significantly influences their densification and conductivity, which are critical for the electrochemical performance of all-solid-state batteries (ASSBs) [112–114]

Fig. 7f illustrates the relationship between the conductivity of the Li6PS5Cl electrolyte and the operating stack pressure, utilizing either titanium plungers or carbon powder as current collectors. The study reveals that when titanium is employed, low stack pressures result in high contact impedance and reduced ionic conductivity. Additionally, hysteresis is observed when pressure is reduced from 70 MPa. In contrast, using carbon powder renders ionic conductivity nearly independent of stack pressure, facilitating more reliable measurements. The choice of the current collector and the applied stack pressure account for the inconsistencies observed in the reported conductivity values for the argyrodite LPSCl electrolyte. Fig. 7g illustrates the room-temperature cycling stability of two comparable all-solid-state batteries, featuring a Li–In|LPSCl|LNO-coated NCA structure. The NCA cathode was coated with LNO to prevent reactions with the electrolyte during cycling. One battery was cycled under a consistent stack pressure of 25 MPa, while the other underwent alternating stack pressures ranging from 5 to 125 MPa every five cycles. As expected, the variation in stack pressure had little impact on cycling stability, which can be attributed to the flexible nature of the electrode materials. The experiments demonstrated that a uniform stack pressure of 25 MPa is appropriate for further investigation into the effects of fabrication pressure.

Fig. 7h presents the correlation between the relative density and ionic conductivity of Li6PS5Cl pellets and the fabrication pressure applied to densify them. Increasing the fabrication pressure from 50 to 250 MPa raised the relative density from 68.3 % to 75.4 % and improved the ionic conductivity from 0.99 mS cm-1 to 2.06 mS cm-1. Additional pressure increases yielded diminishing returns, with a conductivity of 2.28 mS cm-1 achieved at 370 MPa. These findings confirm that the relative density and porosity of the solid-state electrolyte significantly impact its ionic conductivity. Nyquist diagrams (Fig. 7i) reveal that at lower fabrication pressures, a semicircle appears at high frequencies, indicating grain boundary impedance. This effect diminishes as fabrication pressure rises and is no longer observed beyond 250 MPa. Oxide solid-state electrolytes exhibit similar behaviour; sintering enhances relative density, reduces grain boundary effects, and increases ionic conductivity. Notably, sulfide electrolytes maintain high ionic conductivity even with porosity levels exceeding 30 %, with LPSCl surpassing 1 mS cm-1. In contrast, oxide electrolytes require over 90 % relative density due to their higher grain boundary impedance, where a mere 10 % increase in porosity can significantly diminish ionic conductivity.

2.3.4. *Halide-based solid electrolytes (HSEs)*

External pressure plays a critical and multifaceted role in optimizing the performance of halide-based solid-state electrolytes (HSEs) within all-solid-state lithium metal batteries (ASSLMBs). A primary challenge in ASSLMBs is achieving intimate ''solid-solid'' contact between the electrodes and the solid electrolyte, which is crucial for efficient interfacial charge transfer and minimizing cell resistance [115]. Unlike liquid

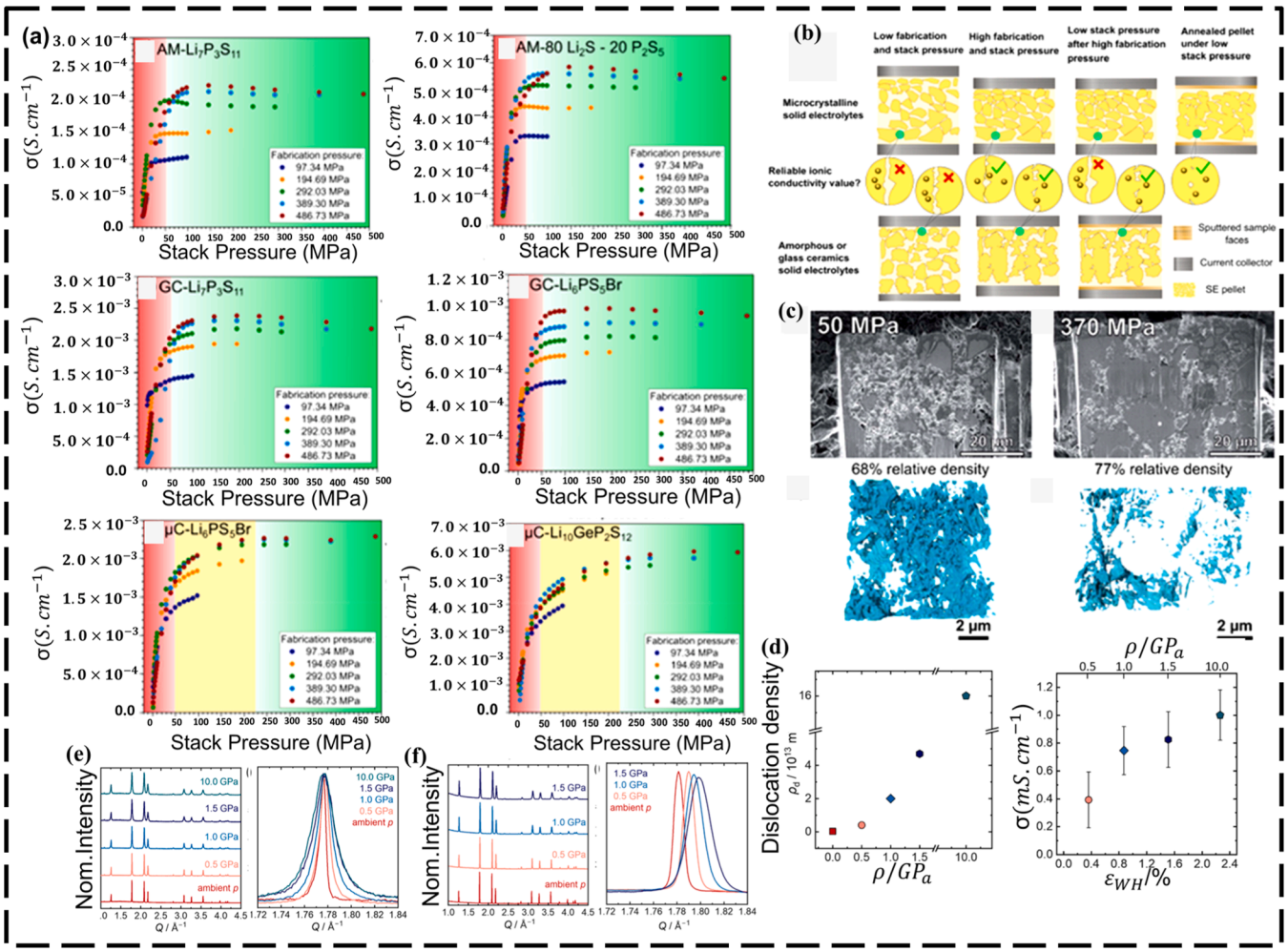

Fig. 6. (a) and (b) illustrate how the architectures of microcrystalline and amorphous solid electrolytes vary under different pressure settings, and how stack pressure influences ionic conductivity at various fabrication pressures (Adapted from Doux et al.) [38]. (c) SEM images of Li_6PS_5Cl electrolyte pellets produced at pressures of 50 MPa and 370 MPa are presented, and the respective relative densities are determined through physical examinations. The emphasis is placed on the FIB cross-sections. The Focused Ion Beam (FIB) reconstructions of the 50 MPa pellet and 370 MPa pellet reveal porosity highlighted in blue (Adapted from Cronau et al.) [103]. Strain as a function of structural dislocations. (d) Dislocation densities derived from Williamson-Hall analysis and effect on ionic conductivity. (e) Ex-situ diffraction exhibits a widening of reflections with increasing pressure. (f) In-situ diffraction showed the rise in strain and the corresponding Q-shift as a function of increasing pressure (Adapted from Zeier et al.) [104].

electrolytes, solid electrolytes often suffer from inherent rigidity, leading to undesirable pores and cracks that reduce contact area and negatively impact performance [116]. Uniform external pressure directly addresses this by deforming solid components, ensuring closer contact at interfaces, and significantly reducing interfacial resistance and porosity, thereby boosting ion and electron transfer efficiency [115]. Furthermore, external pressure is instrumental in suppressing lithium dendrite growth, a major safety and longevity concern. By evenly distributing pressure, it prevents localized stress concentration and the preferential growth of dendrites, directly counteracting the formation of voids at the lithium-electrolyte interface that precede dendrite formation [117]. For instance, increasing external pressure on a sulfide electrolyte (Li6PS5Cl) from 3 MPa to 7 MPa significantly increased the critical current density for dendrite formation from 0.2 to 1mAcm^{-1}, demonstrating pressure's ability to enhance power density [117]. More advanced mechanical constriction techniques, applying 100–250 MPa, can induce materials-level mechanical constriction on order on the order of GPa, controlling localized current densities and physical growth pathways [117].

Beyond interfacial effects, external pressure can profoundly influence the intrinsic bulk properties and phase stability of halide solid electrolytes. The impact on ionic conductivity can be investigated through activation volumes, which reflect atomic volume changes during ion jumps and are derived from pressure-dependent conductivity measurements [118,119]. For example, in lithium argyrodite such as Li_6PS_5Br, activation volumes for Li+ migration were observed to increase with greater Br^-/S^{2-} site disorder and more diffuse Li-ion distributions under pressure, indicating a direct influence on Li-ion diffusion pathway [118]. Moreover, high external pressure can induce structural phase transitions in halide materials, leading to new polymorphs with altered properties. A notable instance is the high-pressure synthesis of $\gamma - Li_3ScCl_6$ from its ambient pressure $\alpha -$ phase at ~3.7 GPa [120]. This transition involves a conversion from cubic close-packing (CCP) to hexagonal close-packing (HCP) of anion, influenced by the cation/anion radius ratio and differential compressibility [120]. Crucially, electrochemical tests of this high-pressure $\gamma -$ Li3ScCl6 polymorph demonstrated improved electrochemical reduction stability, highlighting pressure as a powerful tool for materials synthesis and property tuning beyond compositional engineering [120].

Despite these benefits, the chemical stability of halide solid electrolytes, particularly with the Li metal anode, remains a distinct challenge that external pressure does not directly resolve. Many halide solid electrolytes, such as Li3ClBr, are susceptible to spontaneous decomposition reactions at low operation potentials, forming resistive

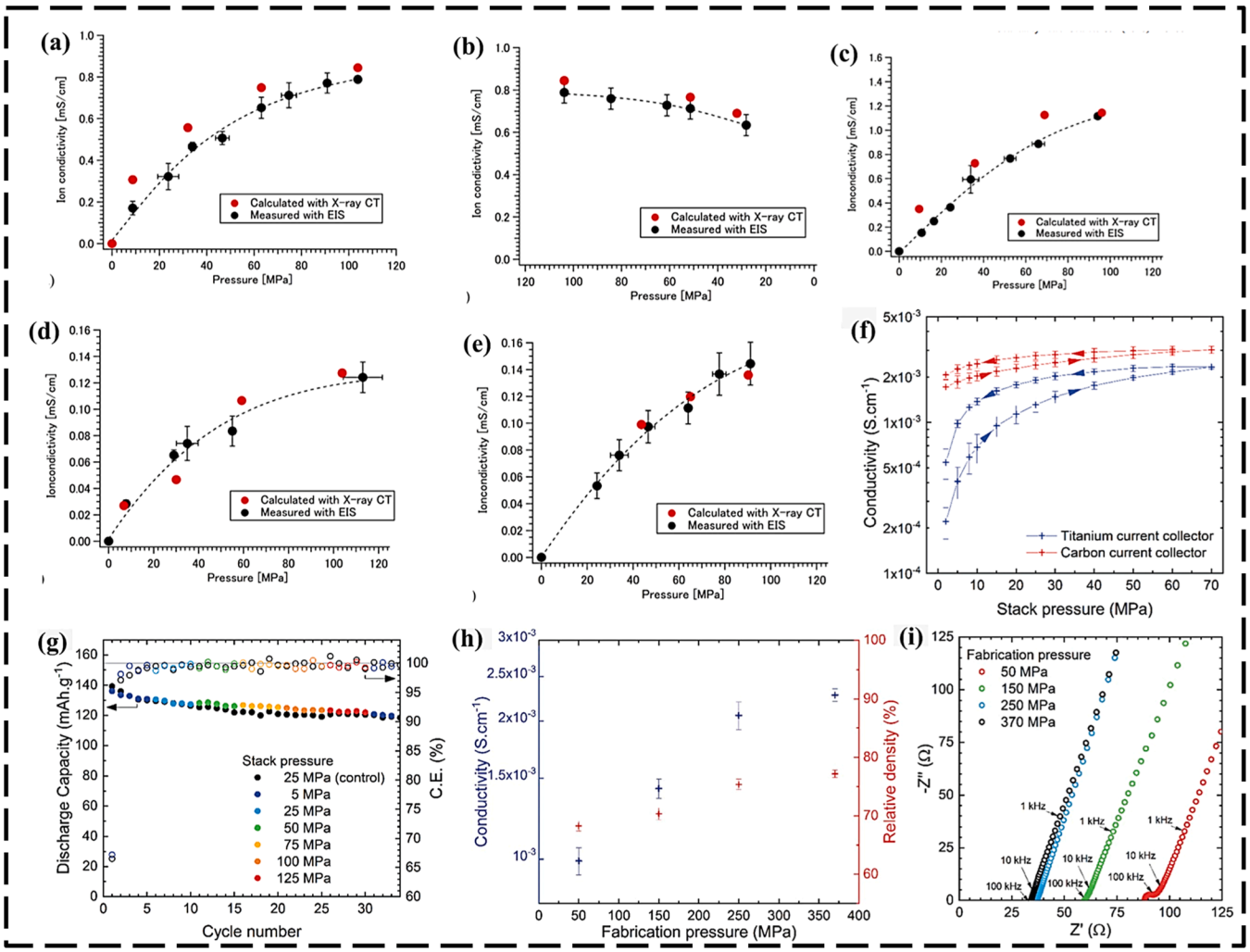

Fig. 7. Illustrates the variation in ionic conductivity with applied pressure: (a) initially, it increases from 0 MPa, and (b) subsequently decreases from 103.0 MPa. The ionic conductivity of different solid electrolytes under applied pressure increased from 0 MPa. (c) Li_6PS_5Cl, (d) LPS glass ceramic, (e) LPS glass (Adapted from Kodama et al.) [107]. (f) Shows the conductivity of Li_6PS_5Cl as it varies with the stack pressure when using titanium plungers or compressed carbon powder as electrodes. The stack pressure was raised to 70 MPa and then lowered to 5 MPa (as indicated by the arrows). The error bars illustrate the standard deviation calculated from 4 samples. (g) shows the impact of stack pressure on the cycling stability (at room temperature) of LiIn|LPSCl|NCA solid-state batteries. Every electrolyte and battery was fabricated under a fabrication pressure of 370 MPa. (h) displays the conductivity and relative density of the Li_6PS_5Cl electrolyte against fabrication pressure, and (i) shows the Nyquist plots of the electrochemical impedance spectra at those pressures. All measurements were taken at a stack pressure of 25 MPa, with error bars representing the standard deviation of 4 samples (Adapted from Doux et al.) [38].

interphases such as LiCl, LiBr, and metallic Y, which increase cell resistance and lead to premature failure [121]. Ab initio molecular dynamics simulations confirm significant instability at the Li/Li3YCl5Br interface, with chemical reactions propagating into the bulk electrolyte [121]. While external pressure is vital for improving physical contact and mechanical stability, research does not explicitly detail its direct influence on these chemical degradation reactions [6]. Therefore, complementary strategies such as fluorine substitution (e.g., in $Li_2ZrCl_{6-x}F_x$) or protective coatings (e.g., Li_3N, LiCl, Li_3P, or self-limiting layers of InF_3/Li_2ZrCl_6) are often employed to suppress these chemical side reactions and mitigate dendrite growth [26,121,122]. This highlights the need for an optimal pressure range, as both insufficient and excessive pressures are detrimental. While inadequate pressure leads to poor contact, excessive pressure can damage electrode porous structures, hinder lithium-ion transport, and potentially cause short circuits or plastic deformation and creep in lithium metal anodes [27,28]. The industry consensus targets operational pressures below 10 MPa, ideally below 1 MPa, a significant gap from the >50 MPa often used in laboratory testing [25]. However, advancements are being made with halide-based $Li_3YBr_2Cl_4$ demonstrating successful operation at pressures as low as 0.1 MPa against a Li-In anode with minimal capacity loss, underscoring the importance of mechanical properties such as hardness over just ionic conductivity for low-pressure performance.

Recent studies indicate that halide-based solid electrolytes exhibit significantly higher fracture toughness and ductility compared to traditional oxide and sulfide electrolytes [123,124]. This improved mechanical performance allows these electrolytes to withstand the mechanical stresses encountered during battery assembly and operation, thereby reducing the risk of failure. The enhanced ductility of halide-based solid electrolytes can be attributed to their unique crystal structures and bonding characteristics [34,123–126]. Additionally, certain processes involving mobile ions facilitate plastic deformation, while the halide lattice demonstrates a remarkable ability to accommodate strain without fracturing. Consequently, the ductile nature of these electrolytes fosters better interfacial contact with electrode materials, which in turn minimizes interfacial resistance and promotes more efficient ion transport.

2.3.5. Ductile and viscoelastic Ga- and Al-based mixed-halide solid electrolytes in external pressure reduction

Gallium (Ga) and aluminum (Al)-based solid electrolytes exhibit intrinsic ductile and viscoelastic mechanical properties, offering a significant advancement in reducing the fabrication and operational pressures associated with all-solid-state batteries (ASSBs). Traditional rigid ceramic oxide electrolytes required high-temperature sintering, typically ranging from 800 °C to 1200 °C, to achieve requisite densification and particle interaction [127,128]. This energy-intensive process often proves incompatible with thermally sensitive electrode materials, thus constituting a substantial manufacturing bottleneck. In contrast, ductile inorganic solid electrolytes exhibit superior ion transport capabilities post-cold pressing, marking a pivotal transition from thermally driven densification to mechanically driven processing or low-temperature phase transitions, which are fundamentally more energy-efficient and scalable for large-scale production [129].

For instance, aluminum-based viscoelastic inorganic glasses (VIGLAS), such as $LiAlCl_{4-2x}O_x$ (LACO) and $NaAlCl_{4-2x}O_x$ (NACO) mixed halides, demonstrate their ability to enable pressure-less solid-state batteries (< 0.1 MPa) [129]. This is due to their polymer-like viscoelasticity, which allows for deformation without cracking. This "clay--like" physical property allows for excellent interfacial contact even under low-pressure or pressure-less conditions, mimicking the infiltration capabilities of liquid electrolytes. This process ensures complete ionic contact without requiring high external pressures during the assembly process. This capability, which mimics liquid infiltration, represents a crucial innovation that enhances the interfacial area for ion transport while maintaining the inherent safety and stability of solid electrolytes. Furthermore, Ga-based mixed-halide solid electrolytes have demonstrated high ionic conductivity and physical flexibility, allowing ASSBs to function without significant stack pressure to maintain conformal cathode-electrolyte interfaces over extended cycling periods [130–132].

During fabrication, the deformability of these ductile electrolytes significantly simplifies the manufacturing process. Traditional brittle solid electrolytes often require high-pressure pressing or hot-pressing techniques to achieve good interfacial contact and minimize voids, which can be energy-intensive and limit scalability. In contrast, the pliable nature of Ga- and Al-based viscoelastic electrolytes allows for easier processing, such as rolling to produce thin films, similar to polymer electrolytes. This inherent flexibility reduces the need for extreme pressures during cell assembly, thereby lowering manufacturing costs and complexity. The ability of these materials to fill porous regions of electrodes, as observed with Ga and Cl signals in energy-dispersive spectroscopy (EDS) mapping, further confirms their capacity to achieve intimate contact without high external forces [130,131].

In terms of operation, the ductile nature of these electrolytes is crucial for maintaining mechanical stability and long-term performance. All-solid-state batteries experience significant volume changes in their electrodes during charge and discharge cycles. Brittle solid electrolytes are prone to fracturing and delamination under these stresses, leading to loss of contact, increased interfacial resistance, and ultimately, battery failure [129,133]. However, ductile viscoelastic electrolytes can accommodate these dimensional changes by deforming rather than cracking. This intrinsic stress-relief mechanism prevents the formation of voids and maintains a stable interface, thereby reducing the need for high applied stack pressure during battery operation. This ability to withstand mechanical deformation ensures consistent ionic transport and prolonged cycle life, making Ga- and Al-based viscoelastic solid electrolytes highly promising for the development of robust and high-performing ASSBs [129,133].

Moreover, the viscoelastic properties of Ga- and Al-based electrolytes are particularly relevant for high-capacity electrode materials, such as silicon anodes, which are subject to substantial volumetric changes (up to 400 %). Rigid inorganic electrolytes frequently fail to accommodate these volumetric fluctuations, resulting in contact loss, void formation, impeded lithium-ion transport, and potential electrode disintegration [129]. In contrast, Al-based VIGLAS electrolytes, characterized by their polymer-like viscoelasticity, low elastic moduli (e.g., LACO: 1.5 GPa, NACO: 3.2 GPa at 30 °C), and glass transition temperatures below room temperature, exhibit the capacity for deformation and superplasticity, enabling viscous flow under stress (Table 2). This inherent deformability ensures sustained interfacial contact under low-pressure operating conditions, typically below 0.1 MPa, effectively buffering stresses associated with electrode expansion and contraction [129,132–134].

Furthermore, the integration of elastic solid electrolytes engineered with soft-rigid dual monomer copolymers exemplifies these advantages, demonstrating exceptional stretchability (1160 % break elongation), high fracture strength (1.7 MPa), and notable shape memory characteristics [135]. These materials can encapsulate active material particles and facilitate rapid ion transport while dissipating considerable mechanical energy through reversible fracture and restoration of non-covalent bonds during cycling. Consequently, this mechanism helps prevent electrode disintegration and enables stable operation under minimal built-in cell pressure (e.g., 52 kPa for pouch cells) [129,131,133]. Finite element simulations further corroborate that such elastic electrolytes yield lower and more uniformly distributed stress within

Table 2
Summarizes the critical mechanical properties of viscoelastic solid electrolytes and their impact on the fabrication and operational pressures of all-solid-state batteries [129,131–135].

Property	Metric/Value	Impact on Fabrication Pressure	Impact on Operation Pressure
Ductility/ Viscoelasticity	Polymer-like behavior, Superplasticity, Viscous flow	Enables cold pressing, melt infiltration, and co-rolling, replacing high-temp sintering	Accommodates electrode volume changes, maintains intimate contact, buffers stress, enables pressure-less operation (<0.1 MPa)
Low Elastic/Shear Modulus	LACO: 1.5 GPa, NACO: 3.2 GPa (at 30 °C); Clay-like: <1 MPa	Facilitates contact with porous electrodes without high external force during assembly	Reduces stress concentration at interfaces, prevents crack propagation, enables stable cycling under low or built-in pressure
Low Melting/ Glass Transition Temperature	VIGLAS: <160 °C; Ga-based: < −50 °C	Allows efficient melt infiltration into electrode structures, akin to liquid electrolytes, ensuring complete ionic contact	Enables "superplasticity" at operating temperatures, allowing the electrolyte to deform and self-heal, maintaining contact during volume changes
High Stretchability /Deformability	Elastic electrolyte: 1160 % break elongation, >77.8 % strain	Facilitates flexible processing methods like rolling for thin film production	Buffers large volumetric changes of electrodes (e.g., Si anodes), preventing contact loss and electrode disintegration
Energy Dissipation Capability	Elastic electrolyte: 1.4 MJ m^{-3} with 82 % loss coefficient (at 400 % tensile strain)	N/A	Actively absorbs and neutralizes mechanical energy from electrode expansion/ contraction, preventing destructive stress accumulation

anodes compared to rigid solid-state electrolytes, underscoring their superior stress management capabilities and enhancing the overall performance and reliability of ASSBs [129,133].

2.4. Influence of external pressure on electrode properties

2.4.1. Lithium metal anode

Utilizing lithium (Li) metal in Li metal batteries is driven by its low reduction potential (−3.04 V vs. standard hydrogen electrode) and the substantial theoretical capacity of lithium, crucial for high-energy-density storage systems [136]. Lithium metal exhibits notable ductility, allowing it to experience deformation through elastic, plastic, and creep mechanisms [137]. Irreversible plastic deformation, resulting from dislocation slip exceeding the critical stress (yield strength), leads to strain hardening. Masias et al. [138] investigated the elastic properties of Li through acoustic methods, specifically pulse-echo techniques (Fig. 8a-c). The materials' respective Young's modulus, shear modulus, and Poisson's ratios were found to be 7.82 GPa, 2.83 GPa, and 0.381.

The stress-strain response of lithium metal under tension and compression was studied in an inert atmosphere, with yield strengths ranging from 0.73 to 0.81 MPa (Fig. 8a-c). During tension and compression, there were apparent variations in the deformation properties. Dislocation increasing proved to be the dominant ingredient in power-law creep in tension, as indicated by the stress exponent of 6.56 [78]. In situ SEM revealed that nanoscale lithium has strengths of 105 MPa at room temperature and 35 MPa at 90 °C, while sub-micrometer lithium dendrites can achieve compression yield strengths of up to 250 MPa, greatly exceeding the strength of bulk lithium [139].

In line with the trend of increasing strength in smaller entities, these groundbreaking discoveries underscore the significant influence of size on the mechanical properties of lithium. When stack pressure is applied during cell operation, the contact resistance between the lithium anode and the electrolyte is decreased. Conversely, if an excessive amount of pressure is applied, short circuits may form either right away or soon after deposition. This issue is linked to the fact that lithium metal can leak through the cracks in the electrolyte due to its inherent ductility, or poor yield strength [72,140]. Although the metal is subjected to forces lower than its yield strength, external pressure affects the creep behavior of lithium metal more than internal stress. Grain boundaries, voids, and fractures are considered defects in solid electrolytes.

In the study, stack pressures of 5, 25, and 75 MPa were applied to the solid sulfide electrolyte in three lithium batteries (Fig. 8d). At 5 MPa, where the pressure is insufficient for lithium penetration into the pores, electroplating occurs solely on the particle surfaces, making it the ideal pressure for the prolonged cycling of lithium batteries (Fig. 8d(iv)) [105]. At 25 MPa (Fig. 8d(v)), lithium successfully penetrated the pores without triggering a short circuit, and at 75 MPa (Fig. 8d(vi)), lithium infiltrated through the interconnected pores, creating electron pathways. Throughout the charge and discharge cycles, the additional pressure from the plated lithium expanded the dendrites within the

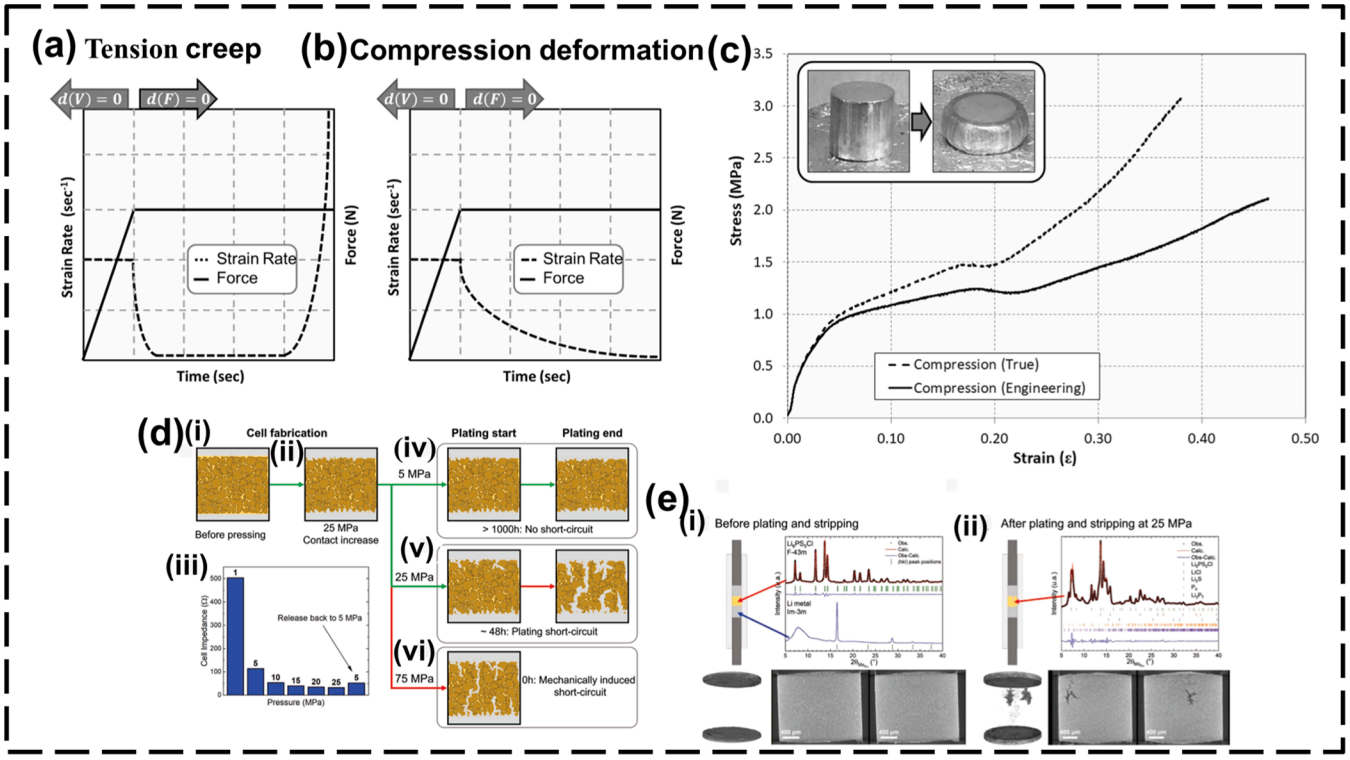

Fig. 8. (a, b) shows the response of lithium (12.3 mm height, 12.7 mm diameter) to compressive pressure and deformation at ambient temperature. (c) illustrates the compressive stress-strain characteristics of lithium at room temperature, with a sample size of 12.3 mm in height and 12.7 mm in diameter (Adapted from Masias et al.) [142]. (d) A schematic illustrating how the short-circuit behavior of lithium metal solid-state batteries is influenced by stack pressure. (i) Insufficient contact was made between the electrolyte and lithium metal during cell assembly, which occurred before the lithium was pressed onto the electrolyte pellet. (ii) Although the pressure was lowered to 5 MPa, the application of 25 MPa pressure improved the electrolyte's wetting, which resulted in (iii) a significant reduction in the cell impedance. (iv) Electroplating and removal occurred at a stack pressure of 5 MPa, preventing lithium from penetrating the solid-state electrolyte (SSE) pellet and allowing the cell to function for over 1000 h. (v) After 48 h, dendrites formed, and the cell short-circuited due to lithium's slow migration between the SSE grains below 25 MPa. (vi) A mechanical short circuit was produced by dendrites that were created by lithium seeping into the electrolyte because of excessive stack pressure. (e) presents the configuration for X-ray tomography and X-ray diffraction of a Li | Li_6PS_5Cl | Li symmetric cell cycled at a stack pressure of 25 MPa. (i) Only Li_6PS_5Cl is observed in the electrolyte before plating and stripping, with lithium metal on both sides and no lithium detected in the electrolyte. (ii) shows the state after shorting, where new phases such as Li_2S, LiCl, P_4, and Li_3P_7 are identified in the electrolyte, indicating the formation of a solid electrolyte interphase (SEI) from lithium's interaction with Li_6PS_5Cl. Additionally, the tomography images indicate a considerable presence of low-density dendrites in the electrolyte (Adapted from Doux et al.) [52].

particles, eventually leading to a short circuit. However, cold pressing the sulfide solid electrolyte block at 370 MPa is not expected to affect the short-circuit mechanism. Although creep may be more prevalent, the formation of a dense interfacial layer prevents short circuits in sodium metal electrodes, setting them apart from lithium metal electrodes [141].

2.4.2. Alloy and nonlithium metal anodes

The reversibility of lithium's interactions with different metals such as Mg, Al, Si, and Sn has attracted much interest for their potential application in lithium batteries [63,64,143–147]. This is because lithium can form intermetallic compounds with these metals. Nevertheless, the substantial volume change inherent in the alloying process between lithium and metals significantly impacts the stability of material cycling, often causing cracking, detachment of the active material, and rapid deterioration in battery capacity [148]. Recent research has emphasized the importance of pressure as a critical factor in the performance of alloy anode materials. Silicon, a promising material for future lithium-ion batteries, offers advantages such as abundance and high specific capacity [148,149]. Silicon can expand by about 300 %, allowing it to accommodate 3.75 mol of lithium per mole and form $Li_{15}Si_4$ at room temperature. However, this expansion-contraction cycle makes silicon particles susceptible to cracking and fragmentation, leading to reduced efficiency [150].

Han et al. [151] studied stress dynamics in all-solid-state batteries with composite anodes and found that reducing particle size alleviates stress during charge and discharge cycles. Piper et al. [152] also showed that higher external pressures (3, 150, 230 MPa) on silicon anodes reduce discharge capacity due to restricted volume expansion. However, they also decrease particle cracking, thereby improving cycle life. Cui et al. [153] determined that maintaining a pressure of around 0.6 MPa lowers interfacial resistance and enhances performance, but pressures above 1.0 MPa can lead to overcharging and short circuits. An optimal pressure of 0.6 MPa prevents electrode cracking and promotes lithium deposition, though excessive pressure can cause uneven deposition and fractures in alloy-negative electrodes due to their fragility (Fig. 9).

Prior research has explored various approaches, including size reduction and structural design, to counteract the negative impacts of undesired volume expansion. Wang et al. [154] introduced a Si structure resistant to pressure by encapsulating secondary microparticles with a dense Si shell, each comprising multiple Si nanoparticles. To maintain structural integrity after calendaring, the design incorporated a silicon skin layer for increased mechanical stability and a porous interior structure for volume expansion. This allows for increased capacity and initial Coulombic performance under pressures above 100 MPa. However, challenges with mechanical stability and volumetric energy density persist during electrode calendaring. In traditional liquid electrolyte lithium-ion batteries (LIBs), silicon anodes experience significant volume expansion (300 %) during lithiation, but a critical particle size of about 150 nm helps prevent breakage or pulverization. Nevertheless, during lithiation, silicon particles bigger than 150 nm tend to fracture and break, a characteristic that has been verified in real-world battery applications [155,156].

All-solid-state batteries (ASSBs) have shown effective performance with micron-sized silicon anodes. A study by Tan et al. [157] demonstrated that silicon anodes sized 2 to 5 μm could successfully cycle for 500 cycles, achieving an area capacity exceeding 5 $mAhcm^{-2}$ in a Si/LSPSCl/NMC ASSB. This raises the question of whether the size effect seen in liquid electrolyte lithium-ion batteries (LIBs) is less significant in ASSBs. Tan et al. discovered that micro-sized silicon is effective in ASSBs, but additional research on anode type, structure, and doping is necessary. If confirmed, this could allow for using high-energy density alloy anodes such as aluminum and tin in ASSBs [112].

Alloy anodes that form lithium-based compounds tend to undergo significant volume changes, which can weaken their structure and cause damage over time [158]. Higher pressure is usually required to maintain a good connection between the anode and solid electrolytes (SSEs). For example, silicon anodes have a very high capacity of 3579 mAh/g and can accommodate 3.75 mol of lithium per mole of silicon. However, they expand by about 300 % during charging, leading to cracking and breakdown of the material [159–164].

Studies using tiny lithium-silicon (μ-LixSi) electrodes have shown that during cycling, the internal pressure fluctuates. For instance, a battery with a μ-Li_xSi anode and a stable electrode ($Li_4Ti_5O_{12}$) experienced approximately 0.7 MPa pressure changes during cycling, with pressure decreasing during discharging and increasing when charging. These variations depend on the lithium content in the material, but other factors such as gaps between electrodes and elastic deformation can also influence the stress. Thicker electrolytes help reduce strain, and initial stress hysteresis (lag) may occur but generally stabilizes over time [1]

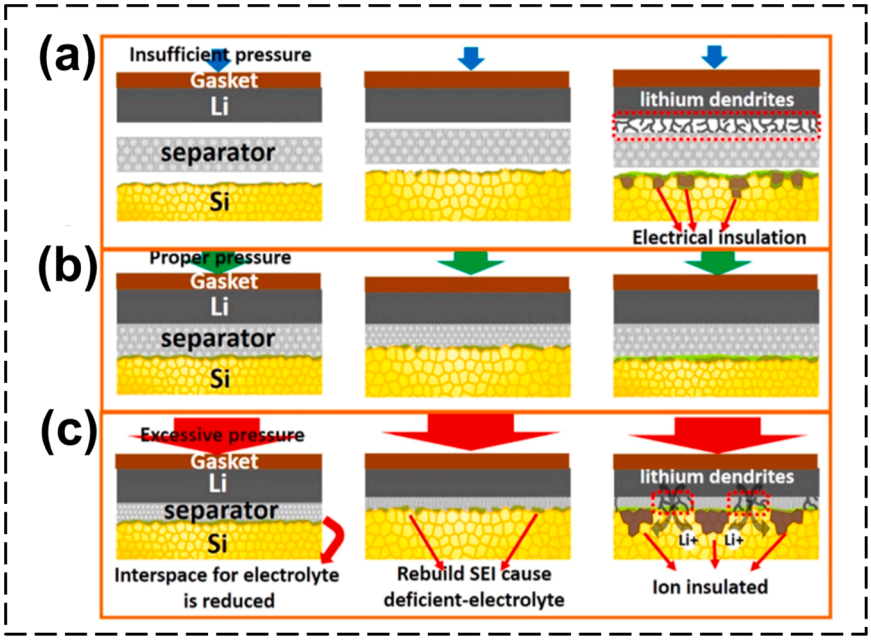

Fig. 9. Illustration of Si anodes at three different pressure conditions: (a) insufficient, (b) suitable, and (c) excessive (Adapted from Cu et al.) [171].

[160,165–169].

Likewise, the indium (In) anode also expands when forming lithium alloys, causing stress and deformation. Imaging techniques revealed that the battery bent considerably during charging at the interface between the electrode and electrolyte. Increasing pressure during charging densifies the electrolyte but also causes cracks at the edges, which could lead to failure if external pressure isn't maintained. During cycling, internal pressure fluctuated, reaching around 2.25 MPa after several cycles [38,52].

Conversely, metals forming solid solutions with lithium, such as Li-Mg and Li-Ag alloys, are more stable and better suited for low-pressure batteries. For example, using Li-Mg alloys allowed batteries to operate at higher speeds with less pressure. A porous structure formed after lithium stripping, helping to sustain good contact and prevent voids [170]. Li-Ag alloys also demonstrate stability over many cycles. The addition of reduced graphene oxide (rGO) to produce rGO/Li-Ag composites helps maintain a consistent connection between the electrolyte and anode, even under very low pressures of about 4.9 MPa [163], enhancing the durability and reliability of these batteries during operation.

2.4.3. Transition metal oxide layered cathode

LiNixMnyCo1-x-yO_2 (NMC) is one of the most widely used and highly promising cathode materials for electric vehicles because of its high specific capacity and operational voltage. However, NMC has a Young's modulus of approximately 200 GPa, which makes it resistant to deformation but susceptible to fracture under certain pressures (Fig. 10a) [172–174]. There are two crystalline forms of NMC: polycrystalline (PC-NMC) and single crystal (SC-NMC). Whereas single-crystal NMC is made up of homogeneous primary particles that are a few microns in size, polycrystalline NMC is created by several particle aggregations, each of which is about 100 nm in size. NMC and sulfide solid electrolytes (SE) are frequently used to generate composite electrodes used in the fabrication of solid-state batteries. Li^+ transport mainly occurs within these electrodes through the "solid-solid" contact. Initially, the particles remain disconnected, resulting in inadequate pathways for lithium ion and electron transport. The introduction of sulfide composite cathodes can enhance battery performance by minimizing the interfacial resistance between particles through the application of significant external pressure. Single-crystal NMC demonstrated superior structural integrity compared to polycrystalline NMC before and after cycling.

Liu et al. [175] found that compressing cathode powders into pellets at pressures of 510 and 1020 MPa indicated that the single-crystal type of NMC is ideal for use in all-solid-state batteries (ASSBs). While SP-NMC811 maintained its structure at 1020 MPa, both LP-NMC811 and SP-NMC811, which are polycrystalline types, experienced significant deformation and cracking at 510 MPa (Fig. 10b). Doerrer et al. [176] found that smaller LPSCl particles exhibited lower ionic conductivity compared to larger ones, emphasizing the importance of the size ratio between solid and active electrolyte powders for effective consolidation and mixing (Fig. 10c, d). Structurally sound composite cathodes were obtained by pressing particles at 500 MPa; however, PC-NMC broke at grain boundaries and only recovered at 50 MPa of pressure. The research discovered that SC-NMC/LPSCl cathodes that were cold-pressed exhibited a discharge capacity of 205 $mAh{\cdot}g^{-1}$ and a Coulombic efficiency of over 85 %. However, because of lithium metal creep, higher stack pressures led to battery short circuits. Although pulverization of NMC, problems with solid-state electrolytes, and electrode cracking can result from pre-compressing positive electrode pellets, they can also improve performance and densification [172,177].

Bruce et al. [178] introduced an approach to maintain high capacity under low external pressure and high rates. These findings highlight the close relationship between cathode capacity and ion transport through the solid electrolyte within the composite. Achieving highly conductive solid electrolytes (SEs) is essential for realizing maximum capacity under realistic current densities and lower stack pressures, such as below 2 MPa for specific applications. The use of Li_3InCl_6 as a solid electrolyte with high ionic conductivity is recommended. Capacity fading is the result of cathode material volumetric changes induced by electrochemical cycling. To improve binding within the active composite material and minimize these volumetric changes, a novel approach

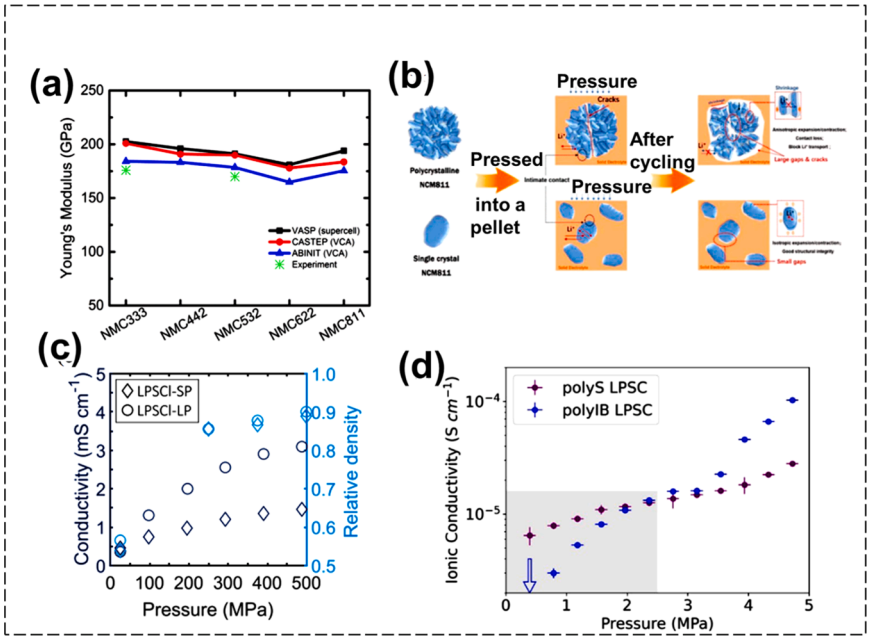

Fig. 10. (a) For five NMC compositions, a comparison of Young's modulus values obtained from the virtual crystal simulation model (CASTEP and ABINIT) and the supercell model (VASP) is shown together with experimental data (Adapted from Sun et al.) [172] (b) During the electrode pressing procedure and electrochemical cycling, the single-crystal and polycrystalline NCM811 composite cathode's cross-section showed morphological alterations (Adapted from Liu et al.) [155] (c) For two distinct solid electrolyte composites, the relationship between ionic conductivity and applied stack pressure is displayed (Adapted from Martin et al.) [92] (d) A diagram showing how LPSCl's ionic conductivity changes in response to various pressure settings (Adapted from Doerrer et al.) [176].

incorporating a buffer layer can be adopted [17,179].

2.4.4. Interfacial delamination in cathode composites

The interfacial contact between the cathode active material and solid electrolyte is a critical bottleneck in all-solid-state batteries (ASSBs), distinguishing them from liquid-electrolyte batteries. The performance limitations of ASSBs are increasingly attributed to interfacial issues, particularly interfacial delamination, which reduces cycle life and battery efficiency by decreasing the active interface area and increasing internal resistance [180]. To enhance the durability and performance of ASSBs, it is essential to understand the mechanisms driving delamination, especially the electrochemical reactions and electrochemo-mechanical interactions involved. Electrochemical reactions at the interface between cathode active materials and solid electrolytes can lead to the formation of resistive layers, such as the cathode electrolyte interphase (CEI), which compromises the integrity of the interface. This effect is particularly pronounced with high-voltage cathodes, such as $LiNi_{0.8}Co_{0.15}Al_{0.05}O_2$ (NCA), in contact with sulfide solid electrolytes, like Li_6PS_5Cl (LPSCl). As LPSCl may decompose, hindering ion transport and promoting mechanical failure in the battery [129,133].

The formation of these highly resistive interphases significantly increases the interfacial resistance, impeding both Li-ion diffusion and charge transfer kinetics at the interface. This increase in resistance translates directly into increased cell polarization, reduced initial discharge capacity, and poor capacity retention over cycling [181]. For instance, solid-state batteries utilizing uncoated NCA with LPSCl demonstrated a substantial increase in interfacial resistance after cycling, reaching approximately 4813 Ω after 100 cycles, in stark contrast to 267 Ω for cells with coated NCA. This resistive layer directly correlated with significantly lower discharge capacity and retention [182–184]. Beyond electronic and ionic impedance, the formation of these interphases contributes to the physical separation of components due to accompanying morphological changes. Initially, compact cathode particles can fracture and disperse into the solid electrolyte matrix, leading to significant contact loss and a reduction in accessible capacity.

Solid electrolytes, while generally more stable than their liquid counterparts, can still exhibit electrochemical instability, particularly at high cathode operating voltages. For example, the garnet-type $Li_7La_3Zr_2O_{12}$ (LLZO), a promising SSE, is susceptible to oxidation at high voltages (e.g., 4.3 V vs Li/Li+). This inherent instability can lead to the decomposition of the solid electrolyte itself and the formation of undesirable secondary phases [185].

Research on NMC622|LLZO interfaces that have been annealed at high temperatures (for instance, 700 °C) has uncovered the creation of resistive decomposition byproducts, including Li_2CO_3, $La_2Zr_2O_7$, and La (Ni, Co)O_3. Performing electrochemical cycling at higher temperatures (like 80 °C) can also lead to the reduction of cathode materials, such as Ni in NMC622, resulting in the emergence of reduced phases (Ni^{2+}, Co^{2+}). The presence of these decomposition byproducts and reduced phases collectively raises interfacial resistance and polarization, causing a noticeable reduction in battery capacity. It is important to note that electrochemical degradation at the interface, such as the reduction of Ni in NMC622, was not detected during cycling at room temperature, indicating that these reactions can be kinetically restrained by operating at lower temperatures or by using a lower charge voltage limit [182–184].

The heterogeneity introduced by the formation of resistive interphases and morphological changes, such as particle fracturing, can lead to a non-uniform current distribution across the interface, creating localized "current hotspots". These hotspots, when combined with kinetic limitations inherent in the cathode active material, can induce local overcharging [186]. This localized overcharging, in turn, generates high-stress states within the particles, ultimately contributing to their fracturing and further void formation. This fracturing directly contributes to delamination by weakening the physical integrity of the cathode composite [182]. This sequence illustrates a critical feedback loop, where electrochemical non-uniformity initiates mechanical damage, which then further impairs electrochemical performance, creating a self-accelerating degradation cycle (Table 3).

2.4.4.1. Effects of volume changes of cathode active materials. During charge (delithiation) and discharge (lithiation) cycles, cathode active materials (CAMs) undergo significant volumetric changes due to lithium ion insertion and extraction, which is inherent to their structure. For instance, graphite anodes experience about 10 % volume change, while silicon anodes can expand up to 400 %. Even small changes, around 7.5 %, can cause delamination [182]. Nickel-rich $LiNixMnyCozO_2$ (NMC) cathodes also exhibit considerable volume fluctuations related to lithium content, creating internal stresses. In the absence of a liquid electrolyte, these volume changes result in strong mechanical interactions that can impact interfacial integrity due to spatial variations in lithium-ion concentration during cycling.

Volumetric changes in cathode active materials (CAMs) during lithiation and delithiation cause tensile and compressive stresses within the composite cathode and at the CAM/solid-state electrolyte interface. Delithiation leads to shrinkage, creating tensile stresses, while lithiation causes expansion and compressive stresses. Under tensile stress, adhesion loss between components can occur, impairing electronic and ionic conduction pathways and reducing battery performance. Stress concentrations can trigger cracks within CAM particles or along interfaces, leading to delamination [182,187,189,191]. This is particularly concerning in high-voltage cathodes like nickel manganese cobalt (NMC), where anisotropic changes in the lattice parameter can create significant stresses among grains, potentially disrupting lithium-ion transfer pathways and isolating sections of the cathode (Table 4).

Traditional inorganic solid electrolytes such as garnets and oxides tend to be rigid and brittle, restricting their capacity to manage volume changes in electrode materials during cycling. This often causes stress buildup, cracks, and weak interfacial contact. The key challenge lies in balancing mechanical strength with the ability to adapt to dynamic volumetric shifts. A promising approach is to develop compliant, ductile, or viscoelastic solid electrolytes that can more effectively accommodate these fluctuations.

- Viscoelastic Inorganic Glasses (VIGLAS), such as $LiAlCl_{4-2x}O_x$ (LACO) and $NaAlCl_{4-2x}O_x$ (NACO), exhibit polymer-like viscoelasticity and superplasticity. These materials are characterized by glass transition temperatures (Tg) that fall below room temperature. This distinctive property enables them to deform under stress without fracturing, effectively accommodating changes in electrode volume.

Table 3
Electrochemical degradation mechanisms and resulting interfacial products at cathode/sse interface [181,187–190].

Degradation Mechanism	Cathode/SSE	Resulting Interfacial Products	Performance/ Delamination Effect
Spontaneous Chemical Reaction	NCA / Li_6PS_5Cl	Highly resistive interphases, fractured NCA particles, needle-like LPSCl	Increased interfacial resistance, physical separation, reduced capacity, poor retention
Electrochemical Oxidation/ Reduction	NMC622 / LLZO (at high voltage/temp)	Li_2CO_3, $La_2Zr_2O_7$, La(Ni,Co)O_3, reduced Ni/Co phases	Increased interfacial resistance, higher polarization, capacity decrease
Non-uniform Current Distribution	General (due to interphases/ morphology)	Current hotspots, local overcharging, high-stress states	Particle fracturing, void formation, reduced accessible capacity, promotes delamination

Table 4
Overview of common cathode active materials and associated volume changes/stress implications [128,181,182,192–197].

Cathode Active Material	Volumetric Change during (De)lithiation	Interfacial Stress and Delamination
$LiNixMnyCozO_2$ (NMC)	Significant, varies with Li content; anisotropic lattice changes	Generates high internal stresses (up to 6 GPa between crystallites), intergranular cracks, and delamination at the CAM/SSE interface
$LiCoO_2$ (LCO)	Moderate to significant	Volume changes contribute to stress and delamination at the CAM/SSE interface
$LiFePO_4$ (LFP)	Moderate	Volume changes contribute to stress and delamination
Silicon (Si)	Up to 400 % expansion	Induces extremely high mechanical stresses, necessitating high stack pressures (50–150 MPa) or elastic electrolytes to maintain contact and prevent disintegration/delamination
Electrode Particles	~7.5 % volume change can induce delamination	Even relatively small changes can trigger delamination if not accommodated by compliant electrolytes

For example, LACO75 displays remarkable deformability, demonstrating over 77.8 % strain under quasi-static loading, along with a measurable viscoelastic creep rate [129,132].

- Elastic Electrolytes: Novel elastic solid electrolytes, typically created from soft-rigid dual monomer copolymers such as dimethyl acrylamide (DMAM) and acrylamide (AM), display remarkable mechanical properties. These include exceptional stretchability, with a break elongation of 1160 %, a high fracture strength of 1.7 MPa, and the ability for shape memory. Importantly, these materials feature outstanding energy dissipation capabilities through the reversible breakage of noncovalent bonds. This mechanism enables the electrolyte to accommodate significant volume changes, effectively preventing electrode disintegration and preserving mechanical integrity [198].
- Pliable Ga-based Electrolytes: Certain inorganic pliable solid electrolytes, potentially incorporating gallium, fluorine, and other halogens (such as $xLiCl–GaF_3$ composites), demonstrate clay-like mechanical properties, characterized by storage and loss moduli below 1 MPa and glass transition temperatures beneath −50 °C. These distinctive mechanical attributes allow them to effectively infiltrate high-loading cathodes similarly to a liquid, ensuring complete ionic conduction pathways and the maintenance of these pathways even during cell operation [199].

Compliant electrolytes, typically characterized by an elastic modulus (E) of <25 GPa, have demonstrated the ability to accommodate up to 25 % changes in particle volume while significantly delaying the onset of delamination [197]. These materials can effectively encase active material particles, even in the presence of internal cracking, thus preserving efficient lithium-ion transport pathways. This inherent mechanical resilience reduces or even eliminates the necessity for high external stack pressures, allowing for stable and safe operation under only built-in pressures (ranging from 52 to 546 kPa) or under very low external pressures (< 0.1 MPa) (Table 5) [130].

Interfacial contact between solid electrolytes and active materials is critical for battery efficiency. Unlike liquid electrolytes, solid electrolytes can develop pores and cracks, which decrease the effective contact area, creating high energy barriers for ion movement and restricting transport pathways. Poor contact also promotes dendrite growth because of uneven current distribution. To boost battery performance, multiple fabrication methods have been introduced to improve initial contact and minimize porosity in composite cathodes.

- Pressing: Both cold pressing, performed at ambient temperature, and hot pressing, which occurs at temperatures ranging from 30 to 150 °C, employ mechanical force and/or increased thermal conditions to enhance the densification of electrolyte pellets. This process subsequently improves the interparticle contact within the material [187,199,200].
- Melt Infiltration: Viscoelastic electrolytes with low melting temperatures (e.g., MACO, below 160 °C) can be melted and effectively infiltrated into the intricate porous structures of electrodes. This process guarantees complete and intimate ionic contact, similar to the behavior of liquid electrolytes, resulting in a significantly increased microscopic contact area. This enhanced adhesion reduces the requirement for external pressure [130–132,134,201].
- Co-rolling Dry Process: The presented sustainable manufacturing method facilitates the concurrent attainment of thin, uniform solid-state electrolyte (SSE) layers alongside high-loading positive electrode layers. Through the implementation of a co-rolling process, this approach significantly enhances the mechanical stability of the resulting structures and fosters the formation of a reinforced, intimately bonded SSE-positive electrode interface. This innovative interface design permits stable operational capabilities even under low stack pressures, exemplified by conditions as low as 2 MPa [202].

High external stack pressure, typically ranging from tens to hundreds of megapascals, is crucial for the fabrication and operation of all-solid-state batteries (ASSBs) with rigid inorganic solid-state electrolytes

Table 5
Overview of the mechanical characteristics of different solid electrolyte categories and their connection to delamination [181–183].

SSE Type	Material	Mechanical Properties	Ability to Accomymodate Volume Change	External Pressure Requirement	Relevance to Delamination
Rigid Inorganic	LLZO, LATP, Garnets	High elastic modulus, brittle, rigid	Poor; cannot buffer volume changes	High (tens to hundreds of MPa)	Prone to stress accumulation, cracking, and contact loss/delamination
Sulfide	Li_6PS_5Cl, $Li_{10}GeP_2S_{12}$	Mechanically softer than oxides, processable	Limited; still requires stack pressure	High (several to hundreds of MPa)	Can experience contact loss and dendrite growth at high pressures
Viscoelastic Inorganic Glass (VIGLAS)	$LiAlCl_{4-2x}O_x$ (LACO), $NaAlCl_{4-2x}O_x$ (NACO)	Polymer-like viscoelasticity, superplasticity (Tg < RT), deformability (>77.8 % strain)	Excellent; deforms without fracturing, enables melt infiltration for intimate contact	Very Low (<0.1 MPa), built-in pressure	Significantly reduces delamination by adapting to volume changes and ensuring intimate contact
Elastic Polymer/Composite	DMAM/AM copolymer, Chitosan-based	High stretchability (1160 %), high fracture strength (1.7 MPa), shape memory, energy dissipation	Excellent; effectively encases particles, buffers stress via noncovalent bond breakage	Very Low (e.g., 52–546 kPa built-in pressure)	Prevents disintegration and maintains contact, reduces need for external pressure
Pliable Ga-based Inorganic	$xLiCl–GaF_3$ composites	Clay-like properties (storage/loss moduli <1 MPa), Tg < −50 °C, formable	Excellent; penetrates cathode like liquid, maintains conduction paths	Low	Resolves cathode–electrolyte interface issues by ensuring complete ionic contact

(SSEs). This pressure helps prevent internal voids, ensures contact between electrodes and SSEs, and reduces delamination risks [181,182]. However, it poses practical challenges such as increased manufacturing costs and reduced battery energy density. Excessively high pressures can also lead to short circuits from lithium dendrite growth. The ideal operating pressure for industrial applications is below 2 MPa [197,203].

The advancement of elastic or viscoelastic SSEs allows for stable operation with minimal external pressure (<0.1 MPa) [204–206]. Additionally, the initial state of charge during battery assembly significantly affects long-term mechanical stability. Assembling half-cells in a state where the active material is expected to shrink during operation increases the risk of delamination. Optimizing the lithiation state of the cathode during assembly can help minimize stress from volume changes, improving cycle life right from the first cycle.

The interfacial delamination in all-solid-state batteries (ASSBs) is primarily driven by interconnected electrochemical reactions and electrochemo-mechanical coupling [182]. This relationship leads to a synergistic degradation pathway, where mechanical stress influences interfacial contact and triggers side reactions, while electrochemical processes induce mechanical deformation [129,182]. A notable example is the formation of resistive interphases, which create current hotspots, leading to mechanical damage like fracturing and void formation, further increasing interfacial resistance and accelerating degradation.

Temperature plays a critical role, as abnormal thermal conditions can enhance strain energy and crack propagation, affecting the stability of the solid electrolyte interphase (SEI) and increasing internal impedance [52,204,205,207]. Understanding this complex thermal-electrochemical-mechanical interaction is vital for battery safety and developing reliable ASSBs. A holistic, multidisciplinary approach to modeling and characterization is necessary to address these coupled challenges, prioritizing multifunctional materials and operando characterization techniques.

2.5. Effects of external pressure on the interface

2.5.1. Electrode and electrolyte interface

The performance of all-solid-state batteries (ASSBs) is greatly impacted by the pressure applied during electrolyte preparation as well as the stack pressure during battery operation. Earlier studies have demonstrated a direct correlation between interfacial contact and stack pressure [77,208,209]. Operating conditions result in a dynamic stack pressure that can fluctuate over time. Capacity and stack pressure in commercial lithium-ion pouch cells were monitored during cycling by Cannarella et al. [210]. The study found that operational pressure in all-solid-state batteries (ASSBs) is affected by initial stack pressure, electrode expansion and contraction, and stress shifts due to changes in electrode volume during charge and discharge. Besides the preparation pressures for electrodes and electrolytes, the stack pressure during operation is essential for ASSB performance. Cannarella et al. [211] discovered that the operating pressure is highly influenced by the initial stack pressure, electrode expansion and contraction, and stress shifts caused by variations in electrode volume during charge and discharge. Although tested in pouch cells, the apparatus utilized to monitor compressive stack stress is similar to ASSB molds, and the expansion of the electrode material volume parallels that in ASSBs.

Stack pressure is prone to the development of interfaces, and when coupled with impedance tracking, it can distinguish between different degradation mechanisms and cell reactions. The formation of Li dendrites, which is dependent on electrolyte density, showed a clear influence on the stack pressure [74]. An electrochemical performance evaluation of all-solid-state batteries (ASSBs) can be performed in real-time by using the dynamic nature of operation pressure as a mechanical sensing approach. Jungy safety andg introduced operando differential electrochemical pressiometry (DEP), demonstrating that the differential pressure related to time or capacity is connected to the specific state of charge (SOC) in all-solid-state batteries (ASSBs). This method shows promise for estimating SOC in graphite electrodes within $LiNi_{0.7}Co_{0.15}Mn_{0.15}O_2$/Gr full cells with different n/p ratios (Fig. 11).

2.5.2. Anode and electrolyte interface

All-solid-state batteries (ASSBs) offer a secure platform for utilizing lithium metal anodes; however, the intricate interfacial interactions between lithium metal and solid electrolytes (SEs) pose challenges. Lithium metal, prone to creep deformation even at room temperature, faces difficulties due to its limited bonding strength. An emerging solution involves applying stack pressure [213,214]. Interfacial impedance, originating from imperfect contact or the formation of interfacial films, is a fundamental component of these interfaces. Wang et al. [215] established a strong correlation between the mechanical and electrochemical properties of the Li-LLZO interface, connecting interfacial resistance to the lithium metal's tensile adhesion strength on LLZO surfaces. It was discovered that removing surface layers improved the contact between Li metal and LLZO, reducing interfacial resistance and strengthening the connection. Interfacial impedance decreases when pressure increases because the interfacial area expands.

Gupta et al. [216] reported that pressure affects the Li-polymer solid electrolyte interface's physical contact area, which in turn affects interface impedance. In the Li-PEO-LiTFSI electrolyte interface, a specified operation pressure is required to attain optimum contact; the impedance is stable when this pressure surpasses a particular threshold. Zhang et al. [72] developed a comprehensive multiscale 3D time-correlated contact model to study the evolution of the lithium-solid electrolyte interface (Fig. 12). This model incorporates factors such as surface roughness, elastoplasticity, creep, and plating/stripping processes. Their findings revealed that the contact area is influenced more by the ratio of stack pressure to lithium yield strength than by stack pressure alone. The elastic-plastic contact influences the development of Li dendrites and pores. External pressure enhances interface contact and hinders void formation [217–221]. Due to inherent flaws at the solid electrolyte (SE) interface, lithium stripping and plating occur only at specific contact points. Yan et al. [222] studied the formation of voids at Li-SE interfacial contacts during delithiation using a creep-contact electrochemo-mechanical model. Their research established conflicting effects of current density and stack pressure on void formation in LLZO. They discovered that creep-induced vacancy transfer in lithium metal helps reduce void development at defective interfaces (Fig. 13a i-iii).

A mechano-electrochemical phase field model was employed by Shen et al. [156] to illustrate the effect of external pressure on lithium dendrites. Critical pressure values, associated with the electrolyte's elastic modulus, influence the formation of smooth and dense lithium dendrites. The relative Young's modulus between lithium metal and the electrolyte dictates dendrite growth, with a lower modulus promoting growth and a higher modulus inhibiting it (Fig. 13b). The study explored the effects of external pressure on lithium dendrite growth in electrolytes with elastic moduli ranging from 0.5 to 2.0 GPa, maintaining a constant pressure of 6.0 MPa. The findings revealed that electrolytes with lower elastic moduli significantly enhance dendrite suppression, requiring less pressure to achieve comparable dendritic structures, while space utilization diminished as the modulus increased. A critical pressure threshold was established that varies with the modulus of the electrolyte, identifying an optimal external pressure limit of at most 5.0 MPa to enhance the performance of lithium metal anodes. This was supported by a phase diagram that aids in pressure management for cell design (Fig. 13d).

Significant polarization is also observed during galvanostatic cycling at a critical stack pressure, which acts as an effective barrier against the formation of voids at a specific current density (Fig. 13e). Pressure compensation aids in achieving uniform electrochemical current distribution across the interface, addressing non-uniformities arising from interface defects during lithium deposition [223–225]. The rigidity of inorganic SEs exacerbates interface contact challenges and crack

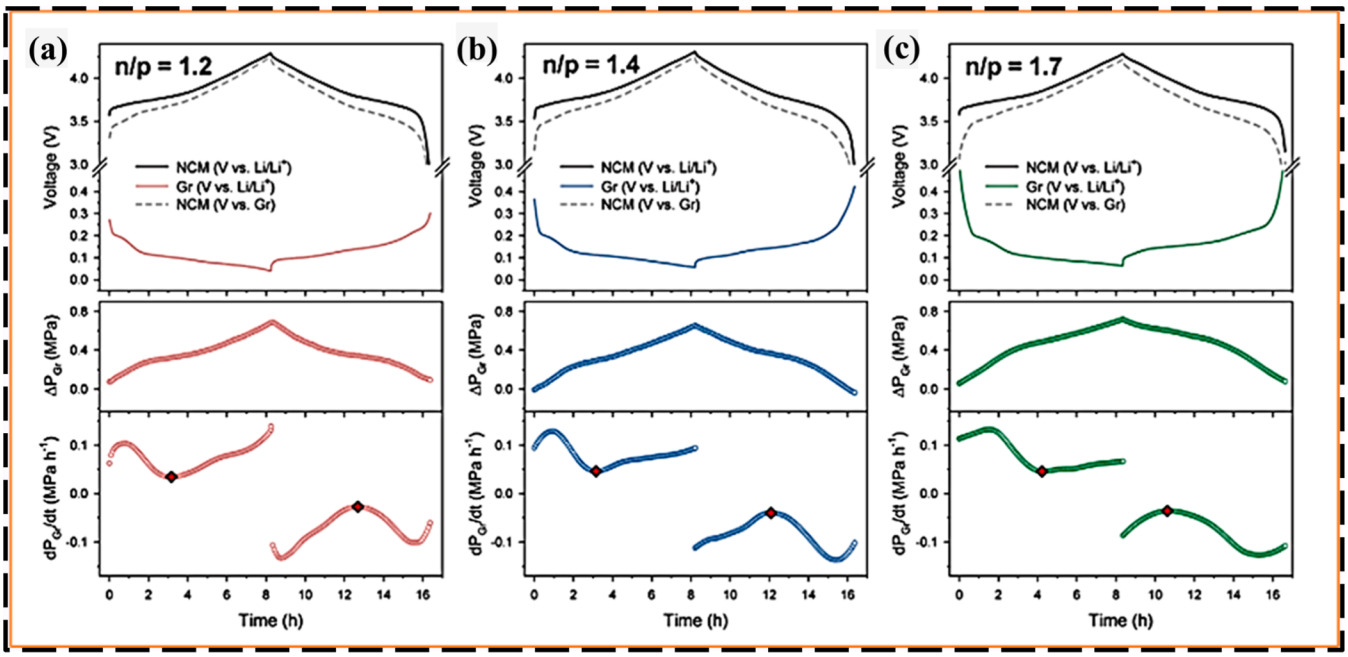

Fig. 11. Shows the results of Differential Electrochemical Pressiometry (DEP) for NCM/Gr all-solid-state three-electrode cells with three different n/p ratios at the 2nd cycle, 0.1C, and 30 °C. It includes charge-discharge voltage profiles for each electrode, corresponding pressure change curves (ΔP), and DEP profiles (dP/dt) of Gr electrodes for NCM/Gr cells with n/p ratios of a) 1.2, b) 1.4, and c) 1.7. The red diamonds indicate the lowest and highest points of the DEP profiles throughout the charging and discharging processes (Adapted from Jun et al.) [212].

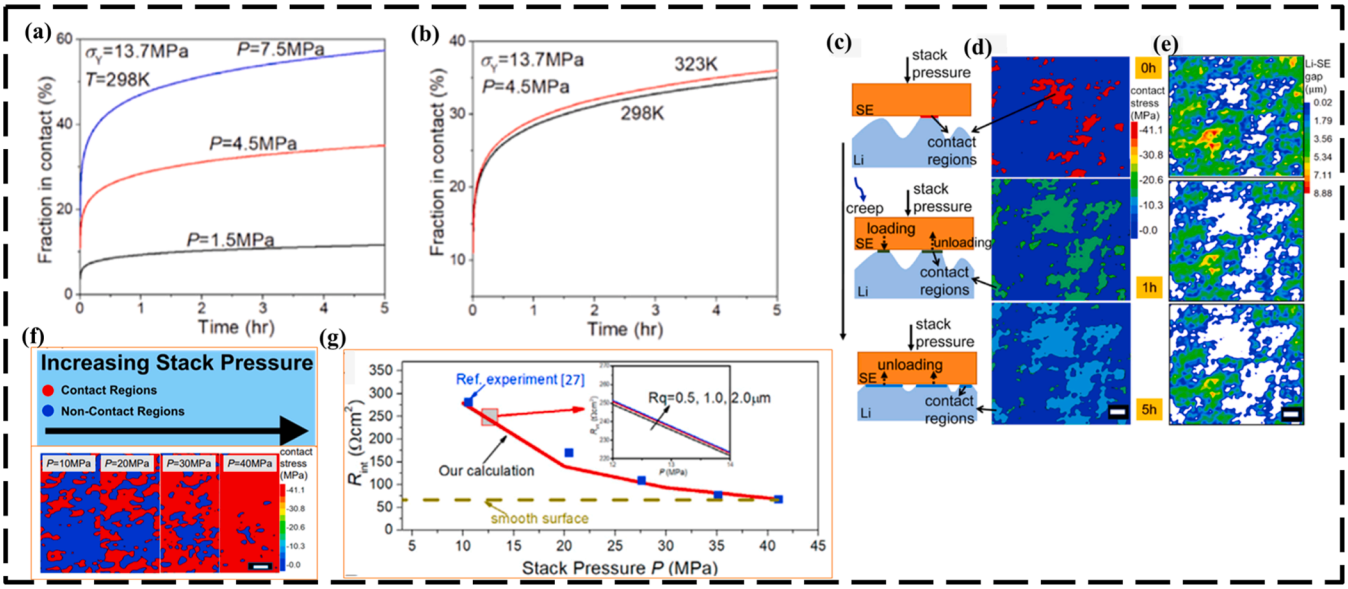

Fig. 12. The contact area between lithium and the solid electrolyte (Li-SE) at different stack pressures is affected by creep-induced variations. Section (a) presents: i) the Li-SE contact area's temporal progression at stack pressures of 1.5, 4.5, and 7.5 MPa; ii) a schematic representation of the interfacial creep process; and iii) the distribution of lithium contact stress over 0, 1, and 5 h at a stack pressure of 4.5 MPa, where blue areas denote no contact stress and red, yellow, and green regions represent contact areas under varying stress levels. The scale bar is 50 μm in length. iv) the Li-SE gap at a stack pressure of 4.5 MPa over 0, 1, and 5 h; v) the evolution of the Li-SE contact area over time at a stack pressure of 4.5 MPa for temperatures of 298 K and 323 K. White areas exhibit zero gap contact, whereas red, yellow, and green regions show non-contact areas. Lithium has an initial roughness of Rq = 2 μm and a yield strength of 14 MPa. The variation in lithium contact stress for a yield strength of 14 MPa at various stack pressures of 10, 20, 30, and 40 MPa is displayed in Part (b), where non-contact locations are indicated by blue regions and contact areas by red regions. The scale bar measures 40 μm. Plotting the estimated interface resistance (red curve) against stack pressure in Part (c), without any charging or discharging procedures, reveals an inverse relationship with pressure, in contrast to the experimental data (blue squares). The computations are calibrated to coincide at a stack pressure of 41 MPa. The horizontal dashed line represents the lowest possible interface resistance for completely smooth surfaces (Adapted from Zhang et al.) [228].

propagation. Despite the theoretical effectiveness of such approaches, issues like lithium dendrite propagation and short circuits in hard ceramic electrolytes have been observed at high lithium deposition rates [173]. Due to the difficulties associated with "solid-solid" contact, understanding the nuances of lithium-metal/SE interactions is essential. Applying pressure enhances the contact between the anode and solid

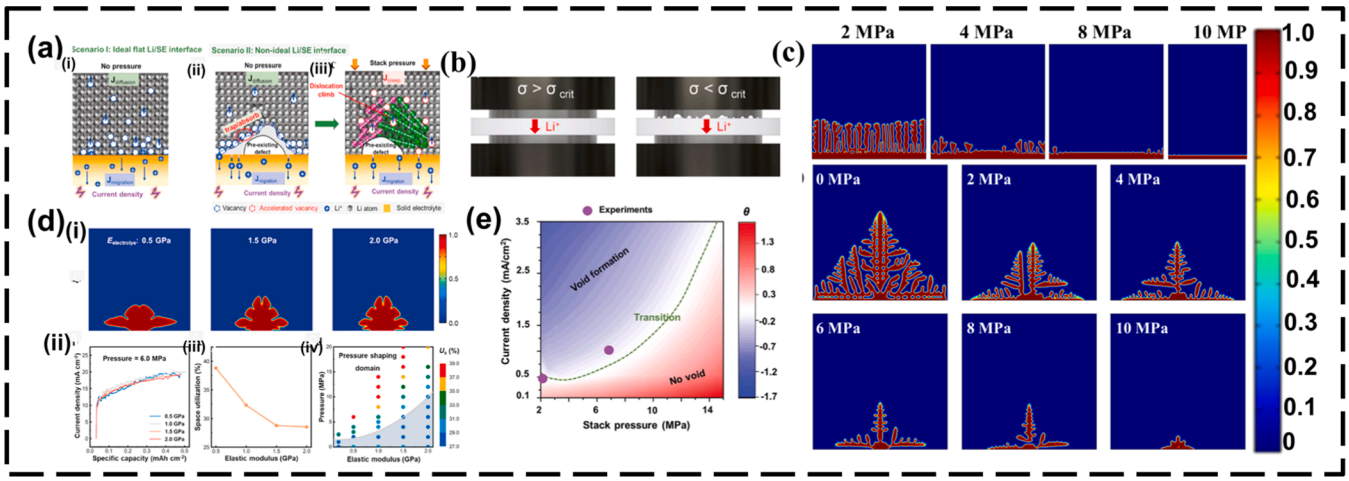

Fig. 13. (a) (i) shows the opposing effects on void formation caused by $J_{migration}$ and $J_{diffusion}$ at a non-ideal, flat Li-SE interface with pre-existing defects. (ii) When vacancies are absorbed or trapped at the surfaces of these defects, $J_{migration}$ exceeds $J_{diffusion}$, making it insufficient to transfer interfacial vacancies into the bulk Li metal, leading to void formation. (iii) When sufficient stack pressure is applied, J_{creep} surpasses $J_{migration}$, facilitating the migration of vacancies from the interface into the bulk Li metal, thus preventing void formation (Adapted from Yan et al.) [222]. (b) The adequacy of the applied pressure for maintaining contact between Li and the electrolyte is demonstrated by the proposed microstructure of the Li-electrolyte interface, which depicts scenarios above and below the critical stack pressure (Adapted from Wang et al.) [229]. (c) Simulation results of single Li dendritic morphological growth as a function of external pressures (0 – 10 MPa) (Adapted from Gao et al.) [230] (d) Lithium dendritic growth in electrolytes with elastic moduli ranging from 0.5 to 2.0 GPa is affected by external pressure. (i) shows the morphology of dendrites at a plating capacity of 0.40 mAh cm^{-2}, along with (ii) variations in current density during electroplating and (iii) the spatial utilization across different electrolytes. (iv) a phase diagram that links the electrolyte's elastic modulus at a plating capacity of 0.4 mAh cm^{-2} to the external pressure that is applied (Adapted from Shen et al.) [231]. (e) The graphic shows the relationship between stack pressure, current density, and void formation, with a green dotted line indicating the critical threshold for void generation. Experimental results are represented by purple circles (Adapted from Yan et al.) [222].

electrolyte, thereby reducing interfacial resistance.

The overall performance of the battery is influenced by the interplay of stack pressure, internal stresses, and the kinetics of interfacial reactions. Ganser et al. [226] extended the Butler-Volmer equation to incorporate mechanical stress, highlighting its enduring positive effects even after pressure removal. For optimal cell performance, stack pressure is crucial, but alkali metals' poor yield strength can induce microcracks in the solid electrolyte, which can cause short circuits even at low pressures (Fig. 13b) [227]. Therefore, managing stress on the lithium metal anode comprehensively should consider interfacial reactions, electrode mechanical properties, and changes over extended cycling periods.

2.5.3. Cathode and electrolyte interface

The presence of porosity in the electrode and electrolyte layers, similar to particle grain boundaries, hinders the transport of ions and electrons, making post-assembly compression critical in the production of all-solid-state batteries (ASSBs) due to the high initial porosity of these layers [232]. Maintaining strong interfacial contact and electrochemical stability between the active material particles and the solid electrolyte (SE) in composite cathodes is essential for ASSB performance [233]. In these composite cathodes, external pressure plays a significant role in charge transport kinetics, with microstructure-based singularities critically influencing these kinetics [234].

Furthermore, both internal and external pressures impact the open-circuit voltage (OCV) of solid-state batteries, with experimental results showing an OCV variation of approximately 1 mV per 100 MPa of pressure [235]. Stress-optimized cathode composites have been proposed to mitigate contact loss due to volume changes and stress-induced issues, especially in NMC materials that are prone to cracking and electrolyte isolation during cycling [236,237]. However, excessive preparation pressure can lead to material extrusion and decreased utilization of active materials.

The impact of stack pressure on interface contact and induced strains in ASSBs has been assessed using computational, experimental, and analytical methods [51,238]. These studies employed digital imaging correlation (DIC) to measure local strain distribution and used computational and analytical models to analyze stress/strain distribution at electrode/electrolyte interfaces (Fig. 15a-b, d-e) [239]. Insufficient contact areas, resulting from the roughness of the electrolyte and cathode material, contribute to elevated interfacial resistance and progressive capacity deterioration. The proximity-induced stress near the interface is positively correlated with stack pressure and electrode moduli (Fig. 15c).

Finite element modeling (FEM) showed that while higher stack pressure (0.26 MPa) enhances interface contact, it also introduces strains that could lead to interface failure (Fig. 15b). Increasing compressive stress expands the range of strain regimes, leading to typical fractures in the deformed electrolyte material (Fig. 15e) and Fig. 16a-d) [51,238]. Induced stress levels at moderate (0.26 and 0.5 MPa) and high (1 MPa) pressures were sufficient to cause cracking, with both crack diameters and openings increasing as stacking pressure rose. Cracking begins at a minimum stacking pressure of 0.26 MPa, while no strain or cracks were observed in a battery under 0.002 MPa pressure [239]. Proper external pressure application is essential for maintaining effective contact with the positive electrode, as the expansion of electrode materials during charge and discharge cycles can damage electrode structures.

Scanning electron microscopy (SEM) analysis of cross-sections before and after cycling revealed enhanced contact between NMC active particles and SE following pressing (Fig. 18). However, voids appeared after charging, which negatively impacted the performance of the all-solid-state system, as the additional SE could not fill these voids [240,241]. High Coulombic efficiency (CE) is maintained by ensuring contact, as demonstrated by the cycling performance of SC-NMC/LPSCl cathodes at different stack pressures. Lower pressures maintained the CE similar to what happened at the first cycle, but gradual contact loss resulted in poor capacity retention after 10 cycles at 2.5 MPa.

The effects of low stack pressure were further highlighted by using an asymmetric pressure design, emphasizing the importance of stress-optimized cathode composites [178]. While appropriate stack pressure reduces interface impedance and contact loss, excessive pressure risks interface deformation and cell failure, underscoring the importance of selecting the right stack pressure for ASSB performance. Given the

impracticality of high external pressures, Yoon Seok Jung and collaborators [242] introduced vulcanized butadiene rubber (BR) as a binder, enabling operation with low or no external pressure for sulfide electrolyte-based all-solid-state Li batteries [243]. The mechanically robust nature of vulcanized BR prevents degradation and reduces the need for external pressure, enhancing electrode performance under realistic pressures. The ongoing research is continuing to explore innovative solutions to these challenges.

Furthermore, before constructing solid-state batteries (SSBs), it is essential to combine the active material, conductive agent, and solid-state electrolyte (SSE) powder effectively on the cathodic side. The effectiveness of this integration can be evaluated through the contact area fraction, which indicates the percentage of the total surface area of the active materials that is in contact with the SSE. The cathode materials exhibit significant hardness, with values ranging from 6 to 18 GPa, and are embedded within rigid SSE particles, creating a stark contrast with the softer lithium metal [245]. Consequently, the deformation, compaction, and rearrangement of these solid particles result in pressure-induced changes at the SSE-cathode interface. Sakka et al. [119] employed X-ray computed tomography (CT) techniques to investigate the effects of mechanical pressure on contact dynamics.

Three distinct states are identified by variations in the contact area. At low pressures, the contact area ratio remains relatively stable. However, as the pressure approaches approximately 50 MPa, the SSE particles significantly fill internal cavities, resulting in a substantial increase in the contact area fraction. Beyond 50 MPa, the improvement in the contact area fraction plateaus, as the deformation of the hard particles is not sufficient to eliminate the voids in the horizontal plane (Fig. 14a) [119]. Moreover, they observed higher interfacial impedance in SSE-Li contacts, which is attributed to inadequate contact between the cathode and the ion-conductive SSE particles.

To gain a comprehensive understanding of the charging and discharging processes at the SSE-cathode interface, it is crucial to explore lithium-ion diffusion and the resulting stress effects across various timescales. Unlike the chemo-plastic deformation characteristic of lithium metal, cathodes generally exhibit chemo-elastic behavior. Chen et al. [245] developed a semi-analytical model (SAM) specifically designed to address these complexities. This model effectively captures the time-dependent chemo-elastic interactions at the SSE-cathode interface, providing valuable insights for measuring and visualizing interfacial stability under applied current conditions [245].

Continuous volume fluctuations at the SSE-cathode interface arise from complex chemical processes and intercalation dynamics. The cyclical expansion and contraction of the electrode lead to a reduction in the interfacial contact area. Utilizing focused ion beam scanning electron microscopy (FIB-SEM), Shi et al. [244] identified the formation of microcavities and cracks in proximity to the cathode particles (Fig. 14b). During cycling of LLZO-based solid-state batteries, two distinct capacity fade behaviors were observed. The first was characterized by a gradual, continuous decrease in capacity attributed to interfacial chemical degradation, while the second pattern features sudden capacity drops interspersed across cycles, indicative of mechanical failure [244]. Ex-situ impedance spectroscopy allowed for disaggregation of the contributions from each interface, revealing that the mid-frequency range is highly responsive to alterations at the SSE-cathode interface. Upon re-evaluation of the battery after the 50th cycle, they observed a

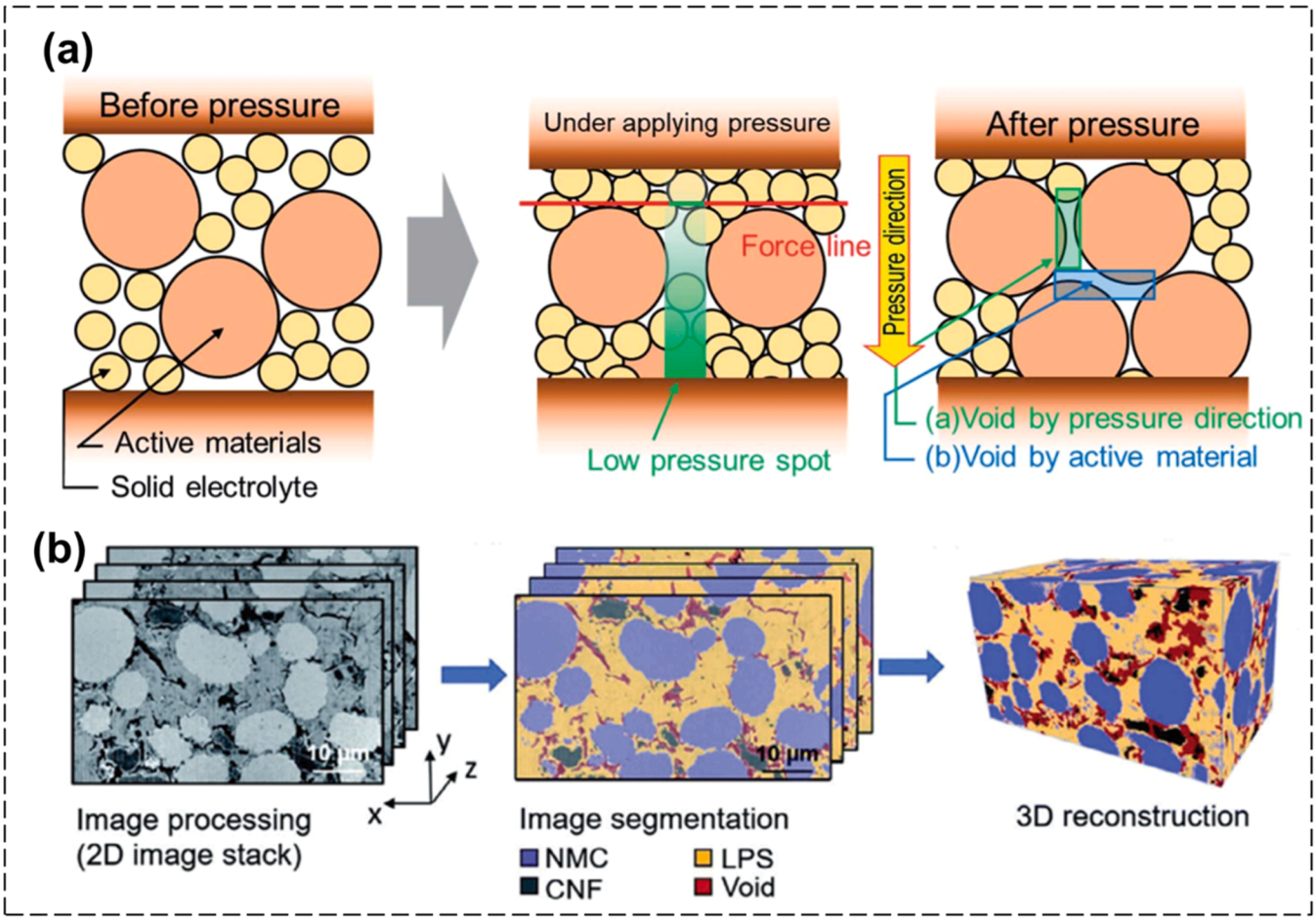

Fig. 14. (a) A schematic showing morphological structural changes in the composite electrode at the interface as a function of pressure (Adapted from Sakka et al.) [119] (b) Presents a FIB-SEM tomography image of the cathode composite (Adapted from Shi et al.) [244].

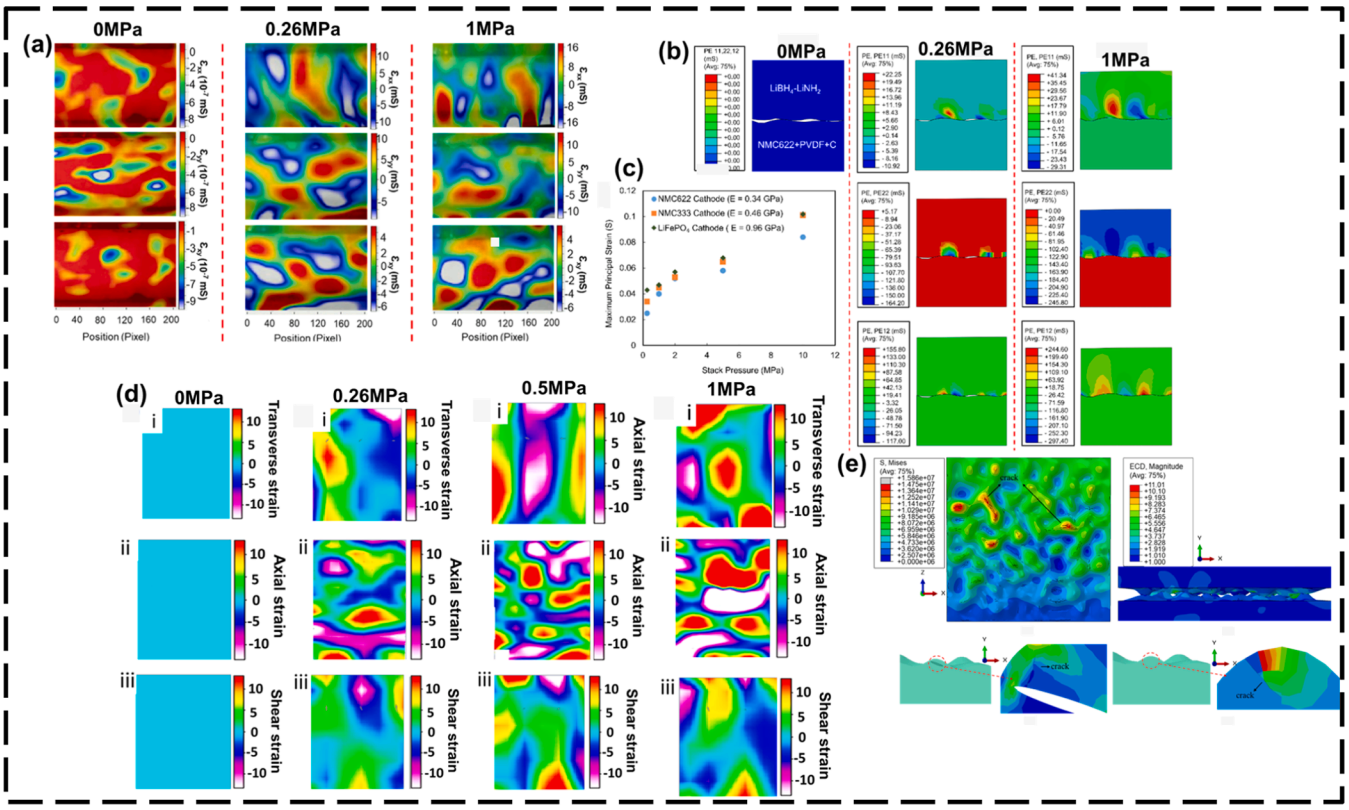

Fig. 15. (a) The interface between the electrolyte and electrode in an all-solid-state battery (ASSB) under stack pressure; (b) The maximum principal strain in the electrolyte for stack pressure; (c) Finite Element Method (FEM) results demonstrating insufficient interfacial contact and plastic strain at 0 MPa (Adapted from Ahmed et al.) [238]. (d) FEM results showing enhanced interfacial contact and significant plastic strain at 0.26 MPa; and (e) FEM results demonstrating improved interfacial contact and significant plastic strain at 1 MPa. DIC strain maps of Al-LLZO electrolyte (f) 0.002 MPa (g) 0.26 MPa (h) 0.5 MPa (i) 1.0 MPa. (i) refers to transverse strain, (ii) refers to axial strain, and (iii) refers to shear strain. (j) Stress distribution in the Al-LLZO layer, (k) Electrical current density in the entire system in the first simulation set. Crack formation inside the Al-LLZO layer under the pressure of 1 MPa, (l) near an elliptical void, (m) with no flaws in the system from the second simulation set (Adapted from Adjah et al.) [239].

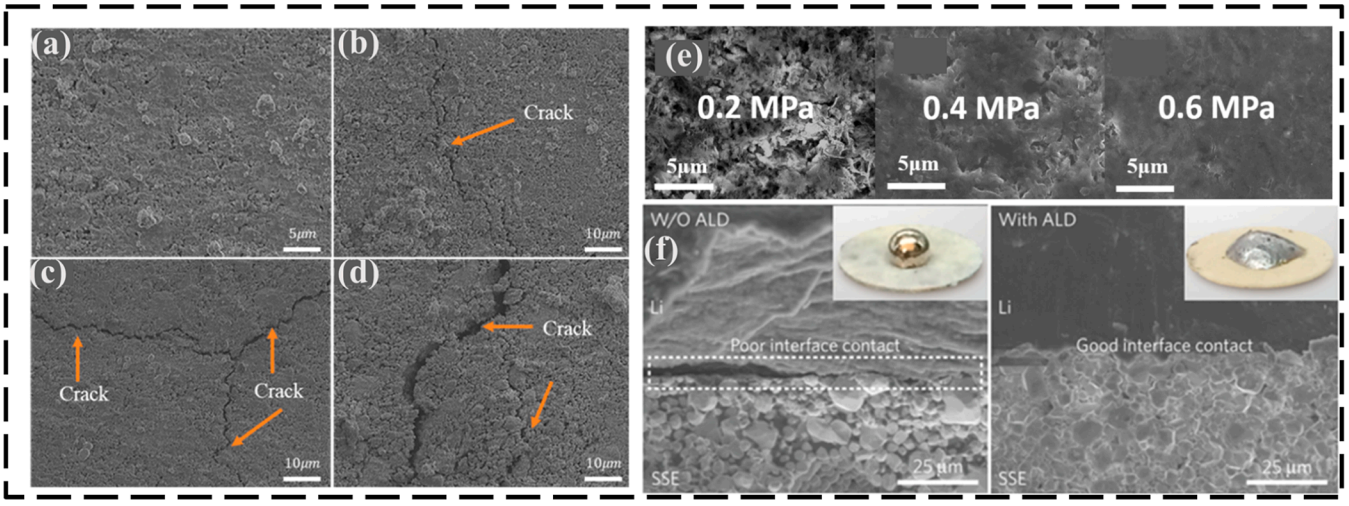

Fig. 16. Illustrates the Al-LLZO electrolyte SEM micrograph after stack pressure at (a) 0.002 MPa, (b) 0.26 MPa, (c) 0.5 MPa, and (d) 1 MPa (Adapted from Adjah et al.) [51]. (e) As the pressure increases from 0.2 MPa to 0.6 MPa, the size of the cracks diminishes. Lithium dendrites are seen at 0.2 MPa, while a dense lithium deposit was observed at 0.6 MPa (Adapted from Cui et al.) [249]. (f) The SEM images reveal that garnet demonstrates poor contact with lithium metal without an ALD-Al_2O_3 coating. With the coating, lithium forms a uniform bond upon heating, as shown in the inset of molten lithium on the treated surface (Adapted from Han et al.) [250].

recovery in capacity alongside a reduction in mid-frequency resistance from 3283 Ω to 2755 Ω, while both low- and high-frequency resistances remained stable [244]. This observation suggests that inadequate interfacial contact between the solid-state electrolyte (SSE) and the cathode is the predominant factor contributing to the observed decline in performance. These results highlight the crucial role of stack and

assembly stresses in maintaining optimal interface integration within solid-state battery systems.

Recent investigations have increasingly focused on sandwich-like composite solid-state electrolytes (SSEs) and their interfacial interactions, alongside ongoing research on SSE-electrode dynamics [246, 247]. Hüttl et al. [248] analyzed the pressure-dependent resistive behavior of a $Li_7P_3S_{11}$ (LPS)-LLZO composite SSE. Their results demonstrate a significant decrease in both low-frequency and high-frequency resistances as pressure increases, a phenomenon mainly attributed to the deformation properties of the softer LPS component.

2.6. Effects of external pressure on dendrite growth

In all-solid-state batteries (ASSBs), applying external pressure influences dendritic development. This pressure can prevent lithium dendrites from spreading by altering the mechanical conditions at the electrode-electrolyte interface. Applied stress improves interfacial contact, reduces nucleation sites, and delays the occurrence of short circuits by causing dendritic deflection. However, the mechanical deformation of cathode materials and electrolytes may facilitate dendrite penetration or create new growth paths.

Zhang et al. [253] and Gao et al. [230] investigated the influence of external pressure on the development of lithium dendrites, applying pressures ranging from 0 to 14 MPa. Their findings demonstrate that as external pressure increases from 0.0 to 14.0 MPa, the lithium dendrites exhibit a smoother morphology with reduced branching (Fig. 13c & Fig. 13d(i)).

When the applied external pressure surpasses the electrochemical stress, the local hydrostatic pressure within the dendrite transitions from negative to positive, altering the growth dynamics from expansion to compression. Notably, the dendritic tip experiences the highest hydrostatic pressure, which acts to inhibit further development of the tip while simultaneously facilitating lateral growth. The presence of smooth and coarse dendrites can considerably decrease the specific surface area while increasing density, aligning with experimental observations. It is crucial to highlight that an increase in external pressure can lead to material failure, which can be predicted using the von Mises yield criterion. When the von Mises stress exceeds the yield strength, the solid electrolyte may fail to recover after the detachment of the lithium dendrite. This can result in the fracturing of the lithium dendrite and its conversion into dead lithium. Consequently, this loss of electrical connectivity between the electrolyte and the lithium dendrite leads to a decline in the battery's coulomb efficiency, (Fig. 17).

The maximum permissible external pressure can be established based on the material properties. The mechanical properties of materials significantly impact their ability to endure external pressure. As the external pressure escalates, the locus of maximum stress transitions from the bifurcation point to the base of the lithium dendrite, culminating in a peak von Mises stress of 19.5 MPa, an increase from 5.8 MPa. Fractures at the dendrite root are more detrimental to Coulombic efficiency compared to those occurring within the branches, highlighting the critical nature of stress concentration in dendritic structures.

Fincher et al. [254] adopted a stress-based methodology to mitigate metal-dendritic failure in solid-state batteries. Their experimental evaluations and a fracture mechanics model indicate that the application of compressive in-plane stress can effectively redirect the growth of lithium metal dendrites within the LLZTO electrolyte, thereby reducing the risk of short circuits. A critical threshold of approximately 150 MPa in in-plane stress has been determined to be sufficient for altering the growth trajectory of dendrites, independent of their initial orientation. These insights offer valuable guidance for selecting material combinations and manufacturing processes that can induce beneficial stresses in laminating solid-state battery architectures, leveraging residual stresses that arise from thermal expansion mismatch.

3. Current approaches for reducing pressure in ASSBs

Recent studies have intensely explored the role of pressure in all-solid-state batteries (ASSBs) [109–114], leading to the development of strategies that reduce operating pressure without sacrificing electrochemical performance, mainly by minimizing stress and preserving interfacial contact. These strategies fall into two broad categories:

- Material Design Strategies

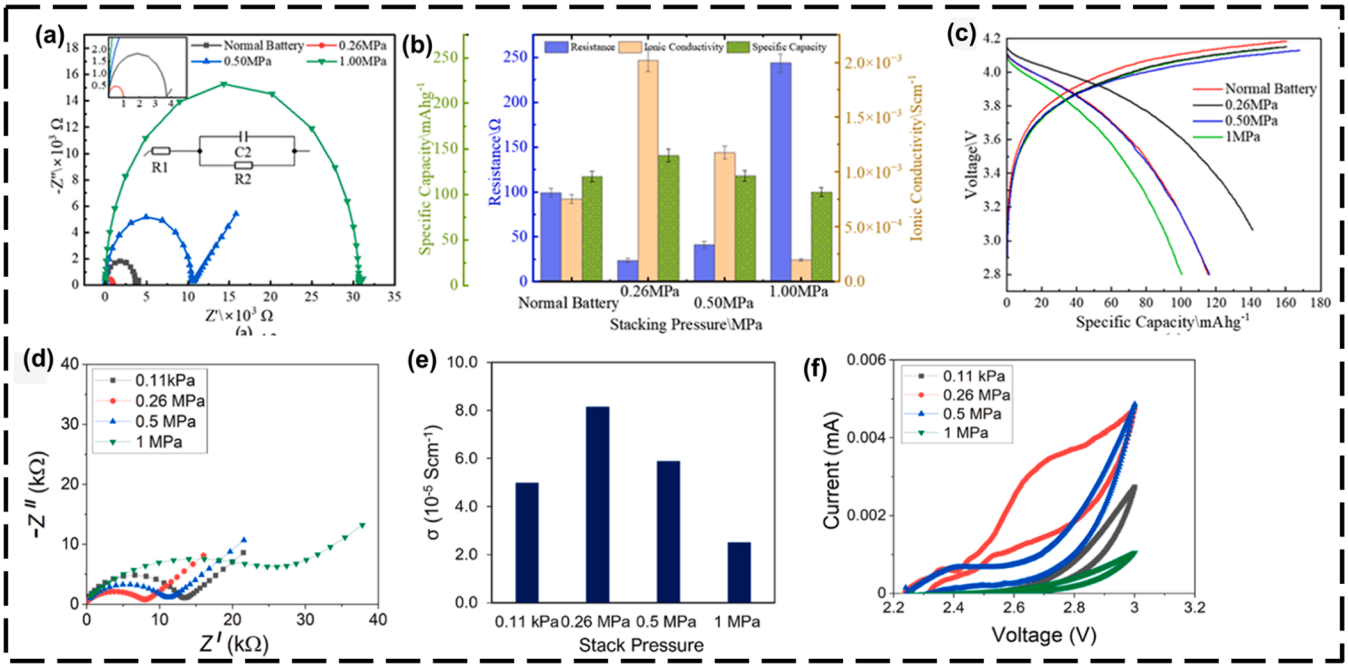

Fig. 17. (a) Impedance Nyquist plot as a function of stack pressure, (b) Resistance, specific capacity, & ionic conductivity as a function of the stacking pressure, (c) Specific capacity vs voltage as a function of stack pressure (Adapted from Adjah et al.) [51] (d) Impedance curves as a function of stack pressure, (e) Effects of stack pressure on ionic conductivity (f) Cyclic voltammogram as a function of stack pressure (Adapted from Ahmed et al.) [251].

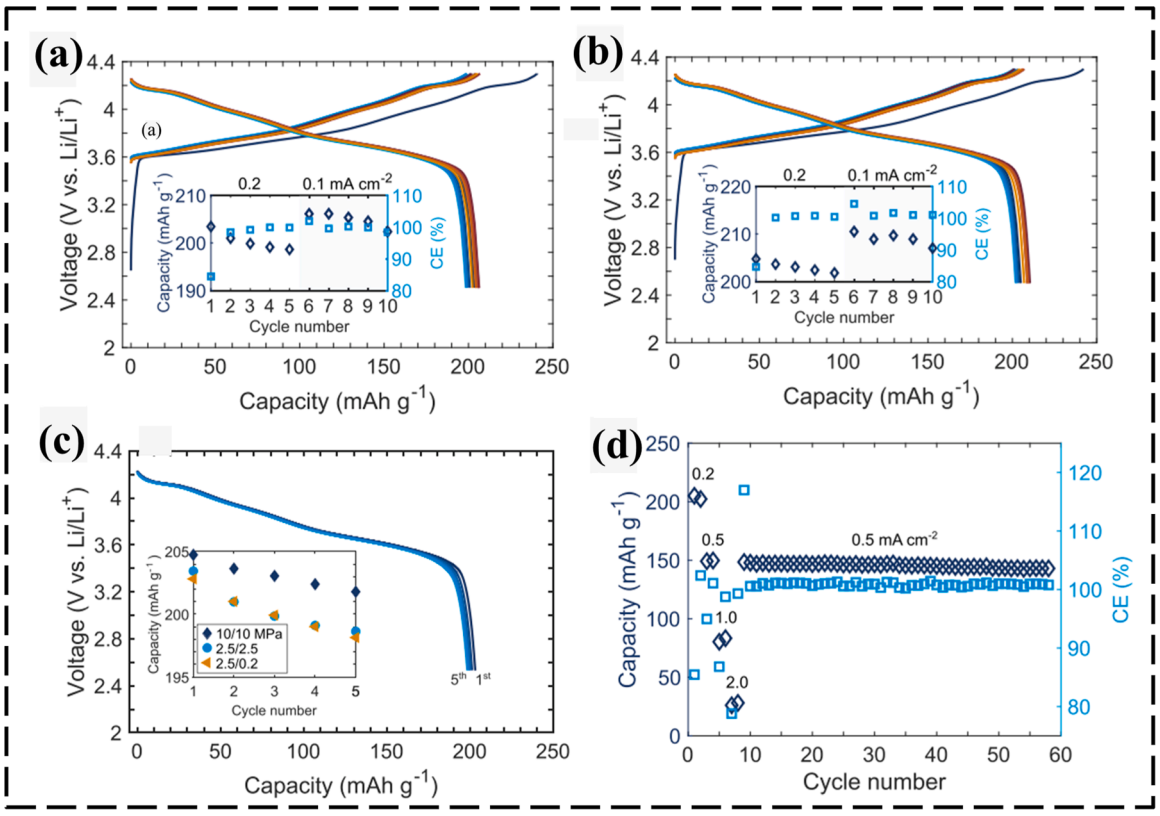

Fig. 18. Illustrates the charge/discharge curves for a composite cathode of SC-NMC/LPSCl coupled with a Li anode, with an inset illustrating capacity fade at (b) 2.5 MPa and (c) 10 MPa. (d) displays the discharge capacity of an LTO/LPSCl anode composite sample cycled at 10 MPa in conjunction with an SC-NMC/LPSCl cathode under varying current densities and an increased number of cycles. Finally, (e) contrasts the SC-NMC/LPSCl composite cathode's capacity fade and performance at various pressures (Adapted from Doerrer et al.) [252].

a) Surface Coating & Bulk Doping: Using elemental diffusion chemistry, a stratified Al/Zr-modified Ni-rich cathode with low volume strain (Δ ≈ 4.15 %) was developed [255]. Its layered architecture and stabilized lattice reduce internal stress, allowing operation at 2 MPa. However, residual volume changes still challenge long-term performance under low pressure.
b) Integrated Electrode Design: A recently developed Li_xTiS_2 cathode, which does not require a solid-state electrolyte (SSE), supports uniform expansion/contraction across the electrode [115]. This improves interfacial contact and performance, though rate capabilities remain limited.
c) Mechanical Equilibrium in Cathode Composites: Stress balance can be achieved by mixing materials with opposite expansion behaviors, such as LCO and NCM, creating a near-zero-strain composite cathode [256]. This approach reduces cycling stress, but maintaining internal contact between components and the SSE is still difficult.
d) Composite Structures for Lithium Metal Anodes: Solutions to lithium anode expansion include embedding the lithium in hollow silver/carbon fiber scaffolds paired with composite electrolytes [257]. These designs improve interfacial contact and reduce plating stress. Alternatives like lithium-carbon nanotube (CNT) composites also enhance lithium diffusion and minimize voids under low pressure [258]. However, adding inactive materials may reduce energy density.
e) Advanced Electrode Binders: Binders like vulcanized butadiene rubber create durable, crosslinked networks, maintaining interparticle contacts and delivering high capacities (~150 mAh g^{-1}) even without external pressure [36]. Block copolymer binders offering both ionic conductivity and mechanical strength enable stable cycling at 1 MPa [259]. Yet, compatibility with inorganic SSEs and high-voltage stability remains problematic.

- Cell Design Strategies
  a) Voltage and Temperature Control: Reducing the charge cut-off voltage (e.g., from 4.4 V to 4.2 V) in $LiNi_{0.83}Mn_{0.06}Co_{0.11}O_2$/$Li_6PS_5Cl$/In-Li cells significantly lowered cathode expansion (6 % → 2.5 %), improving retention from 65 % to 94 % over 50 cycles [260]. Elevated temperatures (e.g., 80 °C) also improved specific capacity at low pressures of ~2 MPa.
  b) Pressure Direction Optimization: The orientation of applied pressure significantly affects performance. Enhancing 3D contact between the electrode and electrolyte improves results under low pressure [261]. An air-based pouch cell holder was designed for isostatic pressure, which benefited cycling stability, though its current use is limited to lab-scale applications.
  c) Spring-Loaded Battery Molds: Springs integrated into battery molds have proven useful. For example, during cycling, spring-loaded cells showed minimal pressure variation (from 5 to 5.21 MPa) and supported higher current densities (up to 1.0 mA cm^{-2}) [262,263]. This controlled pressure fluctuation helps prevent ASSB failure.

4. Perspectives and outlook

The constrained "solid-solid" contact in all-solid-state batteries (ASSBs) refers to the limited interaction between the solid electrodes and solid electrolytes (SEs), which can impede ion mobility and,

consequently, battery performance. External pressure has emerged as a potential solution to enhance this contact, thereby enhancing ion mobility and overall battery efficiency. However, the effects of external pressure can be multifaceted, leading to both beneficial and detrimental effects, causing significant damage to the materials and interfaces involved.

Positive effects of external pressure: Applying external pressure through cold pressing or hot pressing can effectively compact materials and increase the density of inorganic SEs, resulting in improved ionic conductivity and performance. For alloy anodes that undergo significant volume changes during cycling, applying pressure can help maintain structural integrity by preventing detachment and cracking. External pressure can improve the contact area at the anode-electrolyte interface, reducing impedance and promoting better lithium metal behavior. This can mitigate issues like voids and enhance overall battery performance.

Negative effects of external pressure: Excessive pressure can have a detrimental impact on organic polymer electrolytes, causing their polymer chains to fold or tangle, which can hinder ion movement and reduce conductivity. Lithium metal anodes, characterized by low Young's modulus and creep behavior, can infiltrate gaps in the SE when subjected to high pressures, potentially leading to short circuits and dendrite growth, necessitating careful management of the applied pressure to avoid such issues.

An applied pressure can also moderate the lithiation process, which may reduce the overall capacity of alloy anodes. Also, excessive pressure can damage the active particles in cathode materials, making single-crystal nickel manganese cobalt (NMC) materials more suitable for ASSB configurations due to their stability under pressure. While moderate pressure can limit the growth of lithium dendrites (which can cause short circuits), the nonuniformities at the interface can still lead to uneven current distribution, highlighting the need for optimized interface and pressure conditions to ensure uniformity and efficiency.

5. Summary and concluding remarks

External pressure plays a crucial role in enabling effective solid-solid ionic contact in all-solid-state batteries (ASSBs). The responses to applied pressure vary significantly depending on the material class. Sulphide electrolytes typically benefit from pressure-induced densification, which enhances ionic conductivity. Moreover, oxide-based electrolytes are prone to brittleness, limiting the advantages of increased pressure. Polymer electrolytes are mechanically flexible with a drop in conductivity under high compression, which is largely due to structural deformation.

For electrode materials, especially lithium and lithium-alloy anodes, the application of an optimal stack pressure is critical. Proper pressure management can prevent dendritic growth and interfacial cracking, which are detrimental to battery life and safety.

Future research should focus on developing pressure-tolerant interfacial architectures, such as those using graded or adaptive interlayers, to accommodate mechanical mismatches. There is also a need to investigate low-temperature sintering and oscillating pressure methods as scalable, cost-efficient routes to densify solid electrolytes without compromising phase stability. Additionally, pressure-responsive binders and polymer composites that strike a balance between mechanical strength and ionic transport are promising candidates. Finally, benchmarking stack pressure thresholds for different chemistries is essential for transitioning from lab-scale prototypes to industrial-scale pouch cell formats.

This review lays a foundation for the rational design of pressure-engineered ASSBs that balance structural integrity with electrochemical efficiency.

CRediT authorship contribution statement

John Adjah: Writing – review & editing, Writing – original draft, Validation, Resources, Project administration, Methodology, Investigation, Formal analysis, Data curation, Conceptualization. **Benjamin Agyei-Tuffour:** Writing – review & editing, Supervision, Resources, Funding acquisition. **Ridwan A. Ahmed:** Writing – review & editing, Formal analysis. **Desmond Edem Primus Klenam:** Writing – review & editing, Validation, Methodology. **David Dodoo-Arhin:** Writing – review & editing, Supervision. **Emmanuel Nyankson:** Writing – review & editing, Supervision. **Kwadwo Mensah-Darkwa:** Writing – review & editing, Validation, Formal analysis. **Winston Wole Soboyejo:** Writing – review & editing, Resources, Funding acquisition.

Declaration of competing interest

The authors declare that they have no known competing financial interests or personal relationships that could have appeared to influence the work reported in this paper.

Acknowledgment

Technical and financial support from the Global Impact Fund from Worcester Polytechnic Institute is acknowledged. Funding and the contributions from experts from the SUNY Polytechnic Institute are gratefully acknowledged. Support from the University of Ghana through the BANGA-Africa program is also acknowledged.

Data availability

Data will be made available on request.

References

[1] I. Dincer, C. Acar, A review on clean energy solutions for better sustainability, Int. J. Energy Res. 39 (2015) 585–606, https://doi.org/10.1002/er.3329.
[2] Z. Huang, J. Wang, L. Bing, Y. Qiu, R. Guo, Y. Yu, M. Ma, L. Niu, D. Tong, R. M. Andrew, P. Friedlingstein, J.G. Canadell, F. Xi, Z. Liu, Global carbon uptake of cement carbonation accounts 1930–2021, Earth Syst. Sci. Data 15 (2023) 4947–4958, https://doi.org/10.5194/essd-15-4947-2023.
[3] Z. Liu, D. Guan, W. Wei, S.J. Davis, P. Ciais, J. Bai, S. Peng, Q. Zhang, K. Hubacek, G. Marland, R.J. Andres, D. Crawford-Brown, J. Lin, H. Zhao, C. Hong, T. A. Boden, K. Feng, G.P. Peters, F. Xi, J. Liu, Y. Li, Y. Zhao, N. Zeng, K. He, Reduced carbon emission estimates from fossil fuel combustion and cement production in China, Nature 524 (2015) 335–338, https://doi.org/10.1038/nature14677.
[4] J.B. Goodenough, Y. Kim, Challenges for rechargeable Li batteries, Chem. Mater. 22 (2010) 587–603, https://doi.org/10.1021/cm901452z.
[5] David. Linden, T.B. Reddy, Handbook of Batteries, McGraw-Hill, 2002.
[6] T. Shojaei, A. Mokhtar, Carbon mitigation by quota allocation, J. Environ. Manage 304 (2022), https://doi.org/10.1016/j.jenvman.2021.114097.
[7] Z. Cao, R.J. Myers, R.C. Lupton, H. Duan, R. Sacchi, N. Zhou, T.Reed Miller, J. M. Cullen, Q. Ge, G. Liu, The sponge effect and carbon emission mitigation potentials of the global cement cycle, Nat. Commun. 11 (2020), https://doi.org/10.1038/s41467-020-17583-w.
[8] I. Energy, Agency, Global EV Outlook 2024 moving towards increased affordability. www.iea.org, 2024.
[9] I. - International Energy Agency, Global EV Outlook 2023: catching up with climate ambitions. www.iea.org, 2023.
[10] I. Energy Agency, Global EV Outlook 2022 securing supplies for an electric future. www.iea.org/t&c/, 2022.
[11] K. Mizushima, P.C. Jones, P.J. Wiseman, J.B. Goodenough, LixCoO2 (0 < x ~< 1): A New Cathode Material for Batteries Of High Energy Density, North-Holland Publishing Company, 1981.
[12] J. Zheng, M. Gu, A. Genc, J.B. Goodenough, You may also like 4th International colloquium on atomic spectra and oscillator strengths for astrophysical and laboratory plasmas David S Leckrone and Jack Sugar-mitigating voltage fade in cathode materials by improving atomic level spatial uniformity of chemical species bond-length fluctuations in the copper oxide superconductors, 2003.
[13] Y.-S. Hu, Batteries: getting solid, Nat. Energy 1 (2016), https://doi.org/10.1038/nenergy.2016.42.
[14] G. Berckmans, L. De Sutter, M. Marinaro, J. Smekens, J. Jaguemont, M. Wohlfahrt-Mehrens, J. van Mierlo, N. Omar, Analysis of the effect of applying external mechanical pressure on next generation silicon alloy lithium-ion cells, Electrochim. Acta 306 (2019) 387–395, https://doi.org/10.1016/j.electacta.2019.03.138.
[15] H.D. Lim, J.H. Park, H.J. Shin, J. Jeong, J.T. Kim, K.W. Nam, H.G. Jung, K. Y. Chung, A review of challenges and issues concerning interfaces for all-solid-state batteries, Energy Storage Mater. 25 (2020) 224–250, https://doi.org/10.1016/j.ensm.2019.10.011.

[16] F. Zhang, Y. Guo, L. Zhang, P. Jia, X. Liu, P. Qiu, H. Zhang, J. Huang, A review of the effect of external pressure on all-solid-state batteries, ETransportation 15 (2023), https://doi.org/10.1016/j.etran.2022.100220.
[17] D.Spencer Jolly, Z. Ning, J.E. Darnbrough, J. Kasemchainan, G.O. Hartley, P. Adamson, D.E.J. Armstrong, J. Marrow, P.G. Bruce, Sodium/Na β″ alumina interface: effect of pressure on voids, ACS. Appl. Mater. Interfaces. 12 (2020) 678–685, https://doi.org/10.1021/acsami.9b17786.
[18] L.P. Hou, H. Yuan, C.Z. Zhao, L. Xu, G.L. Zhu, H.X. Nan, X.B. Cheng, Q.B. Liu, C. X. He, J.Q. Huang, Q. Zhang, Improved interfacial electronic contacts powering high sulfur utilization in all-solid-state lithium–sulfur batteries, Energy Storage Mater. 25 (2020) 436–442, https://doi.org/10.1016/j.ensm.2019.09.037.
[19] N. Suzuki, N. Yashiro, S. Fujiki, R. Omoda, T. Shiratsuchi, T. Watanabe, Y. Aihara, Highly cyclable all-solid-State battery with deposition-type lithium metal anode based on thin carbon black layer, Adv. Energy Sustain. Res. 2 (2021), https://doi.org/10.1002/aesr.202100066.
[20] T. Famprikis, P. Canepa, J.A. Dawson, M.S. Islam, C. Masquelier, Fundamentals of inorganic solid-state electrolytes for batteries, Nat. Mater. 18 (2019) 1278–1291, https://doi.org/10.1038/s41563-019-0431-3.
[21] R. Koerver, I. Aygün, T. Leichtweiß, C. Dietrich, W. Zhang, J.O. Binder, P. Hartmann, W.G. Zeier, J. Janek, Capacity fade in solid-State batteries: interphase formation and chemomechanical processes in nickel-rich layered oxide cathodes and lithium thiophosphate solid electrolytes, Chem. Mater. 29 (2017) 5574–5582, https://doi.org/10.1021/acs.chemmater.7b00931.
[22] J. Zhang, J. Fu, P. Lu, G. Hu, S. Xia, S. Zhang, Z. Wang, Z. Zhou, W. Yan, W. Xia, C. Wang, X. Sun, Challenges and strategies of low-pressure all-solid-State batteries, Adv. Mater. (2024), https://doi.org/10.1002/adma.202413499.
[23] M. So, G. Inoue, R. Hirate, K. Nunoshita, S. Ishikawa, Y. Tsuge, Effect of mold pressure on compaction and ion conductivity of all-solid-state batteries revealed by the discrete element method, J. Power. Sources 508 (2021) 230344, https://doi.org/10.1016/J.JPOWSOUR.2021.230344.
[24] J. Hu, Z. Sun, Y. Gao, P. Li, Y. Wu, S. Chen, R. Wang, N. Li, W. Yang, Y. Shen, S. H. Bo, 3D stress mapping reveals the origin of lithium-deposition heterogeneity in solid-state lithium-metal batteries, Cell Rep. Phys. Sci. 3 (2022), https://doi.org/10.1016/j.xcrp.2022.100938.
[25] B. Hennequart, M. Platonova, R. Chometon, T. Marchandier, A. Benedetto, E. Quemin, R. Dugas, C. Lethien, J.-M. Tarascon, Atmospheric-pressure operation of all-solid-state batteries enabled by halide solid electrolyte, ACS. Energy Lett. 9 (2024) 454–460.
[26] K. Zhang, Y. He, J. Zhou, X. Wang, Y. Li, F. Yang, Effects of external pressure on cycling performance of silicon-based lithium-ion battery: modelling and experimental validation, RSC Adv. 14 (2024) 29979–29991, https://doi.org/10.1039/d4ra05354k.
[27] P. Roering, G.M. Overhoff, K.L. Liu, M. Winter, G. Brunklaus, External pressure in polymer-based lithium metal batteries: an often-neglected criterion when evaluating cycling performance? ACS. Appl. Mater. Interfaces. 16 (2024) 21932–21942, https://doi.org/10.1021/acsami.4c02095.
[28] X. Gao, B. Liu, B. Hu, Z. Ning, D.S. Jolly, S. Zhang, J. Perera, J. Bu, J. Liu, C. Doerrer, E. Darnbrough, D. Armstrong, P.S. Grant, P.G. Bruce, Solid-state lithium battery cathodes operating at low pressures, Joule 6 (2022) 636–646, https://doi.org/10.1016/j.joule.2022.02.008.
[29] A. Sakuda, A. Hayashi, M. Tatsumisago, Sulfide solid electrolyte with favorable mechanical property for all-solid-state lithium battery, Sci. Rep. 3 (2013), https://doi.org/10.1038/srep02261.
[30] A. Sakuda, A. Hayashi, M. Tatsumisago, Recent progress on interface formation in all-solid-state batteries, Curr. Opin. Electrochem. 6 (2017) 108–114, https://doi.org/10.1016/j.coelec.2017.10.008.
[31] A. Sakuda, A. Hayashi, Y. Takigawa, K. Higashi, M. Tatsumisago, Evaluation of elastic modulus of Li2S-P2S5 glassy solid electrolyte by ultrasonic sound velocity measurement and compression test, J. Ceram. Soc. Jpn. 121 (2013) 946–949, https://doi.org/10.2109/jcersj2.121.946.
[32] C. Lee, S.Y. Han, J.A. Lewis, P.P. Shetty, D. Yeh, Y. Liu, E. Klein, H.W. Lee, M. T. McDowell, Stack pressure measurements to probe the evolution of the lithium-solid-State electrolyte interface, ACS. Energy Lett. 6 (2021), https://doi.org/10.1021/acsenergylett.1c01395.
[33] T.A. Yersak, C. Kang, J.R. Salvador, N.P.W. Pieczonka, M. Cai, Sulfide glass solid-state electrolyte separators for Li metal batteries: using an interlayer to increase rate performance and reduce stack pressure, Mater. Adv. (2022), https://doi.org/10.1039/d1ma00926e.
[34] B. Tao, D. Zhong, H. Li, G. Wang, H. Chang, Halide solid-state electrolytes for all-solid-state batteries: structural design, synthesis, environmental stability, interface optimization and challenges, Chem. Sci. 14 (2023) 8693–8722, https://doi.org/10.1039/d3sc02093b.
[35] Y.G. Lee, S. Fujiki, C. Jung, N. Suzuki, N. Yashiro, R. Omoda, D.S. Ko, T. Shiratsuchi, T. Sugimoto, S. Ryu, J.H. Ku, T. Watanabe, Y. Park, Y. Aihara, D. Im, I.T. Han, High-energy long-cycling all-solid-state lithium metal batteries enabled by silver–carbon composite anodes, Nat. Energy 5 (2020) 299–308, https://doi.org/10.1038/s41560-020-0575-z.
[36] T.Y. Kwon, K.T. Kim, D.Y. Oh, Y.B. Song, S. Jun, Y.S. Jung, Three-dimensional networking binders prepared in situ during wet-slurry process for all-solid-state batteries operating under low external pressure, Energy Storage Mater. 49 (2022) 219–226, https://doi.org/10.1016/J.ENSM.2022.04.017.
[37] D. Zeng, J. Yao, L. Zhang, R. Xu, S. Wang, X. Yan, C. Yu, L. Wang, Promoting favorable interfacial properties in lithium-based batteries using chlorine-rich sulfide inorganic solid-state electrolytes, Nat. Commun. 13 (2022), https://doi.org/10.1038/s41467-022-29596-8.
[38] J.M. Doux, Y. Yang, D.H.S. Tan, H. Nguyen, E.A. Wu, X. Wang, A. Banerjee, Y. S. Meng, Pressure effects on sulfide electrolytes for all solid-state batteries, J. Mater. Chem. Mater. 8 (2020) 5049–5055, https://doi.org/10.1039/c9ta12889a.
[39] R. Yamada, I. Inoue, S. Akasaka, S. Asai, Phase structure and electrical and mechanical properties of PLLA/ionic conductive polyether blends prepared by melt mixing, Polym. J. 51 (2019) 649–656, https://doi.org/10.1038/s41428-019-0176-5.
[40] S. Yu, R.D. Schmidt, R. Garcia-Mendez, E. Herbert, N.J. Dudney, J.B. Wolfenstine, J. Sakamoto, D.J. Siegel, Elastic properties of the solid electrolyte Li7La3Zr2O12 (LLZO), Chem. Mater. 28 (2016) 197–206, https://doi.org/10.1021/acs.chemmater.5b03854.
[41] K. Nagao, M. Nose, A. Kato, A. Sakuda, A. Hayashi, M. Tatsumisago, Preparation and characterization of glass solid electrolytes in the pseudoternary system Li3BO3-Li2SO4-Li2CO3, Solid. State Ion. 308 (2017) 68–76, https://doi.org/10.1016/j.ssi.2017.05.009.
[42] H. Xu, S. Yang, B. Li, Pressure effects and countermeasures in solid-State batteries: a comprehensive review, Adv. Energy Mater. 14 (2024), https://doi.org/10.1002/aenm.202303539.
[43] S. Rajendran, A. Pilli, O. Omolere, J. Kelber, L.M.R. Arava, An all-solid-state battery with a tailored electrode−electrolyte interface using surface chemistry and interlayer-based approaches, Chem. Mater. 33 (2021) 3401–3412, https://doi.org/10.1021/acs.chemmater.1c00747.
[44] J.S. Kim, G. Yoon, S. Kim, S. Sugata, N. Yashiro, S. Suzuki, M.J. Lee, R. Kim, M. Badding, Z. Song, J.M. Chang, D. Im, Surface engineering of inorganic solid-state electrolytes via interlayers strategy for developing long-cycling quasi-all-solid-state lithium batteries, Nat. Commun. 14 (2023), https://doi.org/10.1038/s41467-023-36401-7.
[45] N.J. Taylor, S. Stangeland-Molo, C.G. Haslam, A. Sharafi, T. Thompson, M. Wang, R. Garcia-Mendez, J. Sakamoto, Demonstration of high current densities and extended cycling in the garnet Li7La3Zr2O12 solid electrolyte, 2018.
[46] T. Dussart, N. Rividi, M. Fialin, G. Toussaint, P. Stevens, C. Laberty-Robert, Critical current density limitation of LLZO solid electrolyte: microstructure vs interface, J. Electrochem. Soc. 168 (2021) 120550, https://doi.org/10.1149/1945-7111/ac44be.
[47] H. Xu, Q. Zhu, Y. Zhao, Z. Du, B. Li, S. Yang, Phase-changeable dynamic conformal electrode/electrolyte interlayer enabling pressure-independent solid-State lithium metal batteries, Adv. Mater. 35 (2023), https://doi.org/10.1002/adma.202212111.
[48] H. Huo, J. Liang, N. Zhao, X. Li, X. Lin, Y. Zhao, K. Adair, R. Li, X. Guo, X. Sun, Dynamics of the garnet/Li interface for dendrite-free solid-State batteries, ACS. Energy Lett. 5 (2020) 2156–2164, https://doi.org/10.1021/acsenergylett.0c00789.
[49] R. Xu, F. Liu, Y. Ye, H. Chen, R.R. Yang, Y. Ma, W. Huang, J. Wan, Y. Cui, A morphologically stable Li/electrolyte interface for all-solid-State batteries enabled by 3D-micropatterned garnet, Adv. Mater. 33 (2021), https://doi.org/10.1002/adma.202104009.
[50] P. Shi, J. Ma, M. Liu, S. Guo, Y. Huang, S. Wang, L. Zhang, L. Chen, K. Yang, X. Liu, Y. Li, X. An, D. Zhang, X. Cheng, Q. Li, W. Lv, G. Zhong, Y.B. He, F. Kang, A dielectric electrolyte composite with high lithium-ion conductivity for high-voltage solid-state lithium metal batteries, Nat. Nanotechnol. 18 (2023) 602–610, https://doi.org/10.1038/s41565-023-01341-2.
[51] J. Adjah, K.I. Orisekeh, M. Vandadi, R.A. Ahmed, J. Asare, B. Agyei-Tuffour, D. Dodoo-Arhin, E. Nyankson, N. Rahbar, W.O. Soboyejo, Pressure effects on electrochemical and crack driving forces in aluminium-doped LLZO-based all-solid-state lithium metal batteries, J. Power. Sources 613 (2024) 234873, https://doi.org/10.1016/j.jpowsour.2024.234873.
[52] J.M. Doux, H. Nguyen, D.H.S. Tan, A. Banerjee, X. Wang, E.A. Wu, C. Jo, H. Yang, Y.S. Meng, Stack pressure considerations for room-temperature all-solid-state lithium metal batteries, Adv. Energy Mater. 10 (2020), https://doi.org/10.1002/aenm.201903253.
[53] X. Huang, Y. Lu, Z. Song, K. Rui, Q. Wang, T. Xiu, M.E. Badding, Z. Wen, Manipulating Li2O atmosphere for sintering dense Li7La3Zr2O12 solid electrolyte, Energy Storage Mater. 22 (2019) 207–217, https://doi.org/10.1016/j.ensm.2019.01.018.
[54] R. Hongahally Basappa, T. Ito, T. Morimura, R. Bekarevich, K. Mitsuishi, H. Yamada, Grain boundary modification to suppress lithium penetration through garnet-type solid electrolyte, J. Power. Sources. 363 (2017) 145–152, https://doi.org/10.1016/j.jpowsour.2017.07.088.
[55] M. Cronau, M. Szabo, C. König, T.B. Wassermann, B. Roling, How to measure a reliable ionic conductivity? The stack pressure dilemma of microcrystalline sulfide-based solid electrolytes, ACS. Energy Lett. 6 (2021) 3072–3077, https://doi.org/10.1021/acsenergylett.1c01299.
[56] M. Cronau, M. Szabo, D. Renz, M. Duchardt, L.P. Pescara, B. Roling, Deposition-type lithium metal all-solid-State batteries: about the importance of stack-pressure control and the benefits of hot pressing during initial cycling, Adv. Mater. Interfaces 10 (2023), https://doi.org/10.1002/admi.202202475.
[57] R. Murugan, V. Thangadurai, W. Weppner, Fast lithium ion conduction in garnet-type Li7La 3Zr2O12, Angew. Chem. - Int. Ed. 46 (2007) 7778–7781, https://doi.org/10.1002/anie.200701144.
[58] C.A. Geiger, E. Alekseev, B. Lazic, M. Fisch, T. Armbruster, R. Langner, M. Fechtelkord, N. Kim, T. Pettke, W. Weppner, Crystal chemistry and stability of "Li7La 3Zr2O12" garnet: a fast lithium-ion conductor, Inorg. Chem. 50 (2011) 1089–1097, https://doi.org/10.1021/ic101914e.
[59] J. Sastre, A. Priebe, M. Döbeli, J. Michler, A.N. Tiwari, Y.E. Romanyuk, Lithium garnet Li7La3Zr2O12 electrolyte for all-solid-State batteries: closing the gap

between bulk and thin film Li-ion conductivities, Adv. Mater. Interfaces 7 (2020), https://doi.org/10.1002/admi.202000425.
[60] al - D. Kim, J. Ju Kim, J.W. Park, N. Alloy Tatsuoki Kohno, S. Tsuruta, M. Kanda, J.S. Beck, J.C. Vartuli, W.J. Roth, M.F. Leonowicz, C.T. Kresge, K.D. Schmitt, C. T-W Chu, D.H. Olson, E.W. Sheppard, S.B. McCu IIen, J.B. Higgins, J.L. Schlenker, P. Zavalij, M.S. Whittingham, E.A. Boylan, V.K. Pecharsky, R.A. Jacobson, V. EinEIi, S. RThomas, V.R. Koch, Solid State lonics, Trans Tech Publications Ltd, 1996.
[61] J.A. Dawson, P. Canepa, M.J. Clarke, T. Famprikis, D. Ghosh, M.S. Islam, Toward understanding the different influences of grain boundaries on ion transport in sulfide and oxide solid electrolytes, Chem. Mater. 31 (2019) 5296–5304, https://doi.org/10.1021/acs.chemmater.9b01794.
[62] J. Wolfenstine, H. Jo, Y.H. Cho, I.N. David, P. Askeland, E.D. Case, H. Kim, H. Choe, J. Sakamoto, A preliminary investigation of fracture toughness of Li7La 3Zr2O12 and its comparison to other solid Li-ionconductors, Mater. Lett. 96 (2013) 117–120, https://doi.org/10.1016/j.matlet.2013.01.021.
[63] T. Fuchs, C.G. Haslam, A.C. Moy, C. Lerch, T. Krauskopf, J. Sakamoto, F. H. Richter, J. Janek, Increasing the pressure-free stripping capacity of the lithium metal anode in solid-State-batteries by carbon nanotubes, Adv. Energy Mater. 12 (2022), https://doi.org/10.1002/aenm.202201125.
[64] T. Krauskopf, H. Hartmann, W.G. Zeier, J. Janek, Toward a fundamental understanding of the lithium metal anode in solid-State batteries - an electrochemo-mechanical study on the garnet-type solid electrolyte Li 6.25 Al 0.25 La 3 Zr 2 O 12, ACS. Appl. Mater. Interfaces 11 (2019) 14463–14477, https://doi.org/10.1021/acsami.9b02537.
[65] T. Thompson, J. Wolfenstine, J.L. Allen, M. Johannes, A. Huq, I.N. David, J. Sakamoto, Tetragonal vs. cubic phase stability in Al-free Ta doped Li 7La3Zr2O12 (LLZO), J. Mater. Chem. Mater. 2 (2014) 13431–13436, https://doi.org/10.1039/c4ta02099e.
[66] A. Sharafi, C.G. Haslam, R.D. Kerns, J. Wolfenstine, J. Sakamoto, Controlling and correlating the effect of grain size with the mechanical and electrochemical properties of Li7La3Zr2O12 solid-state electrolyte, J. Mater. Chem. Mater. 5 (2017) 21491–21504, https://doi.org/10.1039/c7ta06790a.
[67] E.A. Il'Ina, O.L. Andreev, B.D. Antonov, N.N. Batalov, Morphology and transport properties of the solid electrolyte Li 7La 3Zr 2O 12 prepared by the solid-state and citrate-nitrate methods, J. Power. Sources. 201 (2012) 169–173, https://doi.org/10.1016/j.jpowsour.2011.10.108.
[68] J. Awaka, N. Kijima, H. Hayakawa, J. Akimoto, Synthesis and structure analysis of tetragonal Li7La3Zr2O12 with the garnet-related type structure, J. Solid. State Chem. 182 (2009) 2046–2052, https://doi.org/10.1016/j.jssc.2009.05.020.
[69] W. Zhao, Y. Zhang, N. Sun, Q. Liu, H. An, Y. Song, B. Deng, J. Wang, G. Yin, F. Kong, S. Lou, J. Wang, Maintaining interfacial transports for sulfide-based all-solid-State batteries operating at low external pressure, ACS. Energy Lett. (2023) 5050–5060, https://doi.org/10.1021/acsenergylett.3c01840.
[70] E. Hirose, K. Niwa, K. Kataoka, J. Akimoto, M. Hasegawa, Structural stability of the Li-ion conductor Li7La3Zr2O12 investigated by high-pressure in-situ X-ray diffraction and raman spectroscopy, Mater. Res. Bull. 107 (2018) 361–365, https://doi.org/10.1016/j.materresbull.2018.07.034.
[71] S. Monismith, J. Qu, Effect of stress State on phase stability and ionic transport in the solid electrolyte Li7La3Zr2O12, J. Phys. Chem. C 125 (2021) 10777–10785, https://doi.org/10.1021/acs.jpcc.1c02149.
[72] X. Zhang, Q.J. Wang, K.L. Harrison, S.A. Roberts, S.J. Harris, Pressure-driven interface evolution in solid-State lithium metal batteries, Cell Rep. Phys. Sci. 1 (2020), https://doi.org/10.1016/j.xcrp.2019.100012.
[73] H.Y. Li, B. Huang, Z. Huang, C.A. Wang, Enhanced mechanical strength and ionic conductivity of LLZO solid electrolytes by oscillatory pressure sintering, Ceram. Int. 45 (2019) 18115–18118, https://doi.org/10.1016/j.ceramint.2019.05.241.
[74] C. Lee, S.Y. Han, J.A. Lewis, P.P. Shetty, D. Yeh, Y. Liu, E. Klein, H.W. Lee, M. T. McDowell, Stack pressure measurements to probe the evolution of the lithium-solid-State electrolyte interface, ACS. Energy Lett. 6 (2021) 3261–3269, https://doi.org/10.1021/acsenergylett.1c01395.
[75] Y. qiang Shao, H. ling Liu, X. dong Shao, L. Sang, Z. tao Chen, An all coupled electrochemical-mechanical model for all-solid-state Li-ion batteries considering the effect of contact area loss and compressive pressure, Energy 239 (2022), https://doi.org/10.1016/j.energy.2021.121929.
[76] J.M. Doux, Y. Yang, D.H.S. Tan, H. Nguyen, E.A. Wu, X. Wang, A. Banerjee, Y. S. Meng, Pressure effects on sulfide electrolytes for all solid-state batteries, J. Mater. Chem. Mater. 8 (2020) 5049–5055, https://doi.org/10.1039/c9ta12889a.
[77] M.J. Wang, R. Choudhury, J. Sakamoto, Characterizing the Li-solid-electrolyte interface dynamics as a function of stack pressure and current density, Joule 3 (2019) 2165–2178, https://doi.org/10.1016/j.joule.2019.06.017.
[78] Y. Zhang, D. Luo, W. Luo, S. Du, Y. Deng, J. Deng, High-purity and high-density cubic phase of Li7La3Zr2O12 solid electrolytes by controlling surface/volume ratio and sintering pressure, Electrochim. Acta 359 (2020), https://doi.org/10.1016/j.electacta.2020.136965.
[79] T. Krauskopf, H. Hartmann, W.G. Zeier, J. Janek, Toward a fundamental understanding of the lithium metal anode in solid-State batteries - an electrochemo-mechanical study on the garnet-type solid electrolyte Li 6.25 Al 0.25 La 3 Zr 2 O 12, ACS. Appl. Mater. Interfaces. 11 (2019) 14463–14477, https://doi.org/10.1021/acsami.9b02537.
[80] P. Yao, H. Yu, Z. Ding, Y. Liu, J. Lu, M. Lavorgna, J. Wu, X. Liu, Review on polymer-based composite electrolytes for lithium batteries, Front. Chem. 7 (2019), https://doi.org/10.3389/fchem.2019.00522.
[81] K. Vignarooban, M.A.K.L. Dissanayake, I. Albinsson, B.E. Mellander, Effect of TiO2 nano-filler and EC plasticizer on electrical and thermal properties of poly (ethylene oxide) (PEO) based solid polymer electrolytes, Solid. State Ion. 266 (2014) 25–28, https://doi.org/10.1016/j.ssi.2014.08.002.
[82] M. Keller, G.B. Appetecchi, G.T. Kim, V. Sharova, M. Schneider, J. Schuhmacher, A. Roters, S. Passerini, Electrochemical performance of a solvent-free hybrid ceramic-polymer electrolyte based on Li7La3Zr2O12 in P(EO)15LiTFSI, J. Power Sources 353 (2017) 287–297, https://doi.org/10.1016/j.jpowsour.2017.04.014.
[83] Y. Su, X. Rong, A. Gao, Y. Liu, J. Li, M. Mao, X. Qi, G. Chai, Q. Zhang, L. Suo, L. Gu, H. Li, X. Huang, L. Chen, B. Liu, Y.S. Hu, Rational design of a topological polymeric solid electrolyte for high-performance all-solid-state alkali metal batteries, Nat. Commun. 13 (2022), https://doi.org/10.1038/s41467-022-31792-5.
[84] X. Xiao, W. Wu, X. Huang, A multi-scale approach for the stress analysis of polymeric separators in a lithium-ion battery, J. Power. Sources 195 (2010) 7649–7660, https://doi.org/10.1016/j.jpowsour.2010.06.020.
[85] Q.H. Nguyen, V.T. Luu, H.L. Nguyen, Y.W. Lee, Y. Cho, S.Y. Kim, Y.S. Jun, W. Ahn, Li7La3Zr2O12 Garnet solid polymer electrolyte for highly stable all-solid-State batteries, Front. Chem. 8 (2021), https://doi.org/10.3389/fchem.2020.619832.
[86] W. Lu, M. Xue, C. Zhang, Modified Li7La3Zr2O12 (LLZO) and LLZO-polymer composites for solid-state lithium batteries, Energy Storage Mater. 39 (2021), https://doi.org/10.1016/j.ensm.2021.04.016.
[87] M.G. Maitra, M. Sinha, A.K. Mukhopadhyay, T.R. Middya, U. De, S. Tarafdar, Ion-conductivity and Young's modulus of the polymer electrolyte PEO-ammonium perchlorate, Solid State Ion. 178 (2007) 167–171, https://doi.org/10.1016/j.ssi.2007.01.006.
[88] J. Lopez, D.G. Mackanic, Y. Cui, Z. Bao, Designing polymers for advanced battery chemistries, Nat. Rev. Mater. 4 (2019) 312–330, https://doi.org/10.1038/s41578-019-0103-6.
[89] T.H. Wang, L.W. Hsu, H.C. Chang, Structural reorganization of imidazolium ionic liquids induced by pressure-enhanced ionic liquid—Polyethylene oxide interactions, Int. J. Mol. Sci. 22 (2021) 1–16, https://doi.org/10.3390/ijms22020981.
[90] H. Xu, Y. Li, A. Zhou, N. Wu, S. Xin, Z. Li, J.B. Goodenough, Li3N-Modified garnet electrolyte for all-solid-State lithium metal batteries operated at 40 °c, Nano Lett. 18 (2018) 7414–7418, https://doi.org/10.1021/acs.nanolett.8b03902.
[91] B. Chen, Z. Huang, X. Chen, Y. Zhao, Q. Xu, P. Long, S. Chen, X. Xu, A new composite solid electrolyte PEO/Li10GeP2S12/SN for all-solid-state lithium battery, Electrochim. Acta 210 (2016) 905–914, https://doi.org/10.1016/j.electacta.2016.06.025.
[92] T.R. Martin, G. Teeter, C.S. Jiang, K. Park, Sulfur polymers as flexible interfacial additives for low stack-pressure solid-State lithium-ion batteries, Batter Supercaps. 6 (2023), https://doi.org/10.1002/batt.202300255.
[93] H. Wang, C. Lin, X. Yan, A. Wu, S. Shen, G. Wei, J. Zhang, Mechanical property-reinforced PEO/PVDF/LiClO4/SN blend all solid polymer electrolyte for lithium ion batteries, J. Electroanal. Chem. 869 (2020) 114156, https://doi.org/10.1016/j.jelechem.2020.114156.
[94] Relationship of ion transport and pressure in PEO_LITFSI solid electrolytes, (n.d.).
[95] H. Wang, C. Lin, X. Yan, A. Wu, S. Shen, G. Wei, J. Zhang, Mechanical property-reinforced PEO/PVDF/LiClO4/SN blend all solid polymer electrolyte for lithium ion batteries, J. Electroanal. Chem. 869 (2020) 114156, https://doi.org/10.1016/j.jelechem.2020.114156.
[96] A. Ohashi, M. Kodama, N. Horikawa, S. Hirai, Effect of Young's modulus of active materials on ion transport through solid electrolyte in all-solid-state lithium-ion battery, J. Power. Sources. 483 (2021), https://doi.org/10.1016/j.jpowsour.2020.229212.
[97] A. Sakuda, A. Hayashi, M. Tatsumisago, Sulfide solid electrolyte with favorable mechanical property for all-solid-state lithium battery, Sci. Rep. 3 (2013), https://doi.org/10.1038/srep02261.
[98] M. Agostini, Y. Aihara, T. Yamada, B. Scrosati, J. Hassoun, A lithium-sulfur battery using a solid, glass-type P2S 5-Li2S electrolyte, Solid. State Ion. 244 (2013) 48–51, https://doi.org/10.1016/j.ssi.2013.04.024.
[99] Y.T. Chen, M.A.T. Marple, D.H.S. Tan, S.Y. Ham, B. Sayahpour, W.K. Li, H. Yang, J.B. Lee, H.J. Hah, E.A. Wu, J.M. Doux, J. Jang, P. Ridley, A. Cronk, G. Deysher, Z. Chen, Y.S. Meng, Investigating dry room compatibility of sulfide solid-state electrolytes for scalable manufacturing, J. Mater. Chem. Mater. 10 (2022) 7155–7164, https://doi.org/10.1039/d1ta09846b.
[100] Y. Nikodimos, W.N. Su, H.K. Bezabh, M.C. Tsai, C.C. Yang, B.J. Hwang, Effect of selected dopants on conductivity and moisture stability of Li3PS4 sulfide solid electrolyte: a first-principles study, Mater. Today Chem. 24 (2022), https://doi.org/10.1016/j.mtchem.2022.100837.
[101] M. Calpa, N.C. Rosero-Navarro, A. Miura, K. Tadanaga, Preparation of sulfide solid electrolytes in the Li2S-P2S5 system by a liquid phase process, Inorg. Chem. Front. 5 (2018) 501–508, https://doi.org/10.1039/c7qi00737j.
[102] K.J. Kim, M. Balaish, M. Wadaguchi, L. Kong, J.L.M. Rupp, Solid-state Li–metal batteries: challenges and horizons of oxide and sulfide Solid electrolytes and their interfaces, Adv. Energy Mater. 11 (2021), https://doi.org/10.1002/aenm.202002689.
[103] M. Cronau, M. Szabo, D. Renz, M. Duchardt, L.P. Pescara, B. Roling, Deposition-type lithium metal all-solid-State batteries: about the importance of stack-pressure control and the benefits of hot pressing during initial cycling, Adv. Mater. Interfaces 10 (2023), https://doi.org/10.1002/admi.202202475.
[104] V. Faka, M.T. Agne, M.A. Lange, D. Daisenberger, B. Wankmiller, S. Schwarzmüller, H. Huppertz, O. Maus, B. Helm, T. Böger, J. Hartel, J. M. Gerdes, J.J. Molaison, G. Kieslich, M.R. Hansen, W.G. Zeier, Pressure-induced dislocations and their influence on ionic transport in Li+-conducting argyrodites,

J. Am. Chem. Soc. 146 (2024) 1710–1721, https://doi.org/10.1021/jacs.3c12323.
[105] J.M. Doux, H. Nguyen, D.H.S. Tan, A. Banerjee, X. Wang, E.A. Wu, C. Jo, H. Yang, Y.S. Meng, Stack pressure considerations for room-temperature all-solid-State lithium metal batteries, Adv. Energy Mater. 10 (2020), https://doi.org/10.1002/aenm.201903253.
[106] M. Cronau, M. Szabo, C. König, T.B. Wassermann, B. Roling, How to measure a reliable ionic conductivity? The stack pressure dilemma of microcrystalline sulfide-based solid electrolytes, ACS. Energy Lett. 6 (2021) 3072–3077, https://doi.org/10.1021/acsenergylett.1c01299.
[107] M. Kodama, S. Komiyama, A. Ohashi, N. Horikawa, K. Kawamura, S. Hirai, High-pressure in situ X-ray computed tomography and numerical simulation of sulfide solid electrolyte, J. Power. Sources 462 (2020), https://doi.org/10.1016/j.jpowsour.2020.228160.
[108] M. Kodama, S. Komiyama, A. Ohashi, N. Horikawa, K. Kawamura, S. Hirai, High-pressure in situ X-ray computed tomography and numerical simulation of sulfide solid electrolyte, J. Power. Sources 462 (2020), https://doi.org/10.1016/j.jpowsour.2020.228160.
[109] Y. Wang, B. Hoang, J. Hoerauf, C. Lee, C.-F. Lin, G.W. Rubloff, S.B. Lee, A. C. Kozen, Hot and cold pressed LGPS solid electrolytes, J. Electrochem. Soc. 168 (2021) 010533, https://doi.org/10.1149/1945-7111/abdb44.
[110] W. Fitzhugh, L. Ye, X. Li, The effects of mechanical constriction on the operation of sulfide based solid-state batteries, J. Mater. Chem. Mater. 7 (2019) 23604–23627, https://doi.org/10.1039/c9ta05248h.
[111] A. Verma, H. Kawakami, H. Wada, A. Hirowatari, N. Ikeda, Y. Mizuno, T. Kotaka, K. Aotani, Y. Tabuchi, P.P. Mukherjee, Microstructure and pressure-driven electrodeposition stability in solid-State batteries, Cell Rep. Phys. Sci. 2 (2021), https://doi.org/10.1016/j.xcrp.2020.100301.
[112] D.H.S. Tan, Y.-T. Chen, H. Yang, W. Bao, B. Sreenarayanan, J.-M. Doux, W. Li, B. Lu, S.-Y. Ham, B. Sayahpour, J. Scharf, E.A. Wu, G. Deysher, H.E. Han, J. Hah, H. Jeong, J.B. Lee, Z. Chen, Y.S. Meng, Carbon-free high-loading silicon anodes enabled by sulfide solid electrolytes, n.d.
[113] S. Chen, D. Xie, G. Liu, J.P. Mwizerwa, Q. Zhang, Y. Zhao, X. Xu, X. Yao, Sulfide solid electrolytes for all-solid-state lithium batteries: structure, conductivity, stability and application, Energy Storage Mater. 14 (2018) 58–74, https://doi.org/10.1016/j.ensm.2018.02.020.
[114] S. Choi, M. Jeon, W.D. Jung, S. Yang, S. Park, H. Il Ji, J.H. Lee, B.K. Kim, B. I. Sang, H. Kim, Robust solid-state interface with a deformable glass interlayer in sulfide-based all-solid-state batteries, Solid. State Ion. 346 (2020), https://doi.org/10.1016/j.ssi.2019.115217.
[115] All Solid-state Battery Performance Under External Pressure Modulation, (n.d.).
[116] H. Nan, C. Zhao, H. Yuan, Y. Lu, X. Shen, G. Zhu, Q. Liu, J. Huang, Q. Zhang, Recent advances in solid-state lithium metal batteries: the role of external pressure and internal stress, Huagong Xuebao/CIESC J. 72 (2021) 61–70, https://doi.org/10.11949/0438-1157.20201201.
[117] Y. Su, L. Ye, W. Fitzhugh, Y. Wang, E. Gil-González, I. Kim, X. Li, A more stable lithium anode by mechanical constriction for solid state batteries, Energy Environ. Sci. 13 (2020) 908–916, https://doi.org/10.1039/c9ee04007b.
[118] V. Faka, M.T. Agne, P. Till, T. Bernges, M. Sadowski, A. Gautam, K. Albe, W. G. Zeier, Pressure dependence of ionic conductivity in site disordered lithium superionic argyrodite Li6PS5Br, Energy Adv. 2 (2023) 1915–1925, https://doi.org/10.1039/d3ya00424d.
[119] Y. Sakka, H. Yamashige, A. Watanabe, A. Takeuchi, M. Uesugi, K. Uesugi, Y. Orikasa, Pressure dependence on the three-dimensional structure of a composite electrode in an all-solid-state battery, J. Mater. Chem. Mater. 10 (2022) 16602–16609, https://doi.org/10.1039/d2ta02378d.
[120] F. Ding, A. Doi, T. Ogawa, H. Ubukata, T. Zhu, D. Kato, C. Tassel, I. Oikawa, N. Inui, S. Kuze, T. Yamabayashi, K. Fujii, M. Yashima, X. Ou, Z. Wang, X. Min, K. Fujita, H. Takamura, A. Kuwabara, T. Zhang, K.J. Griffith, Z. Lin, L. Chai, H. Kageyama, Anionic sublattices in halide solid electrolytes: a case study with the high-pressure phase of Li3ScCl6, Angew. Chem. - Int. Ed. 63 (2024), https://doi.org/10.1002/anie.202401779.
[121] A. Golov, J.X. Lian, J. Carrasco, Interface stability and reaction mechanisms of Li3YCl5Br with high-voltage cathodes and Li metal anode: insights from ab initio simulations, ACS. Appl. Mater. Interfaces. (2024), https://doi.org/10.1021/acsami.4c12938.
[122] P. Ganesan, M. Soans, M.A. Cambaz, R. Zimmermanns, R. Gond, S. Fuchs, Y. Hu, S. Baumgart, M. Sotoudeh, D. Stepien, H. Stein, A. Groß, D. Bresser, A. Varzi, M. Fichtner, Fluorine-substituted halide solid electrolytes with enhanced stability toward the lithium metal, ACS. Appl. Mater. Interfaces. 15 (2023) 38391–38402, https://doi.org/10.1021/acsami.3c03513.
[123] X. Li, J. Liang, J.T. Kim, J. Fu, H. Duan, N. Chen, R. Li, S. Zhao, J. Wang, H. Huang, X. Sun, Highly stable halide-electrolyte-based all-solid-state Li–Se batteries, Adv. Mater. 34 (2022), https://doi.org/10.1002/adma.202200856.
[124] X. Nie, J. Hu, C. Li, Halide-based solid electrolytes: the history, progress, and challenges, Interdiscip. Mater. 2 (2023) 365–389, https://doi.org/10.1002/idm2.12090.
[125] K. Tuo, C. Sun, C.A. López, M.T. Fernández-Díaz, J.A. Alonso, New superionic halide solid electrolytes enabled by aliovalent substitution in Li3−xY1−xHfxCl6 for all-solid-state lithium metal based batteries, J. Mater. Chem. Mater. 11 (2023) 15651–15662, https://doi.org/10.1039/d3ta02781c.
[126] P. Lannelongue, S. Lindberg, E. Gonzalo, A. Golov, F. Bonilla, J.M. Lopez del Amo, T. Marchandier, A. Tron, J. Carrasco, P. López-Aranguren, Stable cycling of halide solid state electrolyte enabled by a dynamic layered solid electrolyte interphase between Li metal and Li3YCl4Br2, Energy Storage Mater. 72 (2024) 103733, https://doi.org/10.1016/J.ENSM.2024.103733.
[127] Y. Li, Z. Ni, J. Geng, Z. Wang, Y. Li, Y. Zhao, H. Shao, Y. Li, S. Xiong, J. Feng, Advancements in electrolytes: from liquid to solid for low-cost and high-energy-density micro-sized silicon-based batteries, Adv. Energy Mater. (2025) 2502284.
[128] T. Yu, Y. Liu, H. Li, Y. Sun, S. Guo, H. Zhou, Ductile inorganic solid electrolytes for all-solid-State lithium batteries, Chem. Rev. 125 (2025) 3595–3662, https://doi.org/10.1021/acs.chemrev.4c00894.
[129] T. Dai, S. Wu, Y. Lu, Y. Yang, Y. Liu, C. Chang, X. Rong, R. Xiao, J. Zhao, Y. Liu, W. Wang, L. Chen, Y.S. Hu, Inorganic glass electrolytes with polymer-like viscoelasticity, Nat. Energy 8 (2023) 1221–1228, https://doi.org/10.1038/s41560-023-01356-y.
[130] Y.-S. Hu, T. Dai, S. Wu, Y. Lu, Y. Yang, Y. Liu, C. Chang, X. Rong, R.-J. Xiao, J. Zhao, Y. Liu, W.-H. WANG, L. Chen, Discovery of inorganic glass electrolytes with polymer-like viscoelasticity, (2023). https://doi.org/10.21203/rs.3.rs-2798828/v1.
[131] Y. Ren, C.W. Nan, Viscoelastic inorganic glass as solid-state electrolyte for batteries, J. Mater. 10 (2024) 707–708, https://doi.org/10.1016/J.JMAT.2023.10.012.
[132] W. Wang, A new room temperature viscoelastic inorganic glass, Mater. Futures 2 (2023), https://doi.org/10.1088/2752-5724/acf7d9.
[133] Y.-S. Hu, T. Dai, S. Wu, Y. Lu, Y. Yang, Y. Liu, C. Chang, X. Rong, R.-J. Xiao, J. Zhao, Y. Liu, W.-H. WANG, L. Chen, Discovery of inorganic glass electrolytes with polymer-like viscoelasticity, (2023). https://doi.org/10.21203/rs.3.rs-2798828/v1.
[134] F.H. Richter, Viscoelastic glass electrolytes, Nat. Energy 8 (2023) 1182–1183, https://doi.org/10.1038/s41560-023-01379-5.
[135] H. Pan, L. Wang, Y. Shi, C. Sheng, S. Yang, P. He, H. Zhou, A solid-state lithium-ion battery with micron-sized silicon anode operating free from external pressure, Nat. Commun. 15 (2024), https://doi.org/10.1038/s41467-024-46472-9.
[136] J.-M. Tarascon, M. Armand, Issues and challenges facing rechargeable lithium batteries, 2001.
[137] Y. Chen, E. Rangasamy, C.R. Dela Cruz, C. Liang, K. An, A study of suppressed formation of low-conductivity phases in doped Li7La3Zr2O12 garnets by in situ neutron diffraction, J. Mater. Chem. Mater. 3 (2015) 22868–22876, https://doi.org/10.1039/c5ta04902d.
[138] A. Masias, N. Felten, R. Garcia-Mendez, J. Wolfenstine, J. Sakamoto, Elastic, plastic, and creep mechanical properties of lithium metal, J. Mater. Sci. 54 (2019) 2585–2600, https://doi.org/10.1007/s10853-018-2971-3.
[139] L. Zhang, T. Yang, C. Du, Q. Liu, Y. Tang, J. Zhao, B. Wang, T. Chen, Y. Sun, P. Jia, H. Li, L. Geng, J. Chen, H. Ye, Z. Wang, Y. Li, H. Sun, X. Li, Q. Dai, Y. Tang, Q. Peng, T. Shen, S. Zhang, T. Zhu, J. Huang, Lithium whisker growth and stress generation in an in situ atomic force microscope–environmental transmission electron microscope set-up, Nat. Nanotechnol. 15 (2020) 94–98, https://doi.org/10.1038/s41565-019-0604-x.
[140] H. Yan, K. Tantratian, K. Ellwood, E.T. Harrison, M. Nichols, X. Cui, L. Chen, How does the creep stress regulate void formation at the lithium-solid electrolyte interface during stripping? Adv. Energy Mater. 12 (2022) https://doi.org/10.1002/aenm.202102283.
[141] C. Hänsel, P.V. Kumar, D. Kundu, Stack pressure effect in Li3PS4 and Na3PS4 based alkali metal solid-State cells: the dramatic implication of interlayer growth, Chem. Mater. 32 (2020) 10501–10510, https://doi.org/10.1021/acs.chemmater.0c03444.
[142] A. Masias, N. Felten, R. Garcia-Mendez, J. Wolfenstine, J. Sakamoto, Elastic, plastic, and creep mechanical properties of lithium metal, J. Mater. Sci. 54 (2019) 2585–2600, https://doi.org/10.1007/s10853-018-2971-3.
[143] C. Yang, K. Fu, Y. Zhang, E. Hitz, L. Hu, Protected lithium-metal anodes in batteries: from liquid to solid, Adv. Mater. 29 (2017), https://doi.org/10.1002/adma.201701169.
[144] T. Krauskopf, B. Mogwitz, C. Rosenbach, W.G. Zeier, J. Janek, Diffusion limitation of lithium metal and Li–Mg alloy anodes on LLZO type solid electrolytes as a function of temperature and pressure, Adv. Energy Mater. 9 (2019), https://doi.org/10.1002/aenm.201902568.
[145] S. Xia, X. Wu, Z. Zhang, Y. Cui, W. Liu, Practical challenges and future perspectives of all-solid-State lithium-metal batteries, Chem. 5 (2019) 753–785, https://doi.org/10.1016/j.chempr.2018.11.013.
[146] D. Cao, X. Sun, Q. Li, A. Natan, P. Xiang, H. Zhu, Lithium dendrite in all-solid-State batteries: growth mechanisms, suppression strategies, and characterizations, Matter 3 (2020) 57–94, https://doi.org/10.1016/j.matt.2020.03.015.
[147] R. Dubey, J. Sastre, C. Cancellieri, F. Okur, A. Forster, L. Pompizii, A. Priebe, Y. E. Romanyuk, L.P.H. Jeurgens, M.V. Kovalenko, K.V. Kravchyk, Building a better Li-garnet solid electrolyte/metallic Li interface with antimony, Adv. Energy Mater. 11 (2021), https://doi.org/10.1002/aenm.202102086.
[148] V. Müller, R.G. Scurtu, M. Memm, M.A. Danzer, M. Wohlfahrt-Mehrens, Study of the influence of mechanical pressure on the performance and aging of Lithium-ion battery cells, J. Power. Sources 440 (2019), https://doi.org/10.1016/j.jpowsour.2019.227148.
[149] M.T. Demirkan, L. Trahey, T. Karabacak, Cycling performance of density modulated multilayer silicon thin film anodes in Li-ion batteries, J. Power. Sources 273 (2015) 52–61, https://doi.org/10.1016/j.jpowsour.2014.09.027.
[150] A.J. Louli, J. Li, S. Trussler, C.R. Fell, J.R. Dahn, Volume, pressure and thickness evolution of Li-ion pouch cells with silicon-composite negative electrodes, J. Electrochem. Soc. 164 (2017) A2689–A2696, https://doi.org/10.1149/2.1691712jes.
[151] S.Y. Han, C. Lee, J.A. Lewis, D. Yeh, Y. Liu, H.W. Lee, M.T. McDowell, Stress evolution during cycling of alloy-anode solid-state batteries, Joule 5 (2021) 2450–2465, https://doi.org/10.1016/j.joule.2021.07.002.

[152] D.M. Piper, T.A. Yersak, S.-H. Lee, Effect of compressive stress on electrochemical performance of silicon anodes, J. Electrochem. Soc. 160 (2013) A77–A81, https://doi.org/10.1149/2.064301jes.
[153] J. Cui, X. Chen, Z. Zhou, M. Zuo, Y. Xiao, N. Zhao, C. Shi, X. Guo, Effect of continuous pressures on electrochemical performance of Si anodes, Mater. Today Energy 20 (2021), https://doi.org/10.1016/j.mtener.2020.100632.
[154] J. Wang, L. Liao, Y. Li, J. Zhao, F. Shi, K. Yan, A. Pei, G. Chen, G. Li, Z. Lu, Y. Cui, Shell-protective secondary silicon nanostructures as pressure-resistant high-volumetric-capacity anodes for lithium-ion batteries, Nano Lett. 18 (2018) 7060–7065, https://doi.org/10.1021/acs.nanolett.8b03065.
[155] X.H. Liu, L. Zhong, S. Huang, S.X. Mao, T. Zhu, J.Y. Huang, Size-dependent fracture of silicon nanoparticles during lithiation, ACS. Nano 6 (2012) 1522–1531, https://doi.org/10.1021/nn204476h.
[156] Y. Sun, J.P. Zhang, C. Wen, L. Zhang, An enhanced approach for biochar preparation using fluidized bed and its application for H2S removal, Chem. Eng. Process.: Process Intensif. 104 (2016) 1–12, https://doi.org/10.1016/j.cep.2016.02.006.
[157] D.H.S. Tan, Y.-T. Chen, H. Yang, W. Bao, B. Sreenarayanan, J.-M. Doux, W. Li, B. Lu, S.-Y. Ham, B. Sayahpour, J. Scharf, E.A. Wu, G. Deysher, H.E. Han, J. Hah, H. Jeong, J.B. Lee, Z. Chen, Y.S. Meng, Carbon-free high-loading silicon anodes enabled by sulfide solid electrolytes, n.d. https://www.science.org.
[158] S. Zhang, G. Yang, X. Li, Y. Li, Z. Wang, L. Chen, Electrolyte and current collector designs for stable lithium metal anodes, Int. J. Miner. Metall. Mater. 29 (2022) 953–964, https://doi.org/10.1007/s12613-022-2442-3.
[159] H. Huo, J. Janek, Silicon as emerging anode in solid-State batteries, ACS. Energy Lett. 7 (2022) 4005–4016, https://doi.org/10.1021/acsenergylett.2c01950.
[160] D. He, M. Yuan, B. Hu, C. Zou, X. Zhao, C. Zhao, J. Wang, H. Ding, Effect of pressure on Si-based anode performance in all-solid-State batteries, J. Phys. Conf. Ser. Inst. Phys. (2024), https://doi.org/10.1088/1742-6596/2679/1/012005.
[161] X. Yin, W. Zheng, H. Tang, L. Yang, P. Zhang, Z.M. Sun, Enhancing ion storage and transport in Ti3C2Tz MXene via a "sacrificial cations" strategy, J. Mater. Chem. Mater. 12 (2024) 8952–8962, https://doi.org/10.1039/d3ta07867a.
[162] Y.-G. Lee, S. Fujiki, C. Jung, N. Suzuki, N. Yashiro, R. Omoda, D.-S. Ko, T. Shiratsuchi, T. Sugimoto, S. Ryu, J.H. Ku, T. Watanabe, Y. Park, Y. Aihara, D. Im, I.T. Han, High-energy long-cycling all-solid-state lithium metal batteries enabled by silver–carbon composite anodes, Nat. Energy 5 (2020) 299–308, https://doi.org/10.1038/s41560-020-0575-z.
[163] Y.S. Park, K. Kim, J.-W. Lee, J.-W. Moon, H.-H. Park, H. Hwang, Effect of cell pressure on the electrochemical performance of all-solid-state lithium batteries with zero-excess Li metal anode, J. Am. Ceram. Soc. 106 (2023) 7322–7330, https://doi.org/10.1111/jace.19322.
[164] S.G. Yoon, B.S. Vishnugopi, E.P. Alsaç, W.J. Jeong, S.E. Sandoval, D.L. Nelson, A. Ayyaswamy, P.P. Mukherjee, M.T. McDowell, Synergistic evolution of alloy nanoparticles and carbon in solid-State lithium metal anode composites at low stack pressure, ACS. Nano 18 (2024) 20792–20805, https://doi.org/10.1021/acsnano.4c07687.
[165] X. Zhang, Q. Xiang, S. Tang, A. Wang, X. Liu, J. Luo, Long cycling life solid-State Li metal batteries with stress self-adapted Li/garnet interface, Nano Lett. 20 (2020) 2871–2878, https://doi.org/10.1021/acs.nanolett.0c00693.
[166] D. Shin, J. Jung, Y. Roh, C. Park, I.J. Kim, H. Kwon, J. Baek, W. Oh, J. Kim, S. Jeong, J. Hwang, Y. Kim, D.H. Yoon, H.-T. Kim, Preferential lithium plating in the interfacial void region in all-solid-State batteries via pressure gradient-driven lithium-ion flux, ACS. Energy Lett. 9 (2024) 1035–1042, https://doi.org/10.1021/acsenergylett.4c00297.
[167] G.W. Baek, Y.J. Kim, M. Lee, Y. Kwon, B. Chun, G. Park, H. Seo, H. Yang, J. Kwak, Progress in the development of active-matrix quantum-dot light-emitting diodes driven by non-Si thin-film transistors, Materials 15 (2022), https://doi.org/10.3390/ma15238511.
[168] W. Ji, X. Zhang, M. Liu, T. Ding, H. Qu, D. Qiu, D. Zheng, D. Qu, M.M. Liu, High-performance all-solid-state Li-S batteries enabled by an all-electrochem-active prelithiated Si anode, 2022.
[169] S.Y. Han, C. Lee, J.A. Lewis, D. Yeh, Y. Liu, H.W. Lee, M.T. McDowell, Stress evolution during cycling of alloy-anode solid-state batteries, Joule 5 (2021) 2450–2465, https://doi.org/10.1016/j.joule.2021.07.002.
[170] T. Asakura, T. Inaoka, C. Hotehama, H. Kowada, K. Motohashi, A. Sakuda, M. Tatsumisago, A. Hayashi, Stack pressure dependence of Li stripping/plating performance in all-solid-State Li metal cells containing sulfide glass electrolytes, ACS. Appl. Mater. Interfaces. 15 (2023) 31403–31408, https://doi.org/10.1021/acsami.3c03552.
[171] J. Cui, X. Chen, Z. Zhou, M. Zuo, Y. Xiao, N. Zhao, C. Shi, X. Guo, Effect of continuous pressures on electrochemical performance of Si anodes, Mater. Today Energy 20 (2021), https://doi.org/10.1016/j.mtener.2020.100632.
[172] H. Sun, K. Zhao, Electronic structure and comparative properties of LiNi x Mn y Co z O 2 cathode materials, J. Phys. Chem. C 121 (2017) 6002–6010, https://doi.org/10.1021/acs.jpcc.7b00810.
[173] E.J. Cheng, K. Hong, N.J. Taylor, H. Choe, J. Wolfenstine, J. Sakamoto, Mechanical and physical properties of LiNi0.33Mn0.33Co0.33O2 (NMC), J. Eur. Ceram. Soc. 37 (2017) 3213–3217, https://doi.org/10.1016/j.jeurceramsoc.2017.03.048.
[174] X. Yan, B. Peng, B. Hu, Q. Chen, PEO-urea-LiTFSI ternary complex as solid polymer electrolytes, Polymer 99 (2016) 44–48, https://doi.org/10.1016/j.polymer.2016.06.056.
[175] X. Liu, B. Zheng, J. Zhao, W. Zhao, Z. Liang, Y. Su, C. Xie, K. Zhou, Y. Xiang, J. Zhu, H. Wang, G. Zhong, Z. Gong, J. Huang, Y. Yang, Electrochemo-mechanical effects on structural integrity of Ni-rich cathodes with different microstructures in all solid-state batteries, Adv. Energy Mater. 11 (2021), https://doi.org/10.1002/aenm.202003583.
[176] C. Doerrer, I. Capone, S. Narayanan, J. Liu, C.R.M. Grovenor, M. Pasta, P.S. Grant, High energy density single-crystal NMC/Li6PS5Cl cathodes for all-solid-State lithium-metal batteries, ACS. Appl. Mater. Interfaces 13 (2021) 37809–37815, https://doi.org/10.1021/acsami.1c07952.
[177] M. Yamamoto, M. Takahashi, Y. Terauchi, Y. Kobayashi, S. Ikeda, A. Sakuda, Fabrication of composite positive electrode sheet with high active material content and effect of fabrication pressure for all-solid-state battery, J. Ceram. Soc. Jpn. 125 (2017) 391–395, https://doi.org/10.2109/jcersj2.16321.
[178] X. Gao, B. Liu, B. Hu, Z. Ning, D.S. Jolly, S. Zhang, J. Perera, J. Bu, J. Liu, C. Doerrer, E. Darnbrough, D. Armstrong, P.S. Grant, P.G. Bruce, Solid-state lithium battery cathodes operating at low pressures, Joule 6 (2022) 636–646, https://doi.org/10.1016/j.joule.2022.02.008.
[179] B. Liu, S.D. Pu, C. Doerrer, D. Spencer Jolly, R.A. House, D.L.R. Melvin, P. Adamson, P.S. Grant, X. Gao, P.G. Bruce, The effect of volume change and stack pressure on solid-state battery cathodes, SusMat 3 (2023) 721–728, https://doi.org/10.1002/sus2.162.
[180] E.P. Alsaç, D.L. Nelson, S.G. Yoon, K.A. Cavallaro, C. Wang, S.E. Sandoval, U. D. Eze, W.J. Jeong, M.T. McDowell, Characterizing electrode materials and interfaces in solid-State batteries, Chem. Rev. (2025), https://doi.org/10.1021/acs.chemrev.4c00584.
[181] T. Zhang, J. Chen, X. Yao, Resist interface delamination and electrolyte cracking in cathodes of solid-state batteries by compliant electrolytes, n.d. https://ssrn.com/abstract=5043691.
[182] K. Guo, P.A. Tamirisa, B.W. Sheldon, X. Xiao, H. Gao, Pop-up delamination of electrodes in solid-State batteries, J. Electrochem. Soc. 165 (2018) A618–A625, https://doi.org/10.1149/2.0831803jes.
[183] M.V. Reddy, C.M. Julien, A. Mauger, K. Zaghib, Sulfide and oxide inorganic solid electrolytes for all-solid-state li batteries: a review, Nanomaterials 10 (2020) 1–80, https://doi.org/10.3390/nano10081606.
[184] X.B. Cheng, R. Zhang, C.Z. Zhao, F. Wei, J.G. Zhang, Q. Zhang, A review of solid electrolyte interphases on lithium metal anode, Adv. Sci. 3 (2015), https://doi.org/10.1002/advs.201500213.
[185] R. Murugan, V. Thangadurai, W. Weppner, Fast lithium ion conduction in garnet-type Li7La 3Zr2O12, Angew. Chem. - Int. Ed. 46 (2007) 7778–7781, https://doi.org/10.1002/anie.200701144.
[186] A. Banerjee, X. Wang, C. Fang, E.A. Wu, Y.S. Meng, Interfaces and interphases in all-solid-State batteries with inorganic solid electrolytes, n.d.
[187] H. Cha, J. Yun, S. Kim, J. Kang, M. Cho, W. Cho, J.W. Lee, Stabilizing the interface between high-Ni oxide cathode and Li6PS5Cl for all-solid-state batteries via dual-compatible halides, J. Power. Sources 617 (2024), https://doi.org/10.1016/j.jpowsour.2024.235157.
[188] J. Kang, H.R. Shin, J. Yun, S. Kim, B. Kim, K. Lee, Y. Lim, J.W. Lee, Chemo-mechanical failure of solid composite cathodes accelerated by high-strain anodes in all-solid-state batteries, Energy Storage Mater. 63 (2023) 103049, https://doi.org/10.1016/J.ENSM.2023.103049.
[189] F. Jin, L. Fadillah, H.Q. Nguyen, T.M. Sandvik, Y. Liu, A. García-Martín, E. Salagre, E.G. Michel, D. Stoian, K. Marshall, W. Van Beek, G. Redhammer, M. Mehraj Ud Din, D. Rettenwander, Elucidating the impact of Li3InCl6-coated LiNi0.8Co0.15Al0.05O2 on the electro-chemo-mechanics of Li6PS5Cl-based solid-State batteries, Chem. Mater. 36 (2024) 6017–6026, https://doi.org/10.1021/acs.chemmater.4c00515.
[190] G. Bucci, B. Talamini, A. Renuka Balakrishna, Y.M. Chiang, W.C. Carter, Mechanical instability of electrode-electrolyte interfaces in solid-state batteries, Phys. Rev. Mater. 2 (2018), https://doi.org/10.1103/PhysRevMaterials.2.105407.
[191] P. Minnmann, L. Quillman, S. Burkhardt, F.H. Richter, J. Janek, Editors' choice—quantifying the impact of charge transport bottlenecks in composite cathodes of all-solid-State batteries, J. Electrochem. Soc. 168 (2021) 040537, https://doi.org/10.1149/1945-7111/abf8d7.
[192] Q. Yao, J. Qu, Interfacial versus cohesive failure on polymer-metal interfaces in electronic packaging - effects of interface roughness, J. Electron. Packag. 124 (2002) 127–134, https://doi.org/10.1115/1.1459470.
[193] D.Spencer Jolly, Z. Ning, J.E. Darnbrough, J. Kasemchainan, G.O. Hartley, P. Adamson, D.E.J. Armstrong, J. Marrow, P.G. Bruce, Sodium/Na β″ alumina interface: effect of pressure on voids, ACS. Appl. Mater. Interfaces 12 (2020) 678–685, https://doi.org/10.1021/acsami.9b17786.
[194] A.J. Louli, J. Li, S. Trussler, C.R. Fell, J.R. Dahn, Volume, pressure and thickness evolution of Li-ion pouch cells with silicon-composite negative electrodes, J. Electrochem. Soc. 164 (2017) A2689–A2696, https://doi.org/10.1149/2.1691712jes.
[195] B. Liu, S.D. Pu, C. Doerrer, D. Spencer Jolly, R.A. House, D.L.R. Melvin, P. Adamson, P.S. Grant, X. Gao, P.G. Bruce, The effect of volume change and stack pressure on solid-state battery cathodes, SusMat 3 (2023) 721–728, https://doi.org/10.1002/sus2.162.
[196] Z.L. Xu, Y. Gang, M.A. Garakani, S. Abouali, J.Q. Huang, J.K. Kim, Carbon-coated mesoporous silicon microsphere anodes with greatly reduced volume expansion, J Mater. Chem. Mater. 4 (2016) 6098–6106, https://doi.org/10.1039/c6ta01344a.
[197] J. Wang, L. Liao, Y. Li, J. Zhao, F. Shi, K. Yan, A. Pei, G. Chen, G. Li, Z. Lu, Y. Cui, Shell-protective secondary silicon nanostructures as pressure-resistant high-volumetric-capacity anodes for lithium-ion batteries, Nano Lett. 18 (2018) 7060–7065, https://doi.org/10.1021/acs.nanolett.8b03065.
[198] X. Zhao, C. Wang, H. Liu, Y. Liang, L.-Z. Fan, A review of polymer-based solid-State electrolytes for lithium-metal batteries: structure, kinetic, interface stability,

and application, Batter. Supercaps. 6 (2023) e202200502, https://doi.org/10.1002/batt.202200502.
[199] S.K. Jung, H. Gwon, G. Yoon, L.J. Miara, V. Lacivita, J.S. Kim, Pliable lithium superionic conductor for all-solid-State batteries, ACS. Energy Lett. 6 (2021) 2006–2015, https://doi.org/10.1021/acsenergylett.1c00545.
[200] A. De Gol, K.B. Dermenci, L. Farkas, M. Berecibar, Electro-chemo-mechanical degradation in solid-State batteries: a review of microscale and multiphysics modeling, Adv. Energy Mater. 14 (2024) 2403255.
[201] T. Dai, S. Wu, Y. Lu, Y. Yang, Y. Liu, C. Chang, X. Rong, R. Xiao, J. Zhao, Y. Liu, W. Wang, L. Chen, Y.-S. Hu, Inorganic glass electrolytes with polymer-like viscoelasticity, Nat. Energy 8 (2023) 1221–1228, https://doi.org/10.1038/s41560-023-01356-y.
[202] D.J. Lee, Y. Jeon, J.P. Lee, L. Zhang, K.H. Koh, F. Li, A.U. Mu, J. Wu, Y.T. Chen, S. McNulty, W. Tang, M. Vicencio, D. Xu, J. Kim, Z. Chen, Robust interface and reduced operation pressure enabled by co-rolling dry-process for stable all-solid-state batteries, Nat. Commun. 16 (2025), https://doi.org/10.1038/s41467-025-59363-4.
[203] J. Zhang, S. Ming, Y. Ning, S. Zhen, Y. Jiang, Y. Liu, X. Wu, Y. Zhang, Z. Wang, High pressure molding Li10SnP2S12 ceramic electrolyte with low-grain-boundary-resistance for all-solid-state batteries, J. Power. Sources 584 (2023), https://doi.org/10.1016/j.jpowsour.2023.233625.
[204] Y. Liu, X. Xu, X. Jiao, O.O. Kapitanova, Z. Song, S. Xiong, Role of interfacial defects on electro–Chemo–Mechanical failure of solid-State electrolyte, Adv. Mater. 35 (2023), https://doi.org/10.1002/adma.202301152.
[205] M.J. Lee, D.O. Shin, J.Y. Kim, J. Oh, S.H. Kang, J. Kim, K.M. Kim, Y.M. Lee, S. O. Kim, Y.G. Lee, Interfacial barrier free organic-inorganic hybrid electrolytes for solid state batteries, Energy Storage Mater. 37 (2021) 306–314, https://doi.org/10.1016/j.ensm.2021.02.013.
[206] A. Gupta, E. Kazyak, N. Craig, J. Christensen, N.P. Dasgupta, J. Sakamoto, Evaluating the effects of temperature and pressure on Li/PEO-LiTFSI interfacial stability and kinetics, J. Electrochem. Soc. 165 (2018) A2801–A2806, https://doi.org/10.1149/2.0901811jes.
[207] J. Pei, X. Bai, P. Xue, L. Ma, R. Long, Z. Liu, W. Liu, All-solid-state battery safety in abnormal thermal situations: crack propagation and lithium dendrite growth, Nano Res. Energy 4 (2025), https://doi.org/10.26599/NRE.2025.9120155.
[208] H. Wang, T. Fujita, A review of research on embodied carbon in international trade, sustainability (Switzerland) 15 (2023). https://doi.org/10.3390/su15107879.
[209] S. Wang, Y. Zhang, X. Zhang, T. Liu, Y.H. Lin, Y. Shen, L. Li, C.W. Nan, High-conductivity argyrodite Li 6 PS 5 Cl solid electrolytes prepared via optimized sintering processes for all-solid-State lithium-sulfur batteries, ACS. Appl. Mater. Interfaces 10 (2018) 42279–42285, https://doi.org/10.1021/acsami.8b15121.
[210] J. Cannarella, C.B. Arnold, Stress evolution and capacity fade in constrained lithium-ion pouch cells, J. Power. Sources 245 (2014) 745–751, https://doi.org/10.1016/j.jpowsour.2013.06.165.
[211] J. Cannarella, C.B. Arnold, Stress evolution and capacity fade in constrained lithium-ion pouch cells, J. Power. Sources 245 (2014) 745–751, https://doi.org/10.1016/j.jpowsour.2013.06.165.
[212] S. Jun, Y.J. Nam, H. Kwak, K.T. Kim, D.Y. Oh, Y.S. Jung, Operando differential electrochemical pressiometry for probing electrochemo-mechanics in all-solid-State batteries, Adv. Funct. Mater. 30 (2020), https://doi.org/10.1002/adfm.202002535.
[213] Q. Tu, L. Barroso-Luque, T. Shi, G. Ceder, Electrodeposition and mechanical stability at lithium-solid electrolyte interface during plating in solid-State batteries, Cell Rep. Phys. Sci. 1 (2020), https://doi.org/10.1016/j.xcrp.2020.100106.
[214] M. Suyama, A. Kato, A. Sakuda, A. Hayashi, M. Tatsumisago, Lithium dissolution/deposition behavior with Li3PS4-LiI electrolyte for all-solid-state batteries operating at high temperatures, Electrochim. Acta 286 (2018) 158–162, https://doi.org/10.1016/j.electacta.2018.07.227.
[215] M. Wang, J. Sakamoto, Correlating the interface resistance and surface adhesion of the Li metal-solid electrolyte interface, J. Power. Sources 377 (2018) 7–11, https://doi.org/10.1016/j.jpowsour.2017.11.078.
[216] A. Gupta, E. Kazyak, N. Craig, J. Christensen, N.P. Dasgupta, J. Sakamoto, Evaluating the effects of temperature and pressure on Li/PEO-LiTFSI interfacial stability and kinetics, J. Electrochem. Soc. 165 (2018) A2801–A2806, https://doi.org/10.1149/2.0901811jes.
[217] L. Xu, J. Li, W. Deng, H. Shuai, S. Li, Z. Xu, J. Li, H. Hou, H. Peng, G. Zou, X. Ji, Garnet solid electrolyte for advanced all-solid-State Li batteries, Adv. Energy Mater. 11 (2021), https://doi.org/10.1002/aenm.202000648.
[218] H. Kim, C. Im, S. Ryu, Y.J. Gong, J. Cho, S. Pyo, H. Yun, J. Lee, J. Yoo, Y.S. Kim, Interface modeling via tailored energy band alignment: toward electrochemically stabilized all-solid-State Li-metal batteries, Adv. Funct. Mater. 32 (2022), https://doi.org/10.1002/adfm.202107555.
[219] X. Li, J. Liang, J.T. Kim, J. Fu, H. Duan, N. Chen, R. Li, S. Zhao, J. Wang, H. Huang, X. Sun, Highly stable halide-electrolyte-based all-solid-State Li–Se batteries, Adv. Mater. 34 (2022), https://doi.org/10.1002/adma.202200856.
[220] B. Chen, J. Zhang, T. Zhang, R. Wang, J. Zheng, Y. Zhai, X. Liu, Constructing a superlithiophilic 3D burr-microsphere interface on garnet for high-rate and ultra-stable solid-State Li batteries, Adv. Sci. 10 (2023), https://doi.org/10.1002/advs.202207056.
[221] W. Chang, R. May, M. Wang, G. Thorsteinsson, J. Sakamoto, L. Marbella, D. Steingart, Evolving contact mechanics and microstructure formation dynamics of the lithium metal-Li7La3Zr2O12 interface, Nat. Commun. 12 (2021), https://doi.org/10.1038/s41467-021-26632-x.
[222] H. Yan, K. Tantratian, K. Ellwood, E.T. Harrison, M. Nichols, X. Cui, L. Chen, How does the creep stress regulate void formation at the lithium-solid electrolyte interface during stripping? Adv. Energy Mater. 12 (2022) https://doi.org/10.1002/aenm.202102283.
[223] J.A. Lewis, F.J.Q. Cortes, M.G. Boebinger, J. Tippens, T.S. Marchese, N. Kondekar, X. Liu, M. Chi, M.T. McDowell, Interphase morphology between a solid-State electrolyte and lithium controls cell failure, ACS. Energy Lett. 4 (2019) 591–599, https://doi.org/10.1021/acsenergylett.9b00093.
[224] J.A. Lewis, J. Tippens, F.J.Q. Cortes, M.T. McDowell, Chemo-mechanical challenges in solid-State batteries, Trends. Chem. 1 (2019) 845–857, https://doi.org/10.1016/J.TRECHM.2019.06.013.
[225] X. Shen, R. Zhang, X. Chen, X.B. Cheng, X. Li, Q. Zhang, The failure of solid electrolyte interphase on Li metal anode: structural uniformity or mechanical strength? Adv. Energy Mater. 10 (2020) https://doi.org/10.1002/aenm.201903645.
[226] M. Ganser, F.E. Hildebrand, M. Klinsmann, M. Hanauer, M. Kamlah, R. M. McMeeking, An extended formulation of Butler-volmer electrochemical reaction kinetics including the influence of mechanics, J. Electrochem. Soc. 166 (2019) H167–H176, https://doi.org/10.1149/2.1111904jes.
[227] C. Hänsel, D. Kundu, The stack pressure dilemma in sulfide electrolyte based Li metal solid-State batteries: a case study with Li6PS5Cl solid electrolyte, Adv. Mater. Interfaces. 8 (2021), https://doi.org/10.1002/admi.202100206.
[228] X. Zhang, Q.J. Wang, K.L. Harrison, S.A. Roberts, S.J. Harris, Pressure-driven interface evolution in solid-State lithium metal batteries, Cell Rep. Phys. Sci. 1 (2020), https://doi.org/10.1016/j.xcrp.2019.100012.
[229] M.J. Wang, R. Choudhury, J. Sakamoto, Characterizing the Li-solid-electrolyte interface dynamics as a function of stack pressure and current density, Joule 3 (2019) 2165–2178, https://doi.org/10.1016/j.joule.2019.06.017.
[230] L.T. Gao, Y. Lyu, Z.S. Guo, External pressure affecting dendrite growth and dissolution in lithium metal batteries during cycles, ACS. Appl. Mater. Interfaces 15 (2023) 58416–58428, https://doi.org/10.1021/acsami.3c13972.
[231] X. Shen, R. Zhang, P. Shi, X. Chen, Q. Zhang, How does external pressure shape Li dendrites in Li metal batteries? Adv. Energy Mater. 11 (2021) https://doi.org/10.1002/aenm.202003416.
[232] J. Lee, T. Lee, K. Char, K.J. Kim, J.W. Choi, Issues and advances in scaling up sulfide-based all-solid-State batteries, Acc. Chem. Res. 54 (2021) 3390–3402, https://doi.org/10.1021/acs.accounts.1c00333.
[233] W. Zhang, D. Schröder, T. Arlt, I. Manke, R. Koerver, R. Pinedo, D.A. Weber, J. Sann, W.G. Zeier, J. Janek, (Electro)chemical expansion during cycling: monitoring the pressure changes in operating solid-state lithium batteries, J. Mater. Chem. Mater. 5 (2017) 9929–9936, https://doi.org/10.1039/c7ta02730c.
[234] K.G. Naik, B.S. Vishnugopi, P.P. Mukherjee, Kinetics or transport: whither goes the solid-State battery cathode? ACS. Appl. Mater. Interfaces. 14 (2022) 29754–29765, https://doi.org/10.1021/acsami.2c04962.
[235] R. Koerver, W. Zhang, L. De Biasi, S. Schweidler, A.O. Kondrakov, S. Kolling, T. Brezesinski, P. Hartmann, W.G. Zeier, J. Janek, Chemo-mechanical expansion of lithium electrode materials-on the route to mechanically optimized all-solid-state batteries, Energy Environ. Sci. 11 (2018) 2142–2158, https://doi.org/10.1039/c8ee00907d.
[236] S. Niu, S. heng, G. Zhu, J. Xu, Q. Qu, K. Wu, H. Zheng, Analysis on the effect of external press force on the performance of LiNi0.8Co0.1Mn0.1O2/graphite large pouch cells, J. Energy Storage 44 (2021), https://doi.org/10.1016/j.est.2021.103425.
[237] J. Gu, R. Xu, B. Chen, J. Zhou, NMC811-Li 6 PS 5 Cl-Li/In all-solid-State battery capacity attenuation based on temperature-pressure-electrochemical coupling model, J. Electrochem. Soc. 170 (2023) 040504, https://doi.org/10.1149/1945-7111/accaac.
[238] R.A. Ahmed, N. Ebechidi, I. Reisya, K. Orisekeh, A. Huda, A. Bello, O.K. Oyewole, W.O. Soboyejo, Pressure-induced interfacial contacts and the deformation in all solid-state Li-ion batteries, J. Power. Sources 521 (2022), https://doi.org/10.1016/j.jpowsour.2021.230939.
[239] J. Adjah, K.I. Orisekeh, M. Vandadi, R.A. Ahmed, J. Asare, B. Agyei-Tuffour, D. Dodoo-Arhin, E. Nyankson, N. Rahbar, W.O. Soboyejo, Pressure effects on electrochemical and crack driving forces in aluminium-doped LLZO-based all-solid-state lithium metal batteries, J. Power. Sources 613 (2024) 234873, https://doi.org/10.1016/J.JPOWSOUR.2024.234873.
[240] J. Adjah, K.I. Orisekeh, R.A. Ahmed, M. Vandadi, B. Agyei-Tuffour, D. Dodoo-Arhin, E. Nyankson, J. Asare, N. Rahbar, W.O. Soboyejo, Cyclic-induced deformation and the degradation of Al-doped LLZO electrolytes in all-solid-state Li-metal batteries, J. Power. Sources 594 (2024) 234022, https://doi.org/10.1016/j.jpowsour.2023.234022.
[241] R. Koerver, I. Aygün, T. Leichtweiß, C. Dietrich, W. Zhang, J.O. Binder, P. Hartmann, W.G. Zeier, J. Janek, Capacity fade in solid-State batteries: interphase formation and chemomechanical processes in nickel-rich layered oxide cathodes and lithium thiophosphate solid electrolytes, Chem. Mater. 29 (2017) 5574–5582, https://doi.org/10.1021/acs.chemmater.7b00931.
[242] S. Jun, Y.J. Nam, H. Kwak, K.T. Kim, D.Y. Oh, Y.S. Jung, Operando differential electrochemical pressiometry for probing electrochemo-mechanics in all-solid-State batteries, Adv. Funct. Mater. 30 (2020), https://doi.org/10.1002/adfm.202002535.
[243] T.Y. Kwon, K.T. Kim, D.Y. Oh, Y.B. Song, S. Jun, Y.S. Jung, Three-dimensional networking binders prepared in situ during wet-slurry process for all-solid-state batteries operating under low external pressure, Energy Storage Mater. 49 (2022) 219–226, https://doi.org/10.1016/j.ensm.2022.04.017.

[244] T. Shi, Y.Q. Zhang, Q. Tu, Y. Wang, M.C. Scott, G. Ceder, Characterization of mechanical degradation in an all-solid-state battery cathode, J. Mater. Chem. Mater. 8 (2020) 17399–17404, https://doi.org/10.1039/d0ta06985j.
[245] M. Chen, L. Xiao, H. Dong, J. Fan, X. Zhang, Pressure-driven contact mechanics evolution of cathode interfaces in lithium batteries, Acta Mech. Solida Sin. 36 (2023) 65–75, https://doi.org/10.1007/s10338-022-00348-x.
[246] Y. Wang, G. Wang, P. He, J. Hu, J. Jiang, L.Z. Fan, Sandwich structured NASICON-type electrolyte matched with sulfurized polyacrylonitrile cathode for high performance solid-state lithium-sulfur batteries, Chem. Eng. J. 393 (2020), https://doi.org/10.1016/j.cej.2020.124705.
[247] Z. Xie, Z. Wu, X. An, X. Yue, P. Xiaokaiti, A. Yoshida, A. Abudula, G. Guan, A sandwich-type composite polymer electrolyte for all-solid-state lithium metal batteries with high areal capacity and cycling stability, J. Memb. Sci. 596 (2020), https://doi.org/10.1016/j.memsci.2019.117739.
[248] J. Hüttl, C. Seidl, H. Auer, K. Nikolowski, A.L. Görne, M. Arnold, C. Heubner, M. Wolter, A. Michaelis, Ultra-low LPS/LLZO interfacial resistance – towards stable hybrid solid-state batteries with Li-metal anodes, Energy Storage Mater. 40 (2021) 259–267, https://doi.org/10.1016/j.ensm.2021.05.020.
[249] J. Cui, X. Chen, Z. Zhou, M. Zuo, Y. Xiao, N. Zhao, C. Shi, X. Guo, Effect of continuous pressures on electrochemical performance of Si anodes, Mater. Today Energy 20 (2021), https://doi.org/10.1016/j.mtener.2020.100632.
[250] X. Han, Y. Gong, K. Fu, X. He, G.T. Hitz, J. Dai, A. Pearse, B. Liu, H. Wang, G. Rubloff, Y. Mo, V. Thangadurai, E.D. Wachsman, L. Hu, Negating interfacial impedance in garnet-based solid-state Li metal batteries, Nat. Mater. 16 (2017) 572–579, https://doi.org/10.1038/nmat4821.
[251] R.A. Ahmed, N. Ebechidi, I. Reisya, K. Orisekeh, A. Huda, A. Bello, O.K. Oyewole, W.O. Soboyejo, Pressure-induced interfacial contacts and the deformation in all solid-state Li-ion batteries, J. Power. Sources 521 (2022), https://doi.org/10.1016/j.jpowsour.2021.230939.
[252] C. Doerrer, I. Capone, S. Narayanan, J. Liu, C.R.M. Grovenor, M. Pasta, P.S. Grant, High energy density single-crystal NMC/Li6PS5Cl cathodes for all-solid-State lithium-metal batteries, ACS. Appl. Mater. Interfaces 13 (2021) 37809–37815, https://doi.org/10.1021/acsami.1c07952.
[253] X. Zhang, Q.J. Wang, K.L. Harrison, K. Jungjohann, B.L. Boyce, S.A. Roberts, P. M. Attia, S.J. Harris, Rethinking how external pressure can suppress dendrites in lithium metal batteries, J. Electrochem. Soc. 166 (2019) A3639–A3652, https://doi.org/10.1149/2.0701914jes.
[254] C.D. Fincher, C.E. Athanasiou, C. Gilgenbach, M. Wang, B.W. Sheldon, W. C. Carter, Y.M. Chiang, Controlling dendrite propagation in solid-state batteries with engineered stress, Joule 6 (2022) 2794–2809, https://doi.org/10.1016/j.joule.2022.10.011.
[255] J. Zhang, J. Fu, P. Lu, G. Hu, S. Xia, S. Zhang, Z. Wang, Z. Zhou, W. Yan, W. Xia, C. Wang, X. Sun, Challenges and strategies of low-pressure all-solid-State batteries, Adv. Mater. (2024), https://doi.org/10.1002/adma.202413499.
[256] R. Koerver, W. Zhang, L. De Biasi, S. Schweidler, A.O. Kondrakov, S. Kolling, T. Brezesinski, P. Hartmann, W.G. Zeier, J. Janek, Chemo-mechanical expansion of lithium electrode materials-on the route to mechanically optimized all-solid-state batteries, Energy Environ. Sci. 11 (2018) 2142–2158, https://doi.org/10.1039/c8ee00907d.
[257] Y. Ren, W. Shin, A. Manthiram, Operating high-energy lithium-metal pouch cells with reduced stack pressure through a rational lithium-host design, Adv. Energy Mater. 12 (2022), https://doi.org/10.1002/aenm.202200190.
[258] T. Fuchs, C.G. Haslam, A.C. Moy, C. Lerch, T. Krauskopf, J. Sakamoto, F. H. Richter, J. Janek, Increasing the pressure-free stripping capacity of the lithium metal anode in solid-State-batteries by carbon nanotubes, Adv. Energy Mater. 12 (2022), https://doi.org/10.1002/aenm.202201125.
[259] G.L. Gregory, H. Gao, B. Liu, X. Gao, G.J. Rees, M. Pasta, P.G. Bruce, C. K. Williams, Buffering volume change in solid-State battery composite cathodes with CO2-derived block polycarbonate ethers, J. Am. Chem. Soc. 144 (2022) 17477–17486, https://doi.org/10.1021/jacs.2c06138.
[260] X. Gao, B. Liu, B. Hu, Z. Ning, D.S. Jolly, S. Zhang, J. Perera, J. Bu, J. Liu, C. Doerrer, E. Darnbrough, D. Armstrong, P.S. Grant, P.G. Bruce, Solid-state lithium battery cathodes operating at low pressures, Joule 6 (2022) 636–646, https://doi.org/10.1016/j.joule.2022.02.008.
[261] Y. Sakka, H. Yamashige, A. Watanabe, A. Takeuchi, M. Uesugi, K. Uesugi, Y. Orikasa, Pressure dependence on the three-dimensional structure of a composite electrode in an all-solid-state battery, J. Mater. Chem. Mater. 10 (2022) 16602–16609, https://doi.org/10.1039/d2ta02378d.
[262] C. Lee, J.Y. Kim, K.Y. Bae, T. Kim, S.J. Jung, S. Son, H.W. Lee, Enhancing electrochemomechanics: how stack pressure regulation affects all-solid-state batteries, Energy Storage Mater. 66 (2024), https://doi.org/10.1016/j.ensm.2024.103196.
[263] S.Y. Ham, H. Yang, O. Nunez-cuacuas, D.H.S. Tan, Y.T. Chen, G. Deysher, A. Cronk, P. Ridley, J.M. Doux, E.A. Wu, J. Jang, Y.S. Meng, Assessing the critical current density of all-solid-state Li metal symmetric and full cells, Energy Storage Mater. 55 (2023) 455–462, https://doi.org/10.1016/J.ENSM.2022.12.013.